NAVAL POSTGRADUATE SCHOOL
Monterey, California

THESIS

PARAMETERIZATION OF HORIZONTAL WIND VELOCITY VARIABILITY

by

Timothy Joseph Dowding

December 1987

Thesis Advisor: Gordon E. Schacher

REPORT DOCUMENTATION PAGE

1a REPORT SECURITY CLASSIFICATION UNCLASSIFIED	1b RESTRICTIVE MARKINGS
2a SECURITY CLASSIFICATION AUTHORITY	3 DISTRIBUTION AVAILABILITY OF REPORT Approved for public release; distribution is unlimited
2b DECLASSIFICATION / DOWNGRADING SCHEDULE	
4 PERFORMING ORGANIZATION REPORT NUMBER(S)	5 MONITORING ORGANIZATION REPORT NUMBER(S)
6a NAME OF PERFORMING ORGANIZATION Naval Postgraduate School 6b OFFICE SYMBOL (If applicable) Code 68	7a NAME OF MONITORING ORGANIZATION Naval Postgraduate School
6c. ADDRESS (City, State, and ZIP Code) Monterey, California 93943-5000	7b ADDRESS (City, State, and ZIP Code) Monterey, California 93943-5000
8a NAME OF FUNDING SPONSORING ORGANIZATION 8b OFFICE SYMBOL (If applicable)	9 PROCUREMENT INSTRUMENT IDENTIFICATION NUMBER
8c. ADDRESS (City, State, and ZIP Code)	10 SOURCE OF FUNDING NUMBERS PROGRAM ELEMENT NO / PROJECT NO / TASK NO / WORK UNIT ACCESSION NO

11 TITLE (Include Security Classification)
PARAMETERIZATION OF HORIZONTAL WIND VELOCITY VARIABILITY

12. PERSONAL AUTHOR(S)
Dowding, Timothy J.

13a TYPE OF REPORT	13b TIME COVERED	14 DATE OF REPORT (Year, Month, Day)	15 PAGE COUNT
Master's Thesis	FROM _____ TO _____	1987, December	153

16 SUPPLEMENTARY NOTATION

17 COSATI CODES			18 SUBJECT TERMS (Continue on reverse if necessary and identify by block number)
FIELD	GROUP	SUB-GROUP	Diffusion; Wind Variability; Turbulence

19 ABSTRACT (Continue on reverse if necessary and identify by block number)

Longitudinal and transverse horizontal wind velocity variability is parameterized based on data collected for the Bureau of Land Management (BLM) between 1980 and 1982. The BLM data sets were used to derive horizontal wind velocity components and standard deviations of these components in the longitudinal (downwind; u, σ_u) and transverse (crosswind; v, σ_v) directions for various time averages. The standard deviations were plotted versus wind speed so that trends in the change of values could be determined. A methodology was used to develop a theoretical algorithm to account for turbulence production mechanisms due to shear, buoyancy and mesoscale processes. Empirical fits were determined for both the u and v wind directions over four different time averages. The results were related to puff growth in the x, y directions and form the basis

20 DISTRIBUTION / AVAILABILITY OF ABSTRACT	21 ABSTRACT SECURITY CLASSIFICATION
☒ UNCLASSIFIED/UNLIMITED ☐ SAME AS RPT ☐ DTIC USERS	Unclassified
22a NAME OF RESPONSIBLE INDIVIDUAL Gordon E. Schacher	22b TELEPHONE (Include Area Code) (408) 646-3411 22c OFFICE SYMBOL Code 06

DD FORM 1473, 84 MAR 83 APR edition may be used until exhausted
All other editions are obsolete

☆ U.S. Government Printing Office 1986—606-243

19 - ABSTRACT - (CONTINUED)

for improving a puff dispersion model for near-coast overwater regions.

Approved for public release; distribution is unlimited

Parameterization of Horizontal Wind Velocity Variability

by

Timothy Joseph Dowding
Lieutenant, United States Navy
B.S., United States Naval Academy, 1978

Submitted in partial fulfillment of the
requirements for the degree of

MASTER OF SCIENCE IN METEOROLOGY AND OCEANOGRAPHY

from the

NAVAL POSTGRADUATE SCHOOL
December 1987

ABSTRACT

Longitudinal and transverse horizontal wind velocity variability is parameterized based on data collected for the Bureau of Land Management (BLM) between 1980 and 1982. The BLM data sets were used to derive horizontal wind velocity components and standard deviations of these components in the longitudinal (downwind; u, σ_u) and transverse (crosswind; v, σ_v) directions for various time averages. The standard deviations were plotted versus wind speed so that trends in the change of values could be determined. A methodology was used to develop a theoretical algorithm to account for turbulence production mechanisms due to shear, buoyancy and mesoscale processes. Empirical fits were determined for both the u and v wind directions over four different time averages. The results were related to puff growth in the x, y directions and form the basis for improving a puff dispersion model for near-coast overwater regions.

TABLE OF CONTENTS

ACKNOWLEDGMENTS

The author wishes to express his appreciation to Dr. Gordon E. Schacher, thesis advisor, for his guidance and assistance throughout the course of this project. One of the purposes for any thesis is to learn something, whether it is to expand a knowledge base on a particular topic, or to merely learn how to think and problem solve. Dr. Schacher's patience reached saintly proportions in an attempt to facilitate the author's learning process. For that, I am most grateful to him. Thanks to Dr. Ken Davidson who reviewed the manuscript and provided timely advice. Also thanks go to Capt. Charlie Roberts and Cdr. Bob Barry, NPS Air-Ocean Sciences Curricular Officers, and to Lcdr. Wayne Shiver, Executive Officer of the Naval Environmental Prediction Research Facility who all provided immeasurable amounts of encouragement over the long road traveled towards earning this degree.

The author is most especially grateful to his wife, Lynn, and sons, David and Daniel who somehow managed to stay patient and maintain a sense of humor throughout the entire NPS experience.

I. INTRODUCTION

Modeling atmospheric transport within the marine atmospheric boundary layer (MABL) has progressed in recent years. The uses of such models are numerous, but for the purposes of this thesis, they were oriented towards the diffusion of airborne contaminants for use in industrial applications such as gaseous releases from offshore oil drilling platforms, and Department of Defense uses such as chemical-warfare defense. To develop such models, people have taken into account certain geophysical, thermodynamic, dynamic processes and developed mathematical algorithms to describe the transport of airborne particles. Previous works by Hojstrup (1982) and Panofsky and Dutton (1984) provided expressions for atmospheric turbulence intensity as a function of shear and buoyancy production mechanisms. Schacher, et al. (1982) performed a series of experiments for the Minerals Management Service (formerly the Bureau of Land Management (BLM)) to obtain empirical data to evaluate the existing models and to parameterize Environmental Protection Agency (EPA) approved Gaussian and trajectory dispersion models specifically for the Southern California coastal regions. Schacher et al. (1986) further utilized these data to parameterize horizontal wind direction variability with three fitting parameters to represent

shear, buoyancy and mesoscale production mechanisms. The purpose of those efforts was to improve the prediction of gaseous dispersion within the MABL.

The purpose of this thesis is to parameterize longitudinal and transverse horizontal wind velocity variability on the basis of the BLM experiments and relate them to longitudinal and transverse puff release growth. The BLM data sets were used to derive horizontal wind velocity components and standard deviations of these components in the longitudinal (downwind; u,σ_u) and transverse (crosswind; v,σ_v) directions for various time averages. The standard deviations were plotted versus wind speed so that trends in the change of values could be determined. A methodology partially based on Hojstrup (1982), and Schacher et al. (1986) was used to develop a theoretical algorithm which accounted for turbulence production mechanisms due to shear, buoyancy and mesoscale processes. Empirical fits were determined for both the u and v wind directions over four different time averages. The results were related to puff growth in the x, y directions and form the basis for improving a puff dispersion model for near-coast overwater regions.

II. DATA ACQUISITION

A. GENERAL DESCRIPTIONS

Data used in this work were collected during the California Coastal Offshore Transport and Diffusion Experiments in 1980, 1981, and 1982. Four experiments were performed, two near Ventura, CA in the Santa Barbara Channel, and two near Pismo Beach, CA, in an open coastal area. These sites were chosen to be representative of areas encountered along the coast. The Environmental Physics Group of the Naval Postgraduate School (NPS) performed measurements aboard the research ship R/V Acania and was responsible for collecting the overwater meteorological data for all four experiments. Studies were performed such that both the winter and summer seasons could be examined. Complete descriptions of the two phases of the experiment were presented by Schacher, et al. (1982). To conform with previous reports, the experiments of Phase I are referred to as BLM 1 and 2, and the experiments of Phase II as BLM 3 and 4. To make this thesis self-contained, portions of the Schacher, et al. (1982) report are included in this thesis.

1. Description of Experiments

The experimental approach was as follows: SF6 gas was released within the outer continental shelf area, outside of three nautical miles (n mi) from shore. During

Phase I near Ventura the ship was approximately five n mi from shore, whereas during Phase II off Pismo Beach the distance was three n mi. The plume location was determined by continuous analyzers in aircraft and ground vehicles, by grab samples from a boat and on land, and by stationary one-hour average samplers on land. The release ship was equipped with a complete set of meteorological instrumentation, including radiosondes, to determine overwater conditions. An aircraft was used to get soundings of mean meteorological parameter profiles. Onshore instrumentation included fixed and tetroon borne sensors and a Doppler acoustic sounder for determining wind profiles. Charts showing the locations of the ship, aircraft trajectories, and ground level sampling during Phase II are in Fig. 2-1.

The sequence of events on a sampling day was approximately as follows: Throughout the early morning the ship reported winds to the shore command station. These data and shore wind informations were used for initial positioning of the ship. Continuous monitoring of the wind was done to determine when the sea breeze had become well established and to position the ship so that at the shoreline the plume would intersect the center of the fixed sampler array. The ship was anchored at a fixed position since movement of the ship during a release would introduce apparent meander to the plume, contaminating the test results. The tracer gas release usually began between 1100

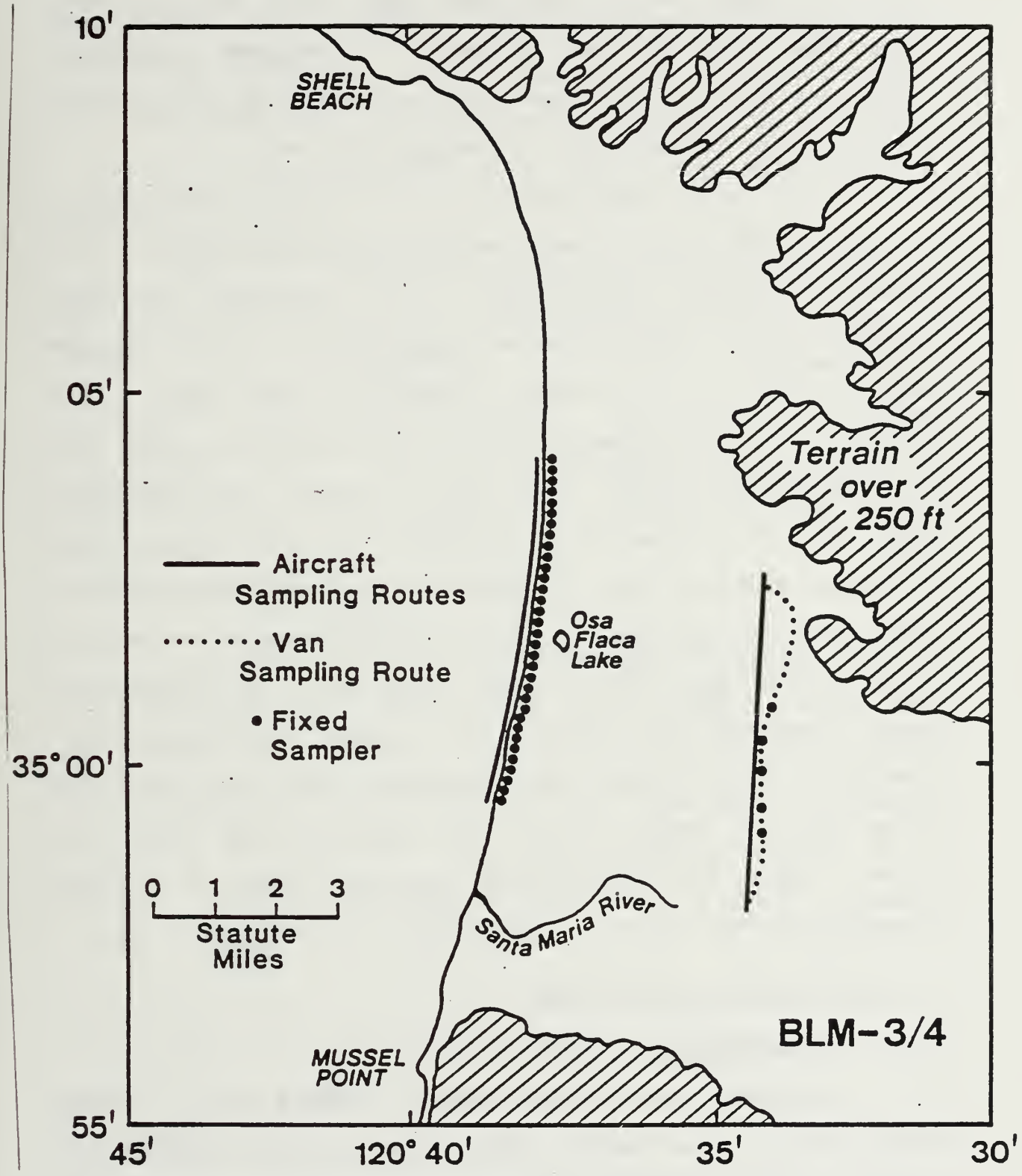

Fig. 2-1 Phase II Sampling Locations and Routes

and 1300 hours. Mobile sampling began about one-half hour after the start of the release. A complete experiment lasted 6-8 hours. The tracer gas was monitored continuously at the source to maintain a constant flow rate.

For all experiments, an aircraft carrying a continuous SF6 analyzer made near shoreline transects of the plume at several elevations. The instrument provided readings of the instantaneous concentrations of SF6 in the ambient air as a function of position and time. This allowed the plume dimensions to be defined in both the horizontal and vertical directions. Ground level transects were made by a similarly equipped van, operating at the shoreline and/or inland. Ground level plume concentrations were determined by placing fixed one-hour average collectors along one or more fixed arrays parallel to the shoreline. These samplers were placed close enough together so that several would be within the narrowest plume expected. The array was wide enough so that the plume would be within its extent even if considerable meander occurred. This necessitated the use of a large number of samplers.

B. ENVIRONMENTAL CONDITIONS

1. Description of Localities

In this section the general nature of the Pismo Beach locality and climatology is described to identify the expected meteorological conditions. Descriptions of the synoptic and local conditions pertaining to the Phase II

experiments are included. Locality descriptions and local conditions during the Phase I experiments are omitted since the data sets from Phase I were not utilized in this work. A chart of the geographical area surrounding Pismo Beach is shown in Fig. 2-2.

The test locations were chosen (1) because they are representative of important types of coastal areas, and (2) because both are candidates for new or increased outer continental shelf oil development. Thus, the areas afford the opportunity to investigate transport under differing meteorological conditions and also satisfy the needs for BLM modeling for regulatory purposes.

a. Pismo Beach, CA (Phase II)

Pismo Beach is approximately 50 miles north of Pt. Conception, in a fairly open coastal area. Pt. Buchon, immediately to the north, has 1000 to 2000 foot high hills projecting some five miles out to sea. The point influences the local flow somewhat but the influence appears to be slight. The immediate inland hills are low giving a weaker land-sea breeze cycle than near Ventura. The experiments were carried out at the mouth of the Santa Maria valley, which steers the local flow slightly. The entrance to the valley at the beach is approximately eight miles wide and the immediate hills on each side of the valley are only one to two hundred feet high, so their effect is small. The area is representative of an open California coastal region

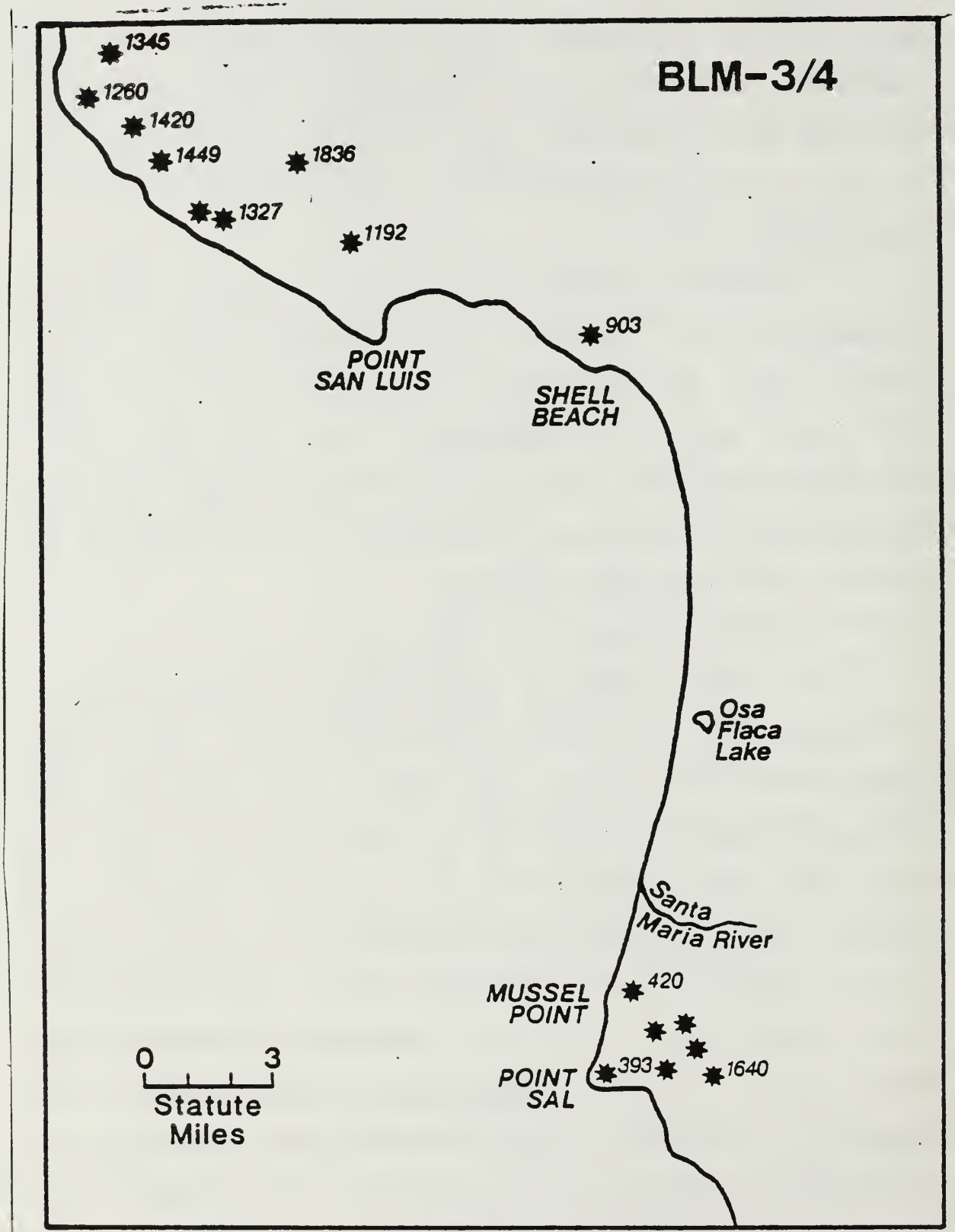

Fig. 2-2 Pismo Beach, California Area

where air mass movement is controlled by the synoptic pressure gradient, giving predominantly northwest flow with a long over-water fetch, and by the land-sea breeze cycle.

2. Synoptic-Scale Seasonal Climatology of the California Coast

The synoptic climatology is the same for the two test areas. General descriptions, according to seasons, for both areas are as follows.

a. Summer

The North Pacific semipermanent subtropical high lies to the west of the area and controls the synoptic-scale flow. Clockwise flow around the high produces northwesterlies along much of the coast, with the local sea-breeze turning the wind more westerly. The general onshore flow is aided by the inland thermal trough which is created by overland heating. Strong subsidence creates the prevalent capping inversion and the occasional passage of weak upper-level troughs will dissipate or lift the inversion for periods of 12-24 hours.

b. Fall

The building of high pressure in the Great Basin causes frequent Santa Ana conditions. Santa Ana conditions are characterized by high pressure areas located over the southern California deserts and lower pressure situated over the southern California coastal regime. The pressure differential between the desert and coast causes very strong, dry, low-level easterly winds to prevail. The

intensity of these winds is exacerbated by being funneled through the numerous canyons, in effect resulting in a hot, dry jet. This jet produces much vertical, shear induced turbulence in the coastal regime MABL. The pattern of storms and upper-level westerlies moves further south breaking up the summer pattern. Frontal passage becomes more frequent than in the summer and the subtropical high becomes displaced or shrinks, resulting in a break up of the coastal marine inversion.

c. Winter

Frontal passage becomes much more frequent and strong surface westerlies often follow the passage. Santa Ana winds can still occur when the sea-level pressure in the Great Basin becomes sufficiently high. Also, the Pacific High and capping inversion can reform between frontal passage occurrences.

d. Spring

As the storm pattern moves north, the Pacific High again becomes the dominant feature. Cold lows pass frequently, followed by strong westerlies.

3. Wind Climatology

Wind climatologies are useful in determining expected conditions and for assessing whether observed conditions are typical. It is not possible to use the climatology to accurately predict local conditions on a day-by-day basis but seasonal patterns are quite reproduceable.

In coastal areas, conditions differ from location to location so that site specific climatologies are needed. Climatological data are presented for Vandenberg Air Force Base (AFB), CA (Det 30, 2WS, 1982) which is near Pismo Beach. Vandenberg AFB is approximately 20 miles from the Pismo Beach experiment area. No closer coastal climatology is available. The data set was obtained at meteorological stations which are two to three miles inland.

Monthly wind averages for Pt. Mugu, CA, including the number of days of occurrence of Santa Ana conditions, are presented in Table 2-1. Santa Ana conditions are widespread so that these data would be approximately correct for Vandenberg AFB also.

Surface wind roses for three-month periods for Vandenberg are shown in Fig. 2-3. Wind speed is indicated by the width of each "vector," wind direction by the angle, and frequency of occurrence by the length. The numbers in each wind rose circle are the percentage of the time the wind is $\leq$ 3 knots. The wind speed averages for Vandenberg AFB are always less than 10 knots.

4. Test Period Weather Description

The following is a description of the synoptic and local conditions during the Phase II test periods. The synoptic conditions were derived from daily weather maps (weekly series), published by the National Oceanic and Atmospheric Administration. The description of local

TABLE 2-1

MONTHLY AVERAGES OF THE MOST FREQUENTLY OBSERVED WIND DIRECTION, PERCENTAGE OF TIME THE WIND SPEED IS GREATER THAN 21 KNOTS, AND THE NUMBER OF DAYS OF SANTA ANA WINDS PER MONTH. THE MAXIMUM NUMBER IS THE MAXIMUM OBSERVED OVER A TEN-YEAR PERIOD.

Month	Most Frequent Wind Direc.	Speed (Kt)	%	% greater than 21 Kt	Santa Ana Occurence Average No. days	Maximum No. days
JAN	NE	10	15.5	2.3	9.3	16
FEB	W	9	12.3	1.8	5.2	12
MAR	W	10	18.3	1.1	2.8	8
APR	W	10	26.7	1.4	0.6	2
MAY	W	9	28.7	0.3	0.3	2
JUN	W	8	27.5	0.0	0.0	1
JUL	W	7	25.2	0.0	0.0	0
AUG	W	8	23.6	0.0	0.0	0
SEP	W	7	19.5	0.1	0.4	4
OCT	W	7	16.3	0.5	2.7	8
NOV	NE	7	12.1	1.0	7.0	19
DEC	N	5	12.8	1.4	9.3	18

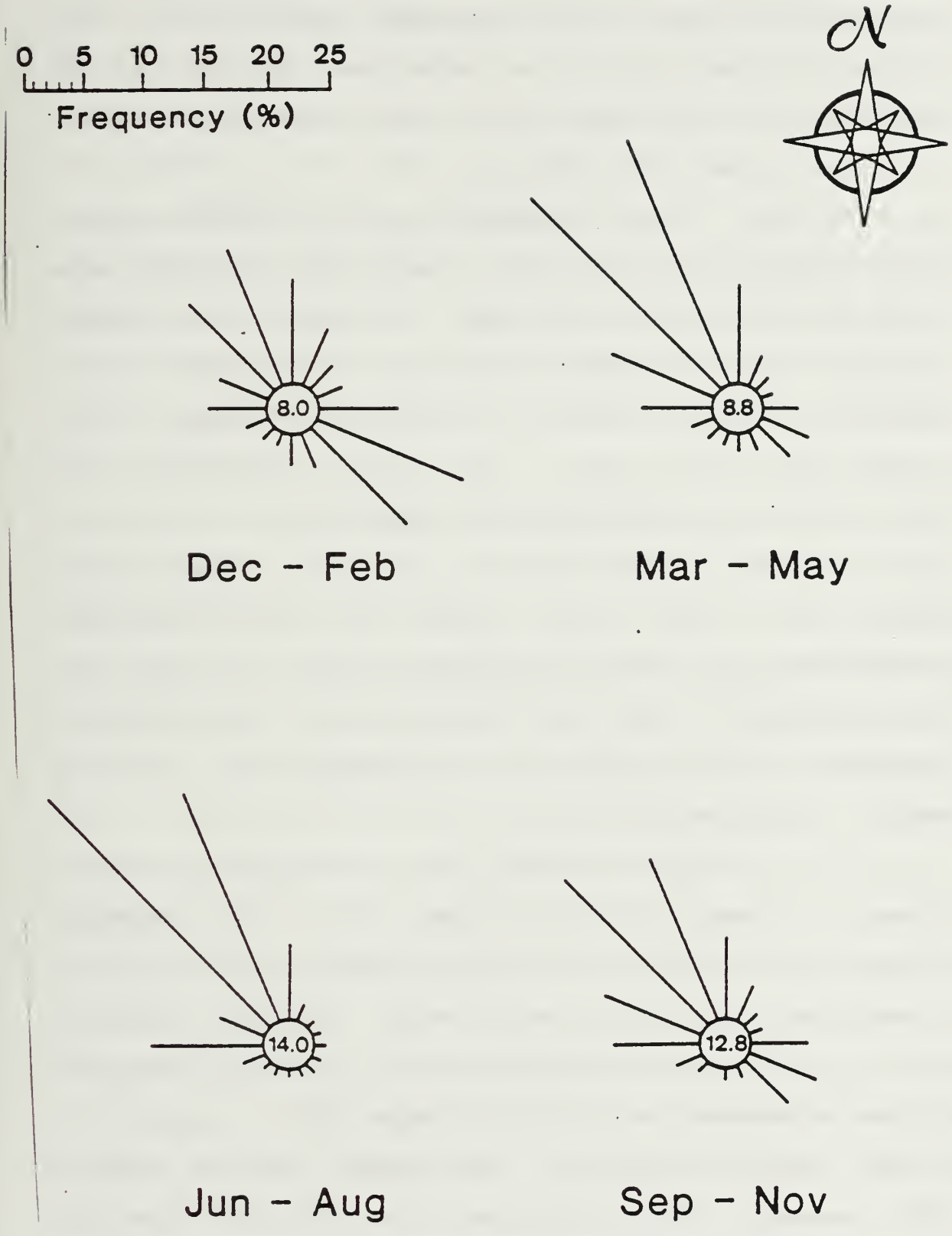

Fig. 2-3 Climatological Wind Roses for Vandenberg AFB

conditions is based on the overwater meteorological data obtained on the R/V Acania which was operated by the Department of Oceanography of the Naval Postgraduate School.

a. Synoptic Descriptions

(1) BLM-3 (December 1981). Synoptic-scale features and associated west coast flow patterns were typical for this time of the year. An upper-air north-south ridgeline over the western states was the dominant feature and led to generally weak surface pressure gradients off the southern California coast. The Mexican thermal low and afternoon sea breeze determined the flow associated with the ridge's presence. Also typical for the time of year was the passage of a fast moving upper wave, and associated precipitation and moderate northwest winds. Another wave was approaching at the end of the period. More detailed descriptions of the synoptic-scale features and resulting coastal flow pattern follows.

On 7 December a 500 mb ridgeline extended North-South from eastern British Columbia to southern California. It had a slow eastward progression in advance of an approaching upper-level trough extending southward from a closed low centered over the Gulf of Alaska. Coastal winds on 8 December were easterly during most of the day due to the unusual location of the Mexican thermal trough. Light westerly winds occurred from 1000 to 1600 in conjunction with the local sea-breeze.

The approaching upper-level trough crossed the west coast on 10 December and a surface front passed the experimental area late on the same day. An extensive precipitation area existed along the west coast from Southern California to Washington state. Coastal winds progressed from southerly on 9 December to northerly on 10 December with the frontal passage. The northerly gradient flow behind the front combined with the afternoon sea breeze led to a maximum onshore wind of 15 kts during the afternoon of 11 December.

A weak North-South ridgeline was re-established over the West Coast on 11 December and existed through 14 December. A fast moving upper level short wave (trough) moved through the weak ridge and crossed the West Coast in the vicinity of northern Washington on 15 December. The associated surface front reached northern California but did not affect the experimental area. During the 12 to 16 December period the coastal wind directions and speeds exhibited flow associated with a Mexican thermal trough and the afternoon sea breeze. The winds were east to northeast except for the afternoon (1100-2400) when onshore flow (northwest) occurred with speeds of 10-15 kt.

The upper-level ridge intensified on 16 December and the associated large surface high region extended from eastern British Columbia to Nevada. The increased gradient on the western side of the surface high

led to general easterly winds on 17 December with no discernable influence from the sea-breeze effects.

(2) BLM-4 (June 1982). The synoptic-scale conditions and resulting precipitation and coastal wind regimes were atypical for the early summer season. The Mexican thermal trough should dominate this region, with resulting light coastal winds influenced by the sea-breeze during this period. Two upper-level troughs passed over the west coast during the period. The first (22 June) was a fast moving short wave and the second (28-30 June) was a deep system associated with a closed low at 500 mb, which became nearly stationary over central California. Both systems had considerable north-south extent which led to the southern California surface pressure patterns reflecting their passage. This resulted in a greater than normal offshore pressure gradient and a fairly steady onshore wind, lacking the usual strong land-sea breeze cycle. Hence, strong onshore winds occurred.

During the 21-23 June period, an upper-level trough was moving from off the west coast into the mountain states. A surface trough extended from western British Columbia into northern California which was an intensification of the northern extension of the Mexican thermal trough.

During the 24-26 June period, a more intense upper-level trough was developing off the west

coast. A surface trough line extended from upper Mexico to Washington and the offshore pressure gradient was moderate. By 25 June, a closed 500 mb low had formed west of the Oregon-Washington coastline. The trough and low intensified as they progressed slowly eastward. Precipitation was observed along the northern California coast on both 25 and 26 June and a cold front existed over northern California on 26 June.

During the 27 June--1 July period, the upper-level trough and closed low moved across the west coast. The closed low moved south-eastward and was centered over central California on 30 June. Widespread precipitation occurred over the central and northern California coastal regions on 27 and 28 June and extended southward into the experimental area during the 29-30 June period. A closed surface low and associated frontal systems formed over northern Utah on 28 June. Because of the offshore pressure gradient, winds remained southwest to northwest during this period. They were maximum on 27 June (15-20 kt) and decreased gradually, to a 5-10 kt range, on the remaining days as the above systems moved across the coast and inland.

C. EQUIPMENT

1. R/V Acania

The R/V Acania served as the platform for the offshore release of the SF6 tracer gas, and provided

continuous measurement of several critical meteorological parameters. These measurements were performed to document atmospheric transport and stability conditions of the overwater boundary layer during each test day. The following subsections describe the equipment that was used for the experiments.

2. Sensors

A complete set of meteorological equipment is used on the ship when it is outfitted for atmospheric research. The purpose is to obtain as complete a characterization of the atmospheric boundary layer (ABL) as is possible. Basically, there is need for a determination of the dynamic and mean parameters from the surface to the top of the ABL, often defined by a temperature inversion. For the purposes of the work described here, the dynamics of the layer are especially important because they are the driving mechanism behind dispersion from low altitude releases, and mean properties are needed in order to parameterize models in terms of readily measured quantities.

A side view of the R/V Acania with the locations of the meteorological sensors is shown in Fig. 2-4. The ship has two masts, located on the bow, dedicated to the sensors. The foreward mast is on the tip of the bow and the sensors located there were at a height of 7 m above the mean water level; the second mast is 5 m behind the bow with sensors at 20.5 m above the mean water level. This mast telescopes

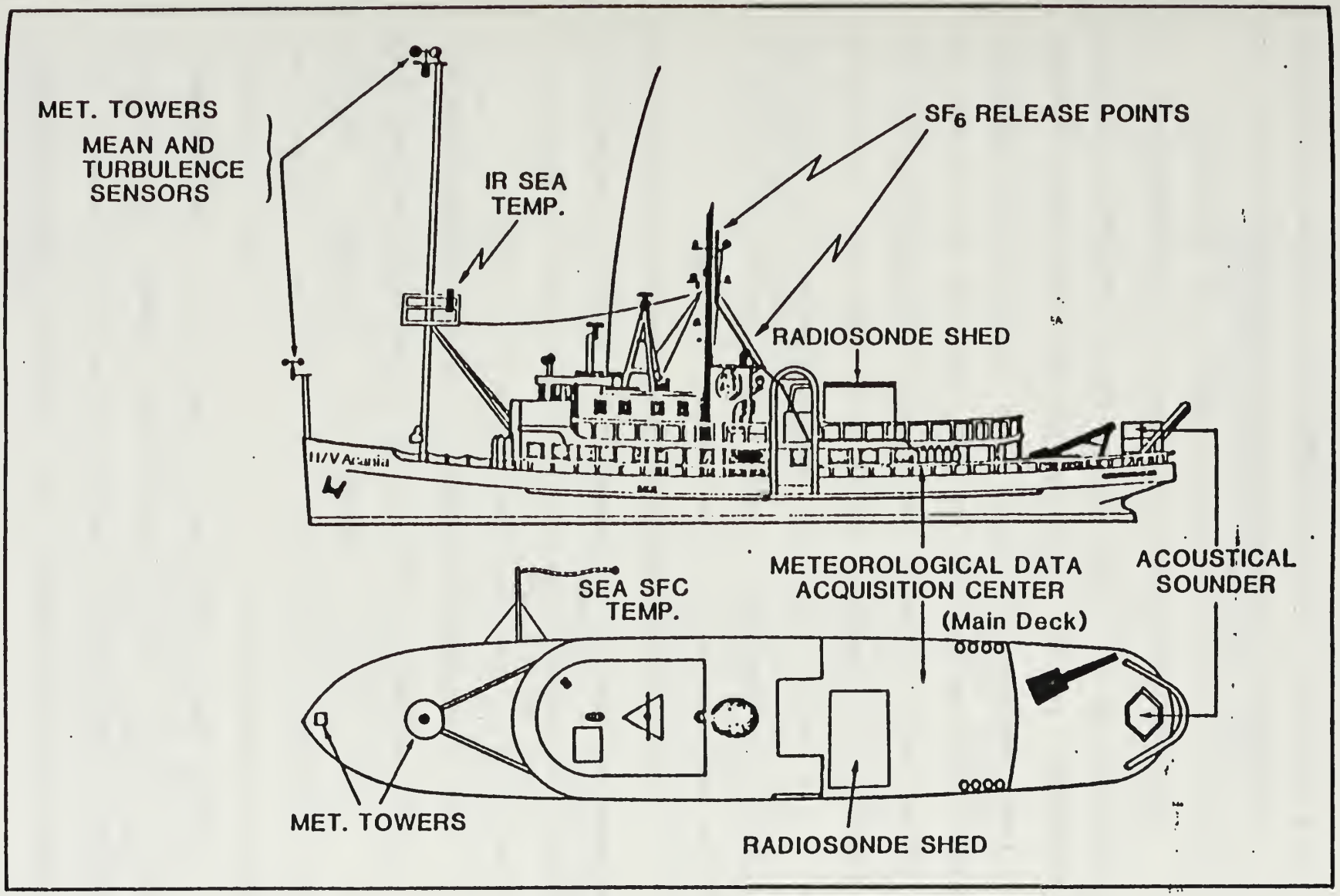

Fig. 2-4 R/V Acania, with Equipment Locations

down to a personnel platform so that the sensors can be made easily accessible. The platform also holds sensors that do not need to be elevated (aerosol counter and IR sensors).

The ship is approximately 40 m long, 7 m wide, and only 7 m high (9 m at the ship's stack). The low profile and narrowness of the ship cause minimal disturbance to the air flow, making it ideal for overwater atmospheric research. The sensors on the high mast are well above any significant ship influence but there is some distortion of the flow at the elevation of the foreward mast. For this reason only data from the upper station are used in subsequent data analysis. Lower mast sensors are used as a backup in the event of an upper sensor failure.

A summary of the monitoring equipment and associated meteorological parameters measured is given in Table 2-2. Details of the various pieces of equipment can be found in a previous report (Naval Postgraduate School, 1980).

3. Data Acquisition Methods and Recording Procedures

Four methods of data acquisition and recording were used: strip charts, analog tape recorders, computer controlled data acquisition and recording systems, and spectral analysis.

Strip chart recording was used only for the acoustic sounder, relative wind direction and speed, and the wind fluctuation signals from the hot films (TSI system). The internal strip chart was the only output available from the

TABLE 2-2

METEOROLOGICAL MEASUREMENTS MADE ABOARD
THE RV/ACANIA AND THE EQUIPMENT USED

Measurement	Equipment
Relative Wind Speed	MRI 1022 Wind System
Relative Wind Direction	"
Air Temperature (T)	100 Ohm Rosemount platinum resistor in a Gill aspirator
Dew-Point Temperature (T_D)	General Eastern 1200 AP cooled mirror dew pointer, modified for 4 wire resistance
Sea-Surface Temperature (T_S)	100 Ohm Rosemount platinum resistor and thermal ballast in a floating tube and Barnes PRT-5 infrared radiometer (a)
Wind-Speed Fluctuation (U')	TSI Constant Temperature Resistance Bridge and 60u platinum coated quartz resistance probes
Three Axis Wind Velocity and Fluctuation (b)	Kaijo-Denki Ultrasonic Anemometer
Ship Roll and Roll Rate Ship Pitch and Pitch Rate (b)	Pendulums on the ship's pitch and roll axes
Inversion Height (Z_i)	Aerovironment 300 acoustic sounder
Temperature Profile	Radiosonde
Ship Location	Loran C and Motorola Mini-Ranger III (b)
Aerosol Content (a)	Particle Measurement Systems Optical Counters
Cloud Cover and Weather Conditions	Weather observations

TABLE 2-2 (CONTINUED)

Measurement	Equipment
Microturbulence	Hot films at 60 feet
Wave height	Observation estimates

a) Not used on BLM-4
b) Used only on BLM-4

acoustic sounder. The other strip chart data were seldom used for analysis. These recordings were made because they provide an immediate check on shipboard conditions.

The analog tape recorder was essentially a back-up instrument. Every possible signal was recorded in this manner. If failure of the primary data acquisition equipment occurred, it was possible to retrieve data by using this recording. The temperatures were measured by resistors, which cannot be readily analog recorded.

The central data acquisition components were the computer controlled data acquisition systems. Two were used: one dedicated to the ultrasonic anemometer and the ship motion sensors, the second devoted to obtaining meteorological data. A computer operated a scanner, voltmeter, and printer, and files data and calculated parameters on its internal cassette tape.

The basic procedure for acquiring data for a given time period and averaging using a computer and scanner was straightforward and will not be described here. Only

average data and calculated parameters were stored to prevent using a large amount of computer memory and/or tape storage. All of the data and parameters were also printed at the end of an averaging period, providing a hard copy output and real time assessment of systems behavior.

The actual averaging used was somewhat complex since both short term averages for turbulence parameters and long term averages for mean parameters needed to be obtained. Averaging periods used were 10 second and one-half hour intervals. A data acquisition cycle takes approximately 1 second so that 10 readings were obtained for each short term average. All 10 second averages were held in computer memory until the end of the one-half hour period, when they and the mean data were averaged for the period. Then both short and long-term averages were stored on tape and all long-term averages printed.

True wind direction, corrected for ship's roll, and the true wind speed were obtained as short term averages from the meteorological data acquisition system. The ultrasonic anemometer outputs were processed to obtain short term averages of the three wind vectors, corrected for ship's pitch and roll.

Spectral analysis had two functions: to determine the power spectral density of turbulence signals and to detect and identify system noise which would invalidate

results obtained by other acquisition methods. Normally, it was used on a regular basis only for the hot-film signals.

III. DATA PROCESSING

A. QUANTITIES OF INTEREST

Data reduction is directed toward producing mean meteorological parameters and parameters which describe the turbulence in the marine layer. The mean quantities are easy to calculate from sensor response functions and the techniques need not be described here. Parameterizing the turbulence requires sophisticated techniques and is subject to error caused by measurement uncertainties and by misinterpretation of the measurements. In this section the several methods used to make these determinations are briefly described. The redundancy in methods provides cross checks on the results.

Measurements made during the data collection expeditions of BLM 3 and 4 were made from a single platform, so only the local turbulence was determined. Local turbulence is driven by a number of forces, which must be considered in developing any parameterization. Some obvious forces are: surface wind shear, convection, mesoscale activity, and swell and wind waves. It is important to establish which are the dominant factors to consider when developing the needed parameterization.

Specific quantities of interest can be categorized as either meteorological parameters or turbulence descriptors as listed below:

Meteorological Parameters :

True wind speed, U,

Friction velocity, U_*,

True wind direction, θ,

Inversion height, Z_i,

Monin-Obukov Length, $L = (T/kg)(U_*^3/H)$,

Surface Virtual Heat flux, $H = \rho C_p U_* \theta_{v*}$,

Convective mixing velocity, $w_* = [(g/T)H/Z]^{1/3}$,

Turbulence Descriptors :

Standard deviation of longitudinal wind velocity, σ_u,

Standard deviation of transverse wind velocity, σ_v,

Standard deviation of wind direction, σ_θ,

In these equations, T = absolute temperature, g = acceleration due to gravity, k = von Karman's constant, ρ = air density, C_p = specific heat at constant pressure, Z_i = the boundary layer depth, and θ_{v*} = the virtual potential temperature scaling parameter. All of these quantities describe various aspects of conditions or turbulence in the atmosphere and are important for describing expected plume/puff properties. Turbulence generated by shear and buoyancy can be accounted for by the local meteorological parameters. Turbulence is also generated by mesoscale processes, which are difficult to account for with only

local parameters. The parameterization methodology is described in Chapter IV.

The meteorological parameters were determined by local measurements of wind speed, air-sea temperature differences, dew-point temperature, and inversion height. The Monin-Obukhov length characterized the state of the surface layer based on the hydrostatic stability. The surface layer momentum, heat, and water vapor fluxes are needed as a measure of forcing in the boundary layer. The scaling parameters can be used to calculate the surface layer fluxes of momentum, heat and water vapor. In a well mixed boundary layer, w_* is the appropriate velocity to use to determine the rate of mixing throughout the convective boundary layer. The stability, friction velocity, dissipation rate, and mixing velocity were all determined using the bulk-aerodynamic method. The method is valuable because it makes use of readily measured quantities. Specifically, it is based on differences in mean temperature, wind, and water vapor at the surface and at some reference height. For a more complete description of this method, see Schacher, et al. (1986).

The next section describes the quality control and error checking procedures performed prior to further data manipulation. This is followed by a description of the process used to derive standard deviations of horizontal

wind velocity components in the downwind (u) and crosswind (v) directions.

B. WIND DATA CALCULATIONS

The objective here was to process the BLM data base in order to determine standard deviations of horizontal wind velocity components in both the longitudinal and transverse relative wind directions ($\sigma_{u,v}$). This information was then plotted and used as a data base to which a theoretical parameterization was empirically fit. In Schacher et al. (1986) a parameterization for overwater wind direction variability was developed by using the standard deviations of wind direction (σ_θ). The vector method used here to derive standard deviations differs from the method used by Schacher et al. (1986) since it conceptually treats contaminant motion differently. The two methods are compared later in this report.

During each step of the data processing phase, provisions were made to double check the resulting values since significant errors are easily made processing turbulence data. Only the BLM 3 and BLM 4 cruises collected σ_u data, therefore, only the data from those two cruises were used here. The deletion of BLM 1 and BLM 2 cruise data reduced the number of data sets from 859 to 705. The remaining data sets were quality checked for validity. In each data set there were between 39 and 150 wind component data elements. There was a possibility that some data were

lost when transferred to the currently used format. This was confirmed by printing out the number of data elements in each set and comparing them to the archived records of what each data set should contain. Data sets with too few wind components were not used. In the final quality control of the BLM 3 data set, 30 out of 401 sets were discarded. This accounted for 7.5% of the sets. In the BLM 4 data, 16 out of 304 sets, 5.3%, were discarded. Once a "clean" data base of 659 data sets was established, test processing of one data set was done. This same test data set was processed by hand to verify the methodology. After this successfully verified the technique, all data sets were processed.

Puff motion may be described by transport and diffusion characteristics. Transport can refer to either the mean trajectory of the puff over a time period, or the meander of the puff center of mass about the mean trajectory within the wind field. Relative diffusion refers to the puff growth about the puff center of mass. These puff mechanisms are influenced by differing scales of turbulence, where turbulence refers to any variation of wind flow from the mean. Large turbulence scales, much larger than the puff size, move the whole puff as an intact entity in the wind field, resulting in meander. Small turbulence scales cause relative motions of parcels of air that are internal to the puff. This relative diffusion causes the puff to grow about its center of mass.

Most data sets contained enough data elements to determine an average particle trajectory over a 30-minute period. Of course, using only the 30-minute average does not fully describe what would actually happen to a small puff release. As described above, meander and diffusion affect a puff as it flows downwind. When a puff is initially released, the size of the puff is small. As the puff moves downstream within the wind field, the puff changes due to forces internal to the puff, or due to external wind shifts. If a puff of length 'l' moves distance 'd' downwind in time 't', then puff growth during small length scales take place, where l = d. Large length scales refer to puff growth that occurs where l << d. These changes can occur within different time scales. Small internal changes may occur at short time intervals within an area relative to only the puff's instantaneous location in space. Large external influences may occur over longer time intervals, such as a wind shift, which causes the whole puff to change its actual location relative to the ground.

In order to study puff growth due to wind variability, the BLM data was processed into specific time averages, then analyzed. Specifically, the wind speed and direction information were vectorized and processed to provide data element sets containing $\overline{U}$, $\overline{\theta}$, $\overline{\sigma}_u$, $\overline{\sigma}_v$ for 1-, 3-, 10- and 30- minute time averaged intervals over each 30-minute period covered by a data set. The vectors were computed using

$$y_i = U_i * \cos(\theta_i),$$

$$x_i = U_i * \sin(\theta_i),$$

and then summed into time bins. (Recall that the original data contained wind speed and direction.) The wind vector components were y_i for the north, and x_i for the east components, respectively. Note that the angular origin is along the cartesian +Y axis to correspond with true north (000^{o}).

The shipboard wind sensors computed time averaged data elements at about 14-second intervals. For the purpose of this research, each one-minute time interval contained four data elements yielding 56-second "minutes." Each data element was summed into the appropriate time averaged bin such that there were 4 elements/1 minute; 12 elements/3 minutes; 40 elements/10 minutes; 120 elements/30 minutes. For each time bin which contained the appropriate number of data elements, the average $\overline{x}$, $\overline{y}$ vectors were computed. The average $\overline{x}$, $\overline{y}$ vectors were converted back into an average $\overline{U}$, $\overline{\theta}$ for the time bin. Standard deviations from each bin were calculated using the formulas:

$$\sigma_u = \left[\frac{\Sigma(ui - \overline{U})^2}{N-1}\right]^{1/2},$$

and

$$\sigma_v = \left[\frac{\Sigma (vi)^2}{N-1} \right]^{1/2} ,$$

where

$$u_i = U_i * \cos(\theta_i - \overline{\theta}(t)) ,$$

and

$$v_i = U_i * \sin(\theta_i - \overline{\theta}(t)) ,$$

where $\theta(t)$ was the average wind direction for each of the four appropriate time bins.

Counters were used to subtotal the number of times each bin was accessed so that after the data were processed, the mean wind speed ($\overline{U}$), direction ($\overline{\sigma}$), and standard deviations ($\overline{\sigma}_{u,v}(t)$) were computed for each of the time periods. The values for the four time averages were then taken and made into grand averages of 30 minutes. For example, 30 one-minute wind speed average values were determined from one 30-minute data set, and all 30 were averaged to get the overall 1-minute average for the entire 30-minute data period. Due to arithmetic properties (e.g., commutative, associative, additive), the 30-minute grand average wind speeds and directions for all four time averages were very similar.

The $\overline{\sigma}_{u,v}(t)$, $U, \overline{\theta}$ values were read into an output file for comparison with the $\overline{U}$, $\overline{\theta}$, $\overline{\theta}_u$, and standard deviation of the wind direction ($\overline{\sigma}_\theta$) values generated by Schacher et al. (1986) and for further processing.

A major strength of the vector method was that it provided a better physical description of wind flow in the boundary layer. This method described an average particle trajectory path based on averaging a series of vectors. The vectors accounted for both direction and magnitude of a particle's velocity, and therefore more accurately described the physical processes occurring as the particle moved. There was a high confidence level in the accuracy of information generated by the vectorization method. The scalar method used previously was strictly a scalar averaging of U,θ without regard to the occasional large variations in the vector magnitude and direction within a data set. By only taking either angular averages, or only speed averages, the scalar method ignores the effects of interaction between sequential vectors having large differences in either/both direction or magnitude. The result was that an average particle trajectory path was less accurately described than by the vector method, making the previous results less usable for our purposes. Fig. 3-1 illustrates an example of each method's averaging of the same two vectors. As can be seen, the vector method produces a more accurate average than the scalar method.

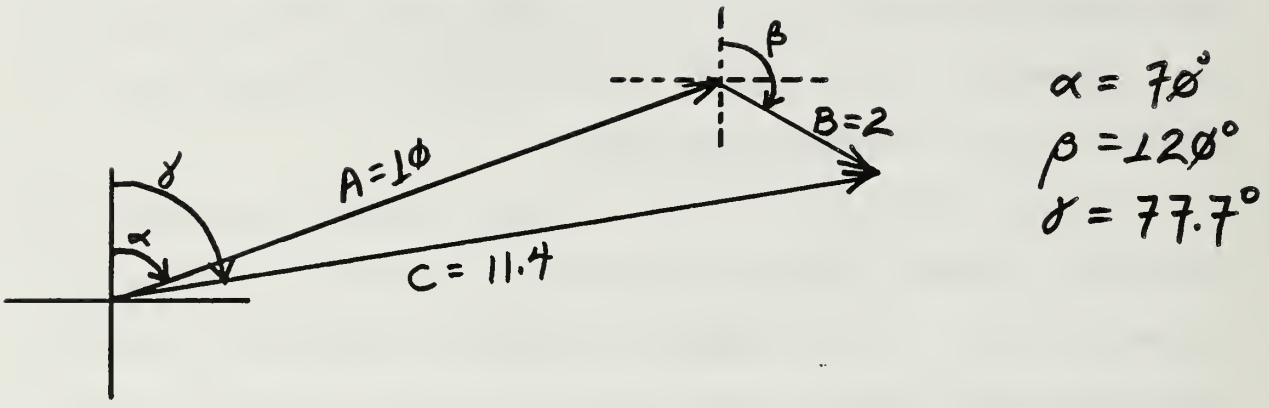

Vector method utilizes vector addition, representing true transport.

Scalar method utilizes straight, unweighted averages

$c' = 6$

$\gamma' = 95^{o}$

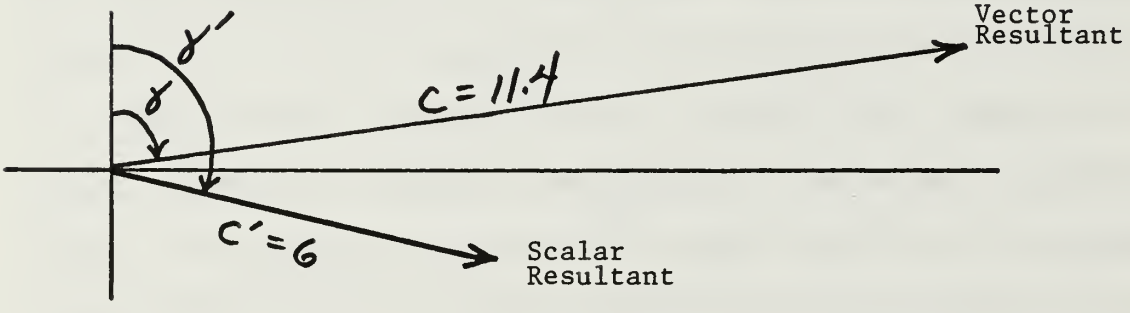

Fig. 3-1 Comparison of Vector versus Scalar Method Used to Average BLM Data. Part a Shows the Results of Vector Averaging, Part b Compares the Two Methods.

The scalar method will produce the correct U if the angles are the same and the correct\theta if the speeds are the same, but makes incorrect assumptions in the relationship between the two vectors when this is not the case. Example 3-1 lists U, θ for a data set showing the differences between scalar & vector averaging for a 30 min time average.

Example 3-1

C= 3 Nu= 121 Total= 121

INPUT I	J	B(I,J)						
1	1	1827	2	1	2032	3	1	1227	4	1	27
1	2	202	2	2	384	3	2	714	4	2	1069
1	3	435	2	3	438	3	3	439	4	3	435
1	4	15	2	4	28	3	4	29	4	4	75
OUTPUT IJ		B(I,J)									
1	1	20	2	1	20	3	1	20	4	1	20
1	2	16	2	2	23	3	2	52	4	2	79
1	3	427	2	3	427	3	3	424	4	3	420
1	4	17	2	4	24	3	4	35	4	4	73

Once processed, all clean data sets (659) were compared to the corresponding Schacher (1986) data sets for comparison of each's results. In virtually every case, the average wind speeds were within $\pm$0.2 m/sec of the earlier values. For any given data set processed by the vector method, the average wind direction value for each of the four time averages was within several degrees of each other. This was not the case for data sets processed with the scalar method. Differences up to 180^{o} occurred between the four time averaged values in some data sets. In comparing

the results from both methods, the wind directions were rarely identical, but differences between the 30-minute averages were $<\pm 20^{o}$ in 98.5% of the cases. Differences between the 1-minute time averages were $<\pm 20^{o}$ in 90.9% of the cases. Example 3-1 shows a typical case where there was a large disparity between the two methods in the 1-minute averages, but showed near agreement for the 30-minute average.

A possible reason for the large fluctuations in average wind direction by the scalar method was not making proper corrections during computations where the wind directions in a data set were scattered around north (000^{o}). An overly simple example is $\overline{\theta} = \Sigma(355^{o} + 005^{o})/2 = 180^{o}$, which is 180^{o} away from the correct average of 000^{o}. In 76.6% of the data sets where the scalar method average wind direction value was greater than 20^{o} different from the vector method's average wind direction value, the wind data were in the quadrant centered around north (000^{o}). This provides a strong indication that incorrect adjustments were made for wind direction values centered around north. Example 3-2 lists the wind directions in a sample data set and provides the scalar wind direction averages for each of the four time averages used. As can be seen in the example, the 1- and 3-minute time averaged values are very close to those derived by Schacher et al. (1986). The vector method

automatically took this possibility into account to ensure these errors did not occur.

Example 3-2

```
C= 3      Nu=121
 1  31     2  27     3  25     4  27     5  26     6  21     7  20     8  22
 9  21    10  16    11  18    12  19    13  18    14  15    15  17    16  17
17  19    18  17    19  18    20  20    21  14    22  13    23  17    24  14
25  13    26  11    27   6    28   4    29   2    30   3    31 359    32 356
33 357    34 356    35 356    36 357    37 356    38   2    39   7    40 360
41 358    42 353    43 359    44 357    45 356    46 352    47 350    48 348
49 348    50 349    51 351    52 350    53 352    54   1    55 353    56 358
57 358    58 357    59 359    60 353    61 358    62 356    63 354    64 354
65 358    66 354    67 355    68 353    69 353    70 355    71 355    72 354
73 352    74 352    75 354    76 354    77 356    78 354    79 354    80 353
81 355    82 351    83 350    84 351    85 350    86 350    87 352    88 347
89 353    90 352    91 351    92 348    93 350    94 348    95 351    96 353
97 355    98 359    99   0   100   3   101   2   102   4   103   4   104   2
105  2   106   4   107   5   108   2   109   4   110   4   111   7   112   7
113  5   114   8   115   7   116   6   117   8   118   8   119   7   120   9
121 10   122  12   123  14   124  11   125  13   126  11   127  13   128  11
129 16   130  13   131  14  1 =  185.28125      3 =  196.841666667  10 =
196.841666667      30 =  196.841666667
```

Other data comparisons included converting σ_v based on the vector method into σ_θ values, using some of the many data sets which contained U, θ, σ_u values that were in close agreement from both methods. This was done using $\sigma_v = \arctan(U * \sigma_\theta)$, where σ_θ is in radians. Numerous random values of σ_v were converted into σ_θ and compared to the Schacher et, al. (1986) values. In all cases tested, the two σ_θ values were in close enough agreement to indicate that the two methodologies produce essentially the same results.

Lastly, a comparison of σ_u values was made. In all cases examined, the scalar method's σ_u values and vectorial

method's $\sigma_{u,v}$ values were consistently a factor of two times within each other. As expected, the σ's increased as the time average increased (i.e.: $\sigma_1 < \sigma_3 < \sigma_{10} < \sigma_{30}$). The rate of increase for the σ's was about the same by both methods. Based on hand calculations, and comparisons to the Schacher et al. (1986) data base, it is concluded that the vectorized data are valid and useful. The next chapter applies turbulence theory to the development of a horizontal wind variability parameterization.

IV. TURBULENCE THEORY

A majority of the theory used here to develop a parameterization is taken from Schacher et al. (1986) and modified to meet the specific needs of this work. The following treatment follows from the results developed by Hojstrup (1982), where expressions were developed for the turbulence intensity as functions of u_* and w_*. Shear and buoyancy production were considered as the two sources of turbulence and were expressed as functions of the convective mixing velocity (w_*) and friction velocity (u_*). Their contributions to the velocity spectra were modeled and the spectra integrated over the appropriate frequency range to determine the velocity variances. The following is a brief description of how the Hojstrup treatment is used to develop algorithms for parameterizing overwater horizontal wind variability from our data.

Scaling parameters were developed as a preliminary step in developing the equations. For some quantity X, the relation between the value at height z (X_z) and surface values of X_s and its scaling parameters is

$$X_z - X_s = (X_*/\alpha_X k) \, [\ln (Z/Z_{oX} - \psi_X(L)] \, , \qquad (5)$$

where the von Karman's constant, k, is 0.35. Rather than use the more conventional k = 0.4, k = 0.35 is used to be consistent with the calculations of U_* and w_* from the data. Z_o is the roughness length and ψ the stability correction function to the logarithmic profile, which is normally written as a function of the Monin-Obukov length (L), as indicated. The turbulence diffusivity ratio is α.

The horizontal, transverse velocity spectrum has two components

$$fS(f) = A(\beta_1)w_*^2 + B(\beta_2)U_*^2, \qquad (6)$$

where f is the frequency, S(f) the spectral intensity, and $A(\beta_1)$ and $B(\beta_2)$ are functions of the variables

$$\beta_1 = f(Z_i/U), \qquad \beta_2 = f(Z/U), \qquad (7)$$

where Z_i is the height of the lowest inversion, and Z is the measurement height. The functions, A and B, were determined by Hojstrup by matching model results to the Kansas (Kaimal 1978) and Minnesota (Kaimal et al. 1976) data, which gives spectral intensity for each component A, and B. A complete description in the methodology is contained in Hojstrup (1981).

Upon integration of the spectral intensity, the velocity variances were found by Hojstrup to be :

$$\sigma_u^2 = 0.6k^{2/3}w_*^2 + 4.8(1-Z/Z_i)^2U_*^2/(1+15Z/Z_i)^{-2/3} , \quad (8)$$

and

$$\sigma_v^2 = 0.7k^{2/3}w_*^2 + 2.7(1-Z/Z_i)^2U_*^2/(1+2.8Z/Z_i)^{-2/3} . \quad (8a)$$

The first terms are normally written as

$$0.6(-Z_i/L)^{2/3}U_*^2 , \quad (9)$$

and

$$0.7(-Z_i/L)^{2/3}U_*^2 . \quad (9a)$$

These equations are applicable only during unstable conditions, since that is when buoyancy driven convection occurs and w_* is defined. During stable conditions, $w_* = 0$, and the first terms in Eqs. (8) and (8a) are zero.

It is apparent that the first term in Equations 8 and 8a contains Z_i, through w_*, because the strength of convective mixing depends on the mixing depth. The second term contains Z_i, through the ratio Z/Z_i, which is present to correct for the decrease in surface shear produced turbulence with height above the surface. The correction factor is 1 at the surface, since the numerator in the second term of Eqs. (8) and (8a) approaches zero there.

Since measurements are all within the surface layer, this factor should not be appropriate, therefore, the height correction in the second term of Eqs. (8) and (8a) are dropped. However, for a very low inversion it may play a role in indicating suppression of turbulence at the measurement height (20 m). Also, it is recognized that the overland spectra from which Hojstrup's model were obtained may not adequately represent the overwater case dealt with here. Thus, the numerical factors are incorporated into the production mechanism parameters C_w and C_u, and the correction factor in the second term is set equal to 1.0. The resulting equations are

$$\sigma_{u,v} = C_w k^{2/3} w_*^2 + C_u U_*^2 \ , \qquad (11)$$

or

$$\sigma_{u,v} = [C_w(-z_i/L)^{2/3} + C_u]\ U_*^2 \ , \qquad (12)$$

where C_w and C_u are constants to be determined from the overwater data. Note that the correction factor in the second term was suppressed; if necessary it could be added later. For simplicity $C_w' = C_w k^{2/3}$ will be used.

The assumption is made that turbulence behaves in similar patterns over water and over land. Similar production mechanisms are expected to be valid for both

regimes, although the magnitudes may be different. If spectral intensities were plotted for both regimes they would be expected to have similar shapes. Both regimes need similar algorithms to describe the geophysical processes contributing to turbulence and as such, both depend on scaling parameters. Hojstrup (1982) has already shown this for the overland regime. It is a goal of this work to extend the methodology of the previous work to the overwater regime.

It may be convenient to write the scaling velocity as a function of the wind speed and drag coefficient,

$$U_* = C^{1/2}U \ . \tag{13}$$

Following Eq. (5), the drag coefficient can be written as

$$C^{1/2} = C_N[1 - C_N^{1/2}\psi/k]^{-1} \ , \tag{14}$$

with the neutral stability drag coefficient

$$C_N^{1/2} = k/\ln(Z/Z_o) \ . \tag{15}$$

For unstable conditions (Businger, 1973)

$$\psi = 2\ \ln[(1+x)/2] + \ln[(1+x^2)/2] - 2\ \tan^{-1}x + pi/2 \ , \tag{16}$$

with

$$x = (1 - 15z/L)^{1/4} ,$$

and for stable conditions

$$\psi = -4.7(Z/L) . \qquad (16a)$$

At this point, the parameterization reduces to using determined values of the stability (Z/L), inversion height (Z_i), wind speed (U), and roughness length (Z_o) or neutral drag coefficient (C_N) and finding the values of C_w and C_u.

The roughness length, or the drag coefficient, over water depends on the wind speed through wind-wave interaction. The Garratt (1977) formulation for the neutral stability drag coefficient,

$$10^3 C_N = 0.75 + 0.067U , \qquad (17)$$

was applied to the buoyancy production component of the regression equation, so that the buoyancy production is represented as

$$U_*^2 = (7.5 \times 10^{-4} + 6.7 \times 10^{-5}U)F(L)U^2 , \qquad (18)$$

with

$$F(L) = [1 - C_N^{1/2} \psi / k]^{-2} \quad . \qquad (19)$$

This is not a closed form solution since L depends on U. All coefficients are determined by an iterative calculation when the data are obtained.

Rather than do another iterative calculation for the results presented here, and in order to clarify the results, F(L) was calculated using the old value of L and Equation 19. Note that ψ for stable conditions was given by -4.7 Z/L. At wind speeds of 10 m/sec or higher, Z/L is near zero since the air-sea temperature difference never can be large enough for buoyancy to overcome shear production at such high wind speeds.

Eqs. (11) and (12) can now be rewritten as

$$\sigma_{u,v}^2 = C_w' w_*^2 + C_u F(L)(7.5 \times 10^{-4} + 6.7 \times 10^{-5} U) U^2, \qquad (20)$$

where

$$C_w' = k^{2/3} C_w = 0.497 \; C_w$$

and,

$$\sigma_{u,v}^2 = [C_w(-Z_i/L)^{2/3} + C_u] F(L)(7.5 \times 10^{-4} + 6.7 \times 10^{-5} U) U^2. \qquad (21)$$

The first form was used for w_* and U parameterizations and the second for stability parameterization and for the effects due to inversion height. Recall that the inversion height correction to C_u (see Eq. (8)) may be needed for low inversions. Another form of Eq. (21) is useful for examining the dependence on stability. It was found by writing the term in square brackets as

$$C_w[(Z_i/Z)(-Z/L)]^{2/3} + C_u \ . \qquad (21a)$$

In Eqs. (21) and (21a) both L and U are left as parameters. Stability did not appear as a sufficient variable.

It is reemphasized that none of the above addressed sources of turbulence other than shear and buoyancy production. The mesoscale process could not be parameterized solely with C_w and C_u, so another term needed to be added to Eq. (20). Mesoscale production is a function of differential heating between the land and sea which contributes to low wind speed turbulence. The contribution due to thermal convection decreases with increasing wind speed such that

$$\sigma_{u,v}(\text{mesoscale}) = C_{ms}/U^N \ . \qquad (22)$$

If N = 2, C_{ms} can be interpreted as the square of an

mixing velocity, w_*, and the friction velocity U_*. Understanding this new velocity is not easy, and here only the new constants were evaluated with no explanation of their meaning. The final algorithm used for the parameterization became

$$\sigma_{u,v}^2 = 0.497 C_w w_*^2 + C_u F(L)(7.5 \times 10^{-4} + 6.7 \times 10^{-5} U)U + C_{ms}/U^N \ , \qquad (23)$$

where the three fitting parameters were functions of the averaging time used to evaluate the variances. The first term represented contributions due to shear, the second term accounts for buoyancy, and the third for mesoscale production mechanisms. Stability was taken into account through F(L). Based on Schacher et al. (1986), it was determined that oversea conditions did not support stability conditions far from neutral for high winds, and that the stability correction was not needed, therefore

$$F(L) = 1.0 \ .$$

The parameterization described in Chapter VI was performed using this algorithm to obtain an empirical fit of the horizontal wind velocity component variances to the data.

V. DATA PROCESSING RESULTS

A. GENERAL

Parameterization of the wind variability required segmenting the data into wind regimes. The situations were different when the wind was dominated by synoptically driven northwest flow than when it was dominated by the sea-breeze cycle. As pointed out in Chapter III, buoyancy, shear and mesoscale production mechanisms are different for various meteorological conditions, which affects the degree to which wind variability exists under a given set of environmental conditions.

In Schacher et al. (1986) multiple data subsets were generated for well known environmental conditions such that a given forcing was dominant and a single parameter could be identified as the dominant factor in parameterizing the wind variability. One subset was the stationary wind regime where the one-hour averaged wind direction remained constant within about 40 degrees and the wind speed was fairly constant, for which mesoscale activity was minimal. In some cases clean data subsets were not available. When more than one parameter was the dominant factor, self-consistency among the dependences was examined to determine dependences on the individual parameters. The analyses focused on dependences on the wind speed, convective mixing velocity,

and stability, with inversion height and wind direction as important auxiliary parameters. The dominant parameters considered for parameterizations were established after examining the following variables:

averaging time,

onshore/offshore flow,

stability,

w_*,

z_i.

B. SCATTERPLOTS

The initial set of plots were scatterplots for $\sigma_{u,v}/U$ versus wind speed (U). The reason for dividing the standard deviations by wind speed was to non-dimensionalize the values and to compare with later theory. The scatterplots were produced for both BLM-3 and BLM-4 data, for each of the four time averaged periods of 1, 3, 10 and 30 minutes. A full set of scatterplots is contained in Appendix A. The large variability that was normally present in fluctuation data is evident. The standard deviation values increase as the averaging time increases. The 1- and 3-minute time averages have a $\sigma_{u,v}/U$ value less than 0.3, increasing to 0.6 for the 10-minute average, and to 1.2 for the 30-minute average. This is a four fold increase in the amount of wind speed variability just from using longer averaging times for the same data. As the time averaging period increased, more time elapsed within which to collect wind direction data.

This allowed dramatic shifts in wind direction to occur within a data set, which in turn, resulted in larger deviations from the mean wind. In a time period of 30 minutes, it was possible for the wind direction to shift up to 180^{o} for some conditions. Over a short time period of 1 minute the amount of wind shift was much less, hence, the smaller standard deviations.

For all four time averages the σ_v variability is less than the corresponding σ_u variability. Even though there is considerable scatter, trends are evident in the plots to demonstrate that there is consistency in the data collected during both cruises. In what follows, the term "variability" will be used to mean the wind speed standard deviation in either the longitudinal (downwind) or transverse (crosswind) directions. It was difficult to obtain quantitative information from scatter plots. They are mainly useful for verifying consistency and trends within the data. In the next section plots of the averaged data are discussed.

C. AVERAGED DATA PLOTS

The data used in the scatterplots were averaged over discrete wind speed ranges of 1 m/sec increments from 0 to 8 m/sec; 2 m/sec increments from 8 to 12 m/sec; and a 3 m/sec increment from 12 to 15 m/sec. The averaged data plots for unrestricted conditions are shown in Appendix B. These figures also contain a print out of the results averaged

over all data, giving the value of the variability for the center of that range; the number of points found in that range; the mean standard deviation of the horizontal wind speed over the averaging period indicated (sigma); and the standard deviations of the data about the mean sigmas. In a following section an algorithm is developed which is empirically fitted to these averaged plots for unrestricted conditions.

D. PRODUCTION MECHANISMS

In the interest of minimizing redundancy of information between here and Schacher et al. (1986), only a short overview is presented of the earlier conclusions regarding dominant meteorological parameters used to develop parameterizations for wind direction standard deviations. Those findings were used here as a stepping off point, forming the basis for the approach used to develop parameterizations of horizontal wind speed variability.

Criteria for stationary conditions were: the one-hour average wind direction remained within a 40 degree sector and the wind speed was fairly constant. Such conditions only occurred when the wind was fairly strong and from a westerly to northwesterly direction. Mesoscale forcing was largely absent during stationary conditions since the strong steady wind flow negated any mesoscale effects due to thermal convection. This factor allowed for the buoyancy contribution to be determined.

Stability was a function of the air-sea temperature difference. Due to the small temperature differentials, only a small range of stabilities was encountered over water. Since buoyancy production occurs only when there is upward heat flux, it was absent during stable conditions.

The shear production contribution was isolated during stationary, stable conditions and was found to be dominant at wind speeds above 7 m/sec. Below that speed, buoyancy production was apparent.

Based on Schacher et al. (1986) no apparent difference in the turbulence was seen for onshore and offshore conditions. Convection normally played a minor role in turbulence production as was evidenced by the turbulence being slightly greater during unstable conditions. This weak dependence on stability led to utilizing stationary conditions to examine turbulence dependence on w_*. Large values of variability at low wind speeds were associated with non-stationary conditions during transition periods in the land-sea-breeze cycle. The forcing for the cycle was differential heating between the land and the sea; a mesoscale process. Low wind speed turbulence produced other than by buoyancy are referred to as "mesoscale" production.

The BLM data were separately processed and averaged for stationary and for stable conditions so that the effects of the various production mechanisms on wind variability could be individually isolated. Appendix C contains averaged plots

of $\sigma_{u,v}/U$ versus U for stable conditions for all four time averaged periods. Stability calculations included the shear and buoyancy production mechanisms, which were a function of mixing depth (Z_i). Since buoyancy production was minimal during stable conditions, the plots in Appendix C for stable conditions give indications of shear production contribution. It can be seen from these plots that the variability decreases as wind speed increases in all cases, as it does during unrestricted conditions. Also, the values of $\sigma_{u,v}/U$ increase from 0.15 to 0.75 for $U < 1.0$ m/s, as the averaging time increases from 1 to 30 minutes; a five-fold increase. Appendix D contains averaged plots of $\sigma_{u,v}/U$ versus U for stationary conditions for all four time averaged periods. As previously mentioned, this situation allows for an estimation of buoyancy production since shear and mesoscale production are minimal. In all eight cases, the plots show that the contribution is relatively constant with respect to wind speed, and that the $\sigma_{u,v}/U$ values are approximately the same.

Schacher et al. (1986) determined that although stability was a good parameter for shear and buoyancy production, it did not account for mesoscale production. Based on the previous work, the optimum conditions for parameterizing mesoscale production was stable conditions, at low wind speeds (< 7 m/sec).

Chapter VI discusses how the theoretical algorithm is used to determine regression variables and generate fitting curves for the averaged data plots. Conclusions are provided with implications for future applications of the parameterization results.

VI. PARAMETERIZATION RESULTS AND CONCLUSIONS

A. PARAMETERIZATION RESULTS

To parameterize horizontal wind velocity variability, wind data were decomposed into longitudinal (downwind) and transverse (crosswind) velocity components over different time averages. Standard deviations of horizontal velocity components were then computed and plotted. Horizontal wind variances were then parameterized using the regression equation

$$\sigma_{u,v}^2 = 0.497 C_w w_*^2 + C_u(7.5 \times 10^{-4} + 6.7 \times 10^{-5} U) U^2 + C_{ms}/U^N , \qquad (23)$$

where the regression variables representing shear (C_w), buoyancy (C_u), and mesoscale (C_{ms}) production are different for the u, and v directions. The three regression parameters are functions of the averaging time used to evaluate the variance.

Presentations of the data in previous sections of this thesis and by Schacher et al. (1986) allowed some conclusions to be drawn about the mechanisms driving horizontal wind variability and the methodologies needed to determine the correct parameterization. Three production mechanisms were identified from the data: namely buoyancy,

shear and a larger scale forcing associated with mesoscale processes. The previous work showed that it was not possible to unambiguously separate the mechanisms. Certain associations between these production mechanisms and associated conditions were used to separate the processes for purposes of developing the parameterization.

Shear production dominated at high wind speeds (> 7 m/sec) and was insignificant at low wind speeds. The shear production contribution was determined from stationary and stable thermal conditions at high wind speeds. Mesoscale forcing was absent during stationary conditions and buoyancy production was absent during stable conditions so that shear production could be isolated and individually parameterized using the second term of Eq. (23). Based on the previous work, it was determined that oversea conditions were near neutral for high winds. Thus, it was assumed that the stability correction was not needed for the values of C_U, C_w, C_{ms} to correctly fit the data. The result was to use $F(L) = 1.0$ in Eq. (23).

Buoyancy production was apparent at low wind speeds (< 7 m/sec) and decreased inversely proportional to wind speed (1/U). Good results were expected when using stationary conditions at low wind speeds to determine buoyancy contributions. This was due to minimal mesoscale production for stationary and minimal shear production at low wind speeds. Figs. 6-1a,b show plots of σ_u/U vs. U for the

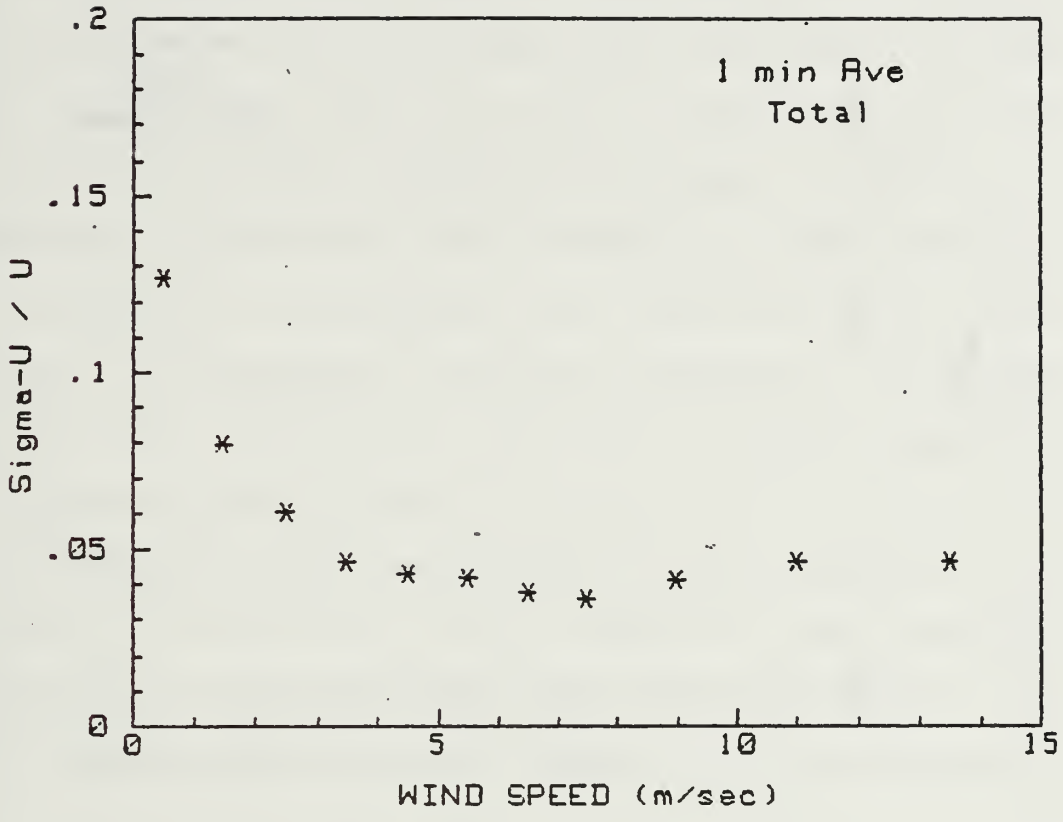

U	#	SIGMA	Std Dev
.5	10	.126	.006
1.5	77	.080	.001
2.5	102	.060	0.000
3.5	91	.046	0.000
4.5	89	.043	0.000
5.5	56	.041	0.000
6.5	60	.038	0.000
7.5	43	.036	0.000
9.0	30	.041	0.000
11.0	17	.046	.001
13.5	14	.046	.001

Fig. 6-1a Averaged BLM-3 and 4 Data for Unrestricted Conditions

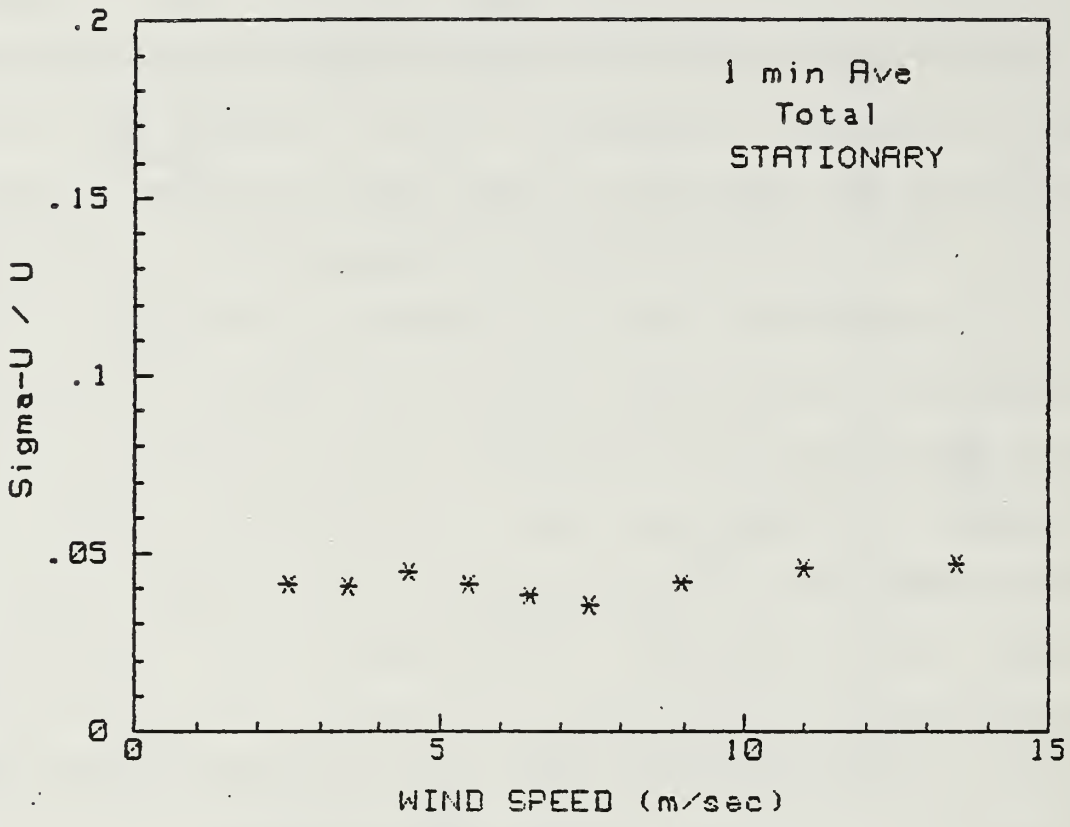

U	#	SIGMA	Std Dev
.5	0	0.000	0.000
1.5	0	0.000	0.000
2.5	2	.041	.002
3.5	7	.041	.001
4.5	17	.045	.001
5.5	20	.041	0.000
6.5	39	.038	0.000
7.5	30	.035	0.000
9.0	27	.041	0.000
11.0	15	.045	.001
13.5	13	.047	.001

Fig. 6-1b Averaged BLM Data During Only Stationary Conditions

1-minute average during unrestricted and stationary conditions, respectively. When comparing the two figures, it is seen that by isolating stationary conditions, buoyancy effects at low wind speeds and shear effects at high wind speeds may be isolated, and thus quantified.

Mesoscale production was deduced by subtracting the shear production contribution from non-stationary, stable conditions. The mesoscale processes dominated at low wind speeds (<5 m/s) under these conditions, since bouyancy and shear production were minimal.

The parameterization for horizontal wind variability was developed by fitting Eq. (23) to the data, then adjusting C_w, C_u, C_{ms} and N to find the best fit. This was done for all four averaging times of 1-, 3-, 10-, and 30-minutes for both σ_u and σ_v.

Appendix E contains the empirical fits of Eq. (23) to the $\sigma_{u,v}/U$ vs. U data for stable, stationary and unrestricted conditions. Sorting on w_* ranges of 0-0.2, 0.2-0.4 and > 0.4 m/sec was done for the latter two cases and the values of the fitting parameters used are shown on the graphs. Figs. 6-2a,b, and c provide examples of w_* sorting for σ_u/U vs. U during stable, stationary and unrestricted condition, respectively. The ranges of 0.0-0.2, 0.2-0.4 and >0.4 m/sec are represented as 0, 2 and 4, respectively. These particular conditions were chosen because a) $w_* = 0$ for stable conditions and C_{ms} can be determined, b)

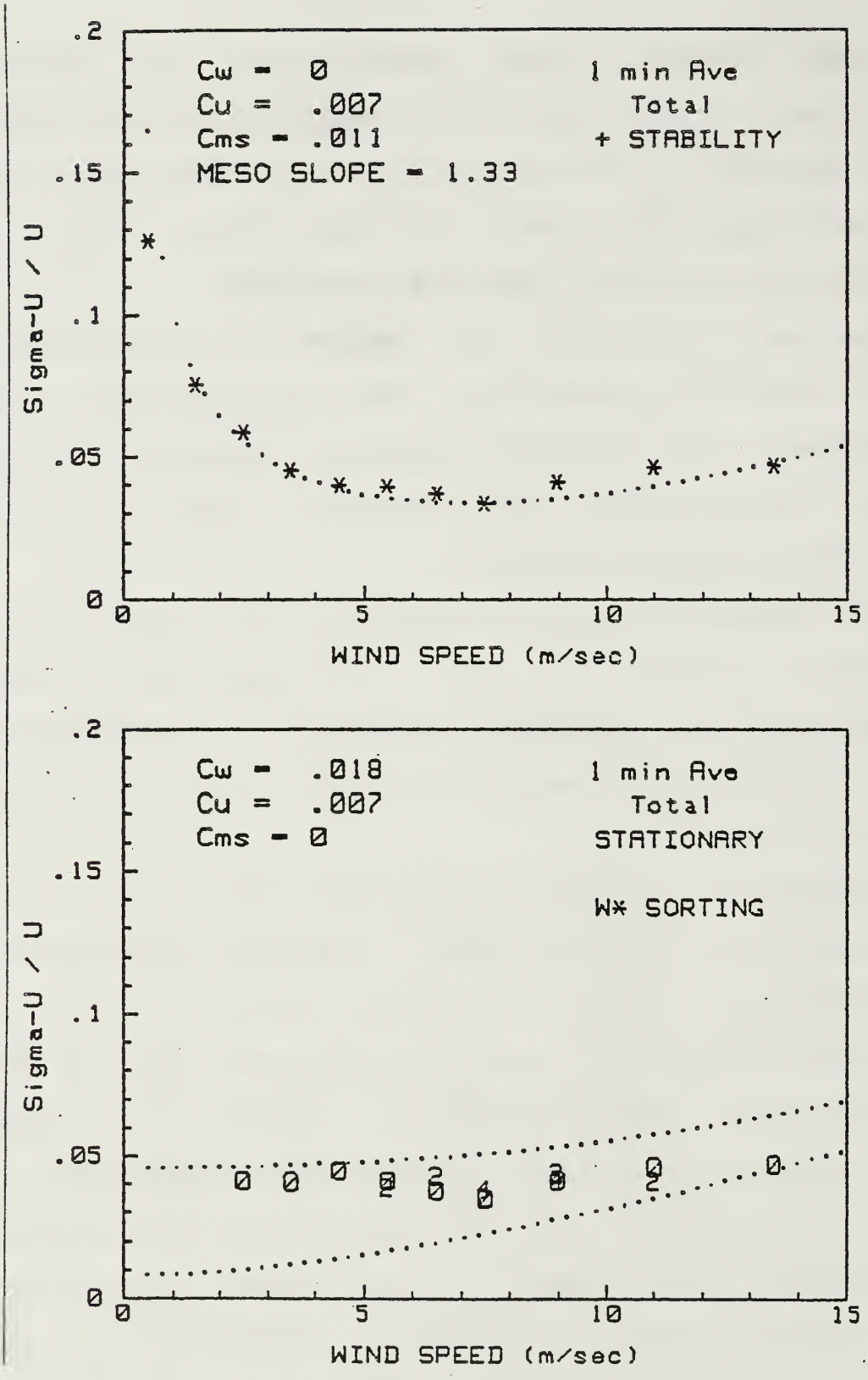

Fig. 6-2 Empirical Fitting Curves for Stable, Stationary, and Unrestricted Conditions for BLM Data

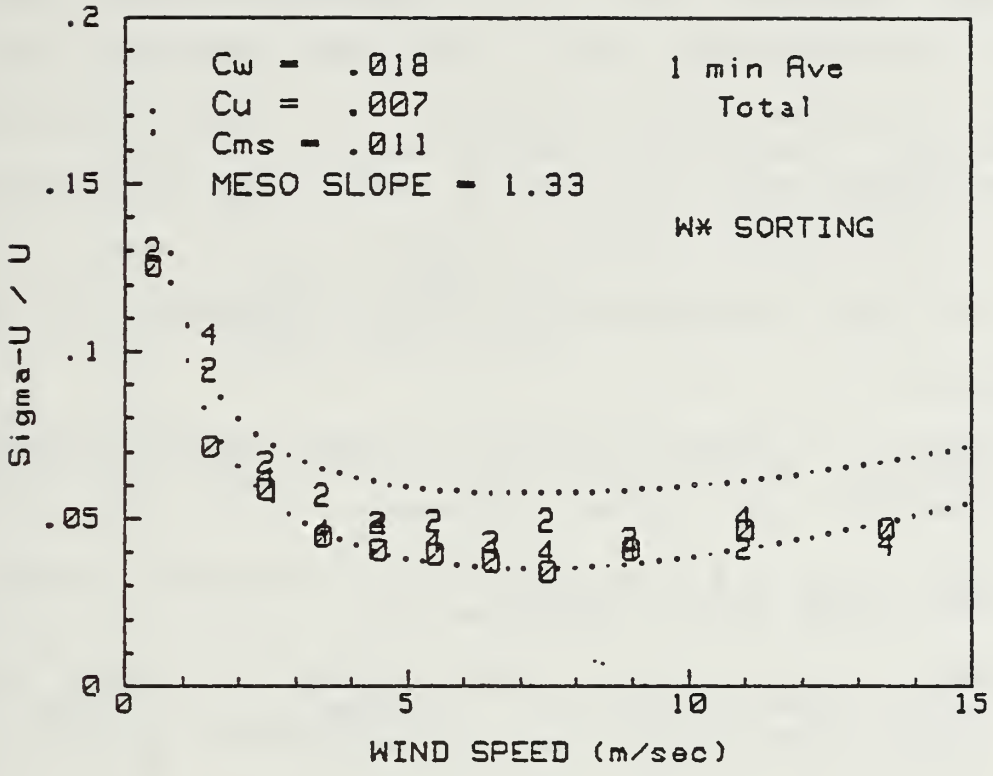

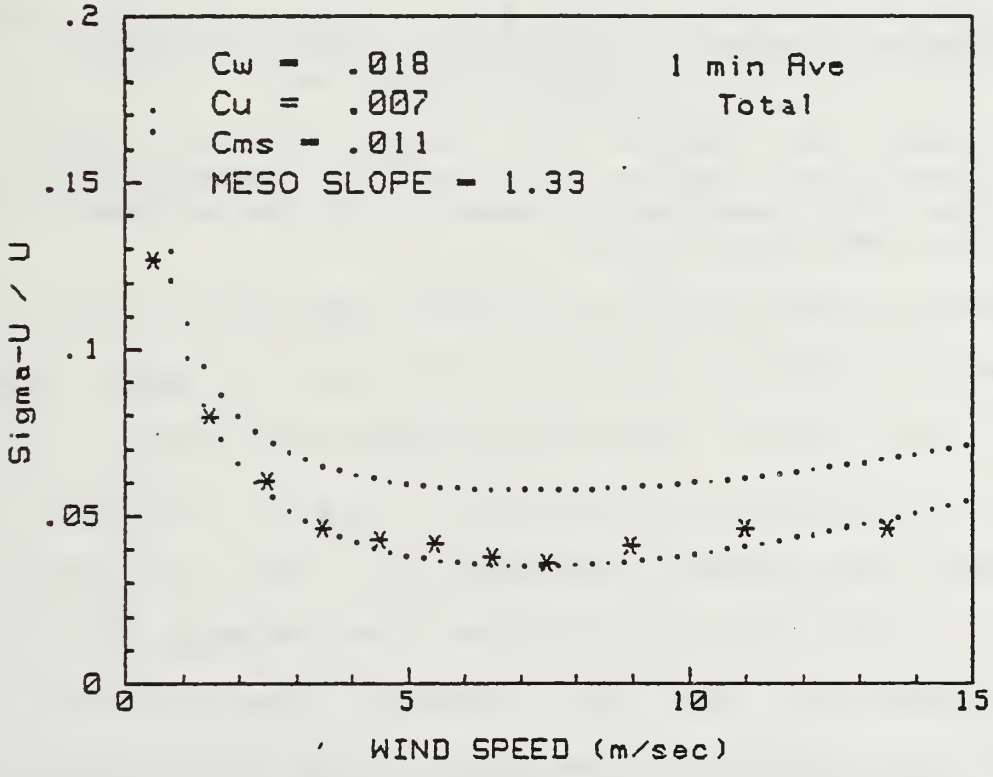

Fig. 6-2 (CONTINUED)

mesoscale production was low for stationary conditions and C_w can be determined, and c) the whole procedure can be checked for unrestricted conditions. For each set of curves the parameters were evaluated by the following procedures. Figs. 6-2a-d contain plots of σ_u/U vs. U for the 1-minute time average, demonstrating the sequence of these procedures.

1. Choose an initial value of C_u based on the difference between the values for stationary, and stable conditions at high wind speeds.

2. Adjust C_{ms} and N to fit the low wind speed portion of the stable data, letting $C_w = 0$.

3. Adjust C_u to correctly fit the high wind speed regime during stable conditions, letting $C_w = 0$. Fig. 6-2a contains an example of the adjustments performed in steps 2 and 3.

4. Choose C_w and adjust to fit the high wind speed regime during stationary conditions, letting $C_{ms} = 0$. Fig. 6-2b contains an example of this step.

5. Check the results by checking the fit that all parameters combined give to the unrestricted data. Fig. 6-2d contains an example of the end results for this particular case.

There are two fitting curves for those cases where $C_w <> 0$. The lower curve is for $w_* = 0.1$ and the upper curve is for $w_* = 0.5$ m/sec. The fitting curves turn upward below 2 m/s as the mesoscale contribution (C_{ms}/U^N) dominates over the shear and buoyancy contributions. Fig. 6-3 shows the σ_u/U vs. U plot for the 30-minute time average (the values representing σ_u/u for the 30-minute time average will hereafter be referred to as σ_{u30}). Using the values of the regression variables presented in Appendix E, σ_{u30}^2 may be

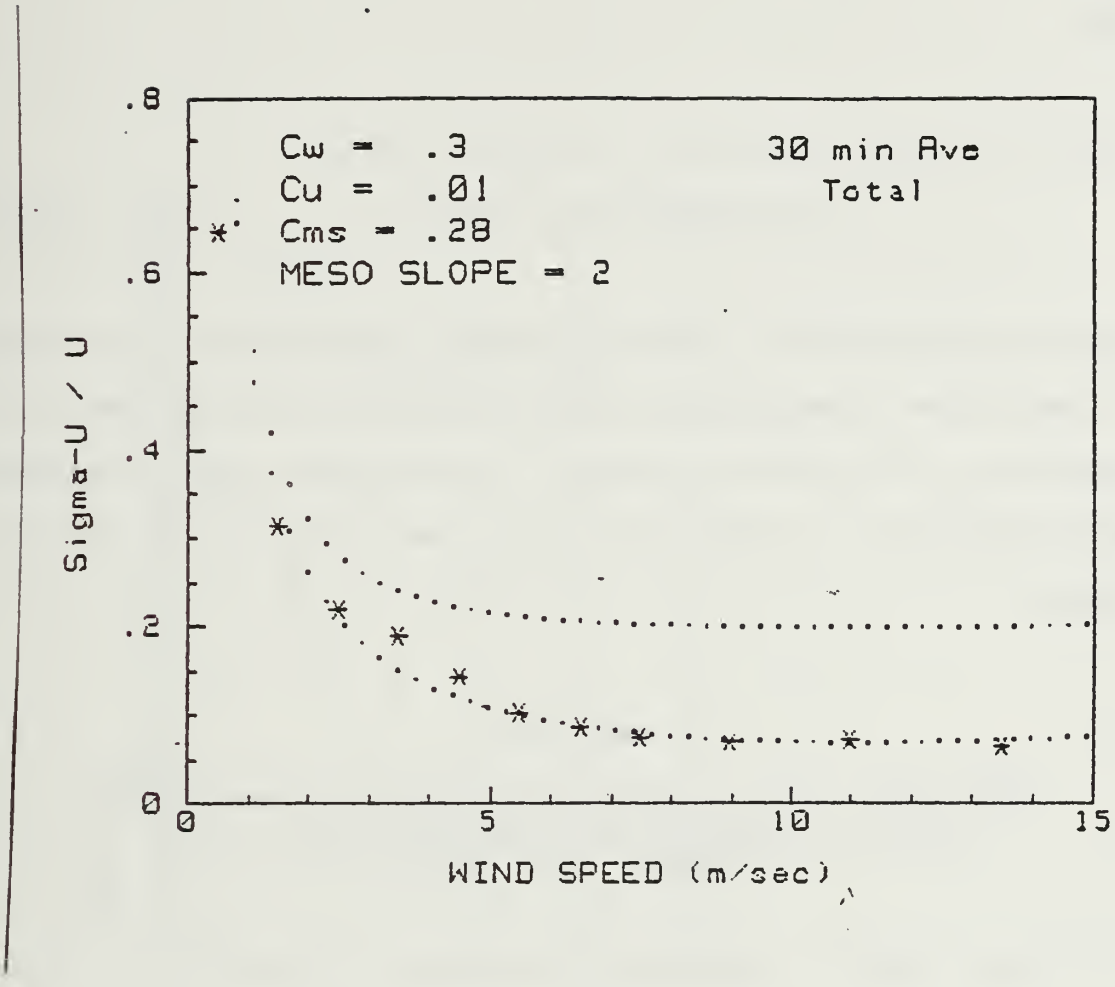

Fig. 6-3 σ_u vs. U Plot of Averaged BLM Cruise 3 & 4 Data with Fitting Curves for High (0.5 m/s) and Low (0.1 m/s) w_* Values

calculated using Equation 23, assuming $w_* = 0.1$ m/sec, such that

$$\sigma_{u30}^2 = 0.497(0.3)(0.1)^2 + (0.01)(7.5\text{x}10^{-4} + 6.7\text{x}10^{-5}U)U^2 + 0.28/U^2 \quad . \qquad (23a)$$

Applying Equation 23a during various wind speeds, the values of the three subcomponents representing shear, buoyancy and mesoscale production mechanism contributions are calculated and displayed in Table 6-1 along with the σ_{u30}^2 and σ_{u30} values.

TABLE 6-1

COMPARISON OF PRODUCTION MECHANISM CONTRIBUTIONS BASED ON EQUATION 23 WITH RESULTANT σ_v AT VARIOUS WIND SPEEDS

U (m/sec)	Shear	Buoyancy	Mesoscale	σ_{u30}^2	σ_{u30}
0.1	1.5E-3	7.5E-8	28.0	28.0015	5.3
0.5	1.5E-3	1.9E-6	1.12	1.1215	1.06
5.0	1.5E-3	2.7E-4	1.3E-2	1.477E-2	0.114
11.0	1.5E-3	1.8E-3	2.3E-3	5.6E-3	7.5E-2

Table 6-1 shows that as expected, at wind speeds below 5 m/sec, mesoscale production dominates.

The values of the empirically derived regression variables are given in Table 6-2. For the purpose of comparison, the values determined by Schacher et al. (1986) for σ_θ^2 are included. The shear and buoyancy values in

TABLE 6-2

FITTING PARAMETER VALUES FOR BUOYANCY, SHEAR, AND MESOSCALE PRODUCTION, BASED ON TIME AVERAGES FOR u, v, AND θ DIRECTIONS

Ave. Time	$C_w(u;v;\theta)$	$C_u(u;v;\theta)$	$C_{ms}(u;v;\theta)$	$N(u;v;\theta)$
1 min	0.018; 0.025; 0.3	0.007; 0.002; 0.45	0.011; 0.017; 0.02	1.33; 2.0; 2.0
3 min	0.033; 0.045; 0.6	0.01; 0.0035; 0.6	0.025; 0.035; 0.06	1.33; 2.0; 2.0
10 min	0.15; 0.09; 1.2	0.01; 0.005; 0.8	0.055; 0.1; 0.12	1.33; 2.0; 2.0
30 min	0.3; 0.27; 1.6	0.01; 0.005; 1.2	0.28; 0.24; 0.25	2.0; 2.0; 2.0

Table 6-2 are about the same size for both σ_u and σ_v. This result is expected based on previous discussions by Panofsky and Dutton (1984) and Hojstrup (1982). No direct comparison should be made between the magnitudes of the regression variables since the actual significance of this work lies in analyzing the values of $\sigma_{u,v}^2$. The values for N are similar for σ_v, but smaller for σ_u.

It was found that the best value of N for the mesoscale term was dependent upon which wind component was examined. In the transverse direction (v) N = 2 for all four time averages. This was expected since Schacher et al. (1986) determined N = 2 for σ_θ and σ_v is directly related to σ_θ. Fig. 6-4a shows the σ_v/U vs. U plot for the 30 minute time average. Fig. 6-4b shows the corresponding σ_θ vs. U plot for the 30-minute average from Schacher et al. (1986). Table 6-3 shows sample values picked off of the graphs. The "σ_θ conversion" column contains the equivalent values of σ_v converted to σ_θ using the formula

$$\{\tan[(\sigma_v/U)*U]\}/U = \sigma_\theta \text{(radians)} ,$$

and compared to the corresponding σ_θ values from Schacher et al. (1986). As seen in Table 6-3, the converted σ_v values are very close to those produced by the previous work, indicating consistency between the two methodologies.

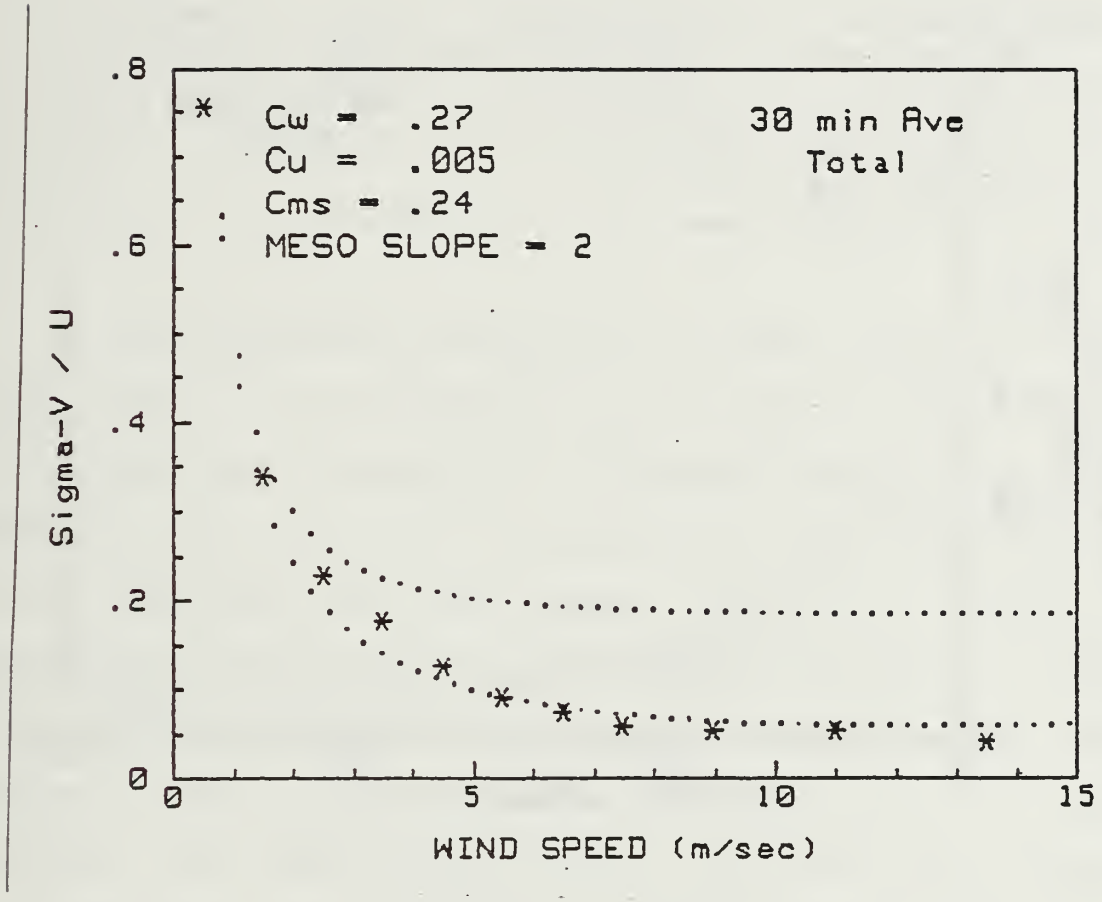

Fig. 6-4a σ_v/V Plot for 30 Minute Time Average, Unrestricted Conditions, Using BLM 3 and 4 Data

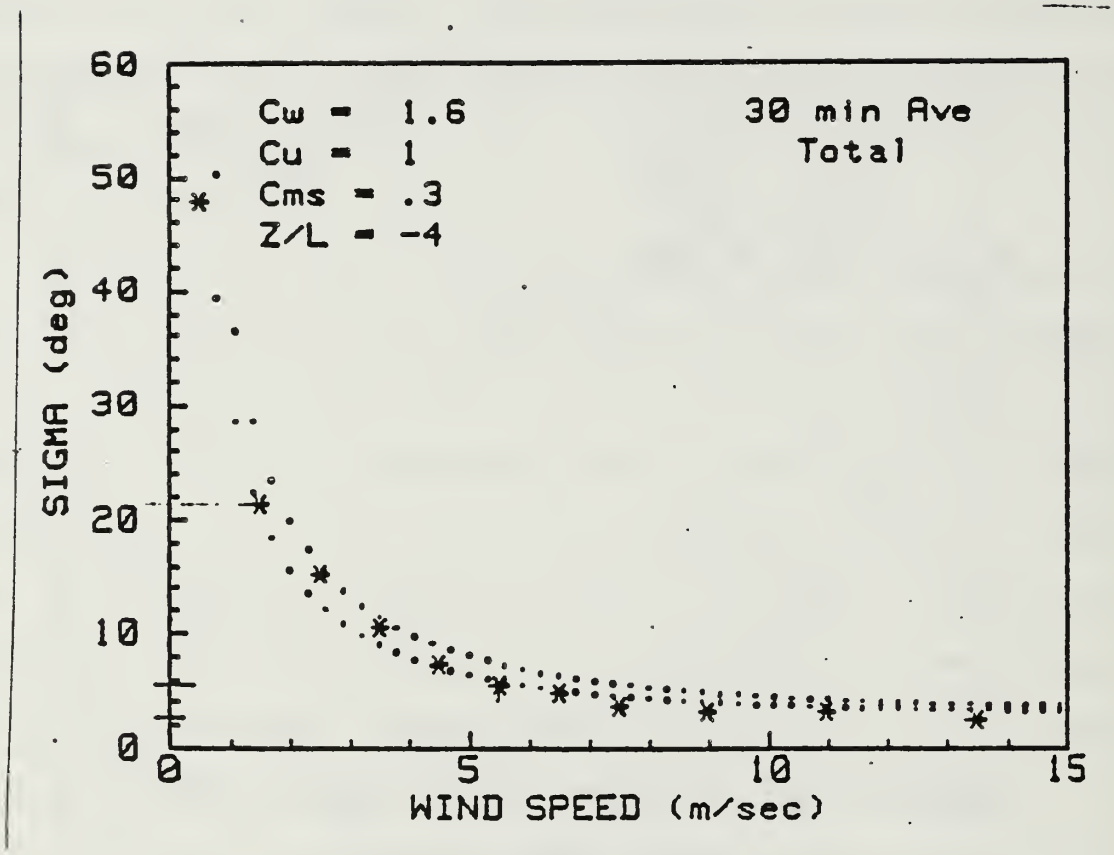

Fig. 6-4b σ_θ vs. U Plot for 30 Minute Time Average, Unrestricted Conditions, Using BLM 1, 2, 3 and 4 Data (from Schacher et al., 1986)

TABLE 6-3

COMPARISON OF σ_θ VALUES CONVERTED FROM σ_v AND FROM SCHACHER ET AL. (1986)

U (m/sec)	σ_v/U	σ_θ (Schacher)	σ_θ (conversion)
1.5	0.34	21.3°	21.3°
5.5	0.09	5.7°	5.6°
11.0	0.055	2.5°	3.6°

In the longitudinal direction (u), many values of N were tried, with N = 1.33 yielding the best fit for the 1, 3, and 10 minute time averages. Figures 6-5a,b compare the fitting curves based on N = 2.0 and N = 1.33, respectively. It is seen that the more gradual slope of N = 1.33 is required to properly fit the low wind speed data. Oddly though, N = 2 provided the best fit for the 30-minute time average. Since previous works (Schacher et al., 1986; Hojstrup, 1984; Panofsky and Dutton, 1984) utilize 30-minute time averages, it is necessary to emphasize findings based on the 30-minute averaging which shows N = 2.0 for both the u and v directions. The implication is that mesoscale effects are about the same in both directions. The different values for each fitting parameter suggest that the production mechanisms affect puff growth differently in the downwind than in the crosswind directions.

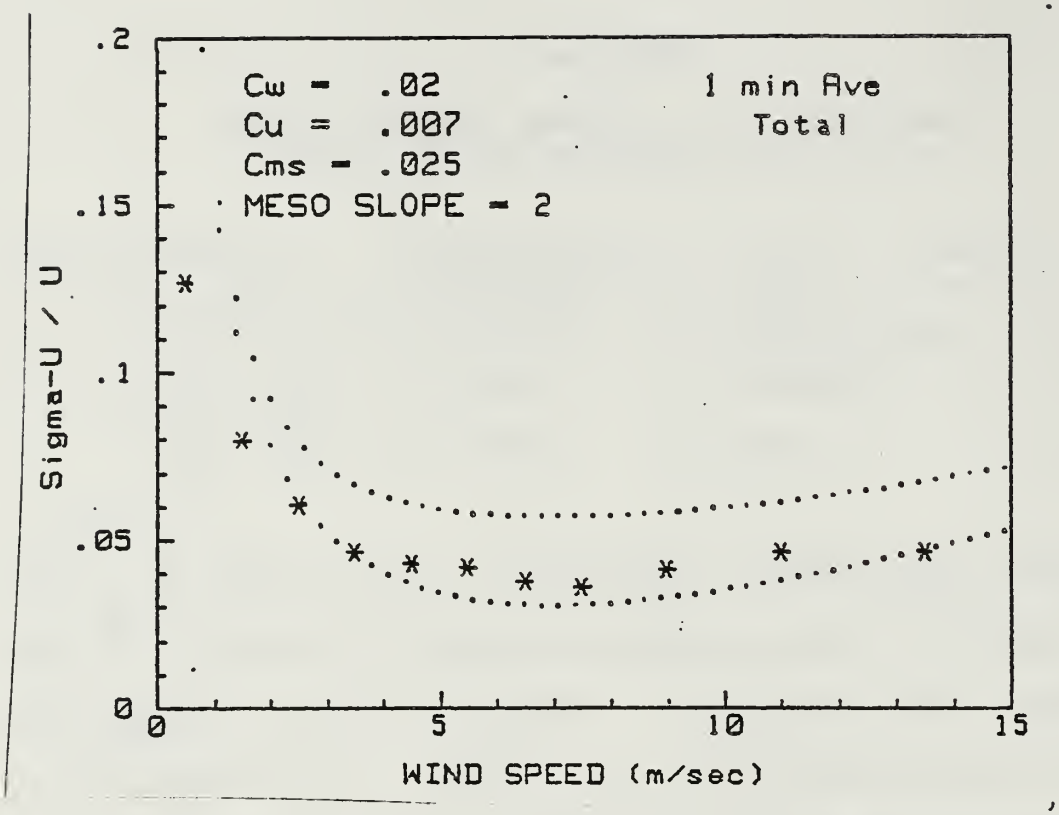

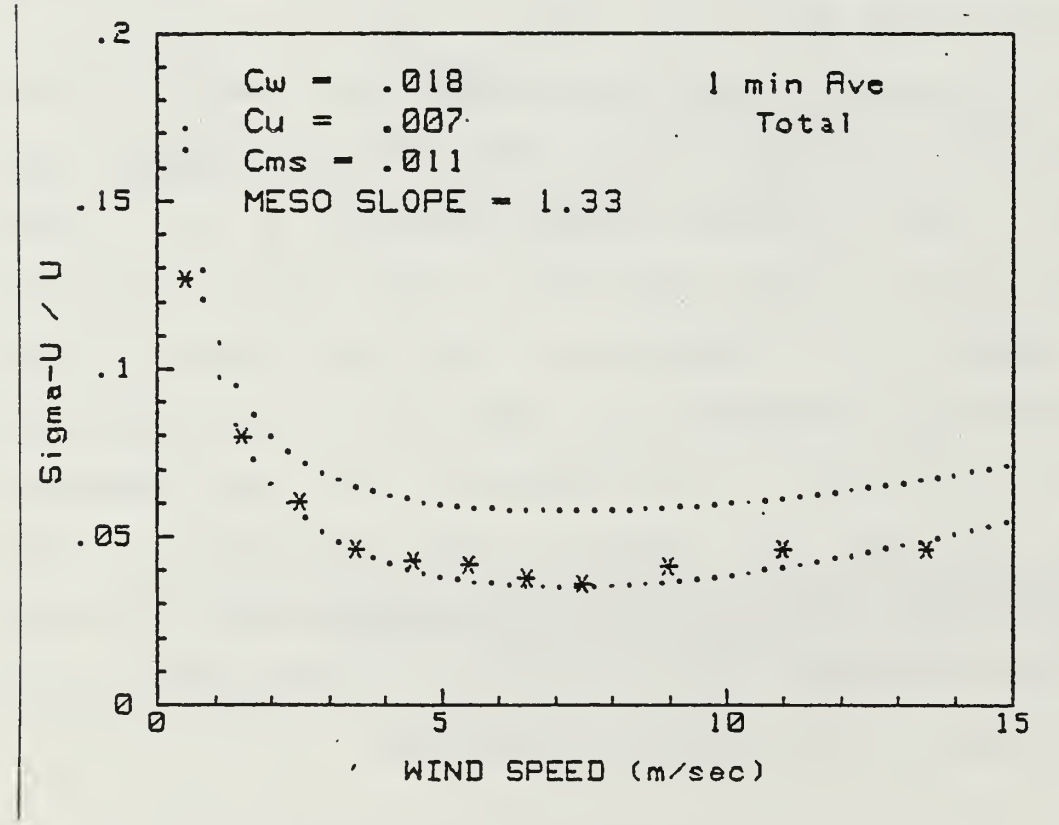

Fig. 6-5 Comparison of Empirical Curves Using Mesoslopes of 2.0 Versus 1.33

B. RATIOS

Panofsky and Dutton (1984) proposed the simple expression

$$\sigma_u = A * u_* \ , \qquad (24a)$$

and

$$\sigma_v = B * u_* \ , \qquad (24b)$$

for purely shear driven, mechanical turbulence. A and B were presumably constants for a given surface roughness, assuming convection was unimportant. He also assumed that σ_u was slightly larger than σ_v. Based on various experiments over flat terrain the mean values for the constants A and B, for 30 minute time averages were

$$A = 2.39 \pm 0.03 \ , \qquad \text{and}$$

$$B = 1.92 \pm 0.05 \ , \qquad \text{such that,}$$

$$A/B = 1.25 \pm 0.05 \ .$$

These values agreed well with corresponding wind tunnel measurements. The assumption here is that turbulence is shear driven and is quantified by the σ/u_* ratios, therefore, only u_* is a function of the generation mechanism. Under this assumption, A and B should be universal constants based on the integral of the velocity spectra over the time scale of interest.

Based on observations at various locations, it was seen that as the surface roughness increased, the values of A and B increased. Conversely, over open ocean having a small surface roughness, it would be expected that A and B decrease, perhaps being several times smaller than the above values. Table 6-4 shows the values of A and B based upon the BLM data.

TABLE 6-4

RATIOS OF STANDARD DEVIATIONS OF HORIZONTAL VELOCITY COMPONENTS TO FRICTION VELOCITY; A FOR LONGITUDINAL, B FOR TRANSVERSE

Time (min)	A	B
1	0.15	0.12
3	0.20	0.17
10	0.28	0.25
30	0.39	0.37

As expected, the open ocean values are much less than those over flat terrain, about one order of magnitude smaller. Since A and B deviate from the Panofsky and Dutton (1984) values, there is a strong possiblity that other production mechanisms independent of z_o must exist. Possibilities could include buoyancy and mesoscale effects as proposed by Schacher et al. (1986), or terrain/orographic effects.

By assuming that the BLM data were obtained in the surface layer over uniform terrain, Eq. (24) becomes

$$\sigma_u/u_* \tilde{=} \sigma_v/u_* \ , \qquad (25)$$

assuming A is about the same size as B.

Using Equation 25, a final comparison was made using the ratio of σ_u/σ_v. The values used in Panofsky and Dutton (1984) resulted in a ratio of

$$\sigma_u/\sigma_v = 1.25 \pm 0.05 \ .$$

The ratios σ_u/σ_v are significant because they address the actual growth of a puff.

Table 6-5 shows the σ_u/σ_v ratios for each time average based on the processed BLM data.

TABLE 6-5

RATIOS OF STANDARD DEVIATIONS OF HORIZONTAL VELOCITY COMPONENTS

Time (min)	σ_u/σ_v +0.05
1	1.37
3	1.31
10	1.24
30	1.27

As shown in Table 6-5, the σ_u/σ_v ratios based on the BLM data are about the same as Panofsky and Dutton (1984) for overland. Note that the values in Table 6-5 decrease as the

time average increases. Based on Panofsky and Dutton (1984), it is expected that the σ_u/σ_v ratios for the 30-minute time averaged values should be approximately 1.25. Using the parameterization constants from Table 6-2, σ_u/σ_v ratios for the various production mechanisms can be computed. Shown below are the ratios of each production mechanism in the longitudinal (u) vs. transverse (v) directions (u/v) based on the empirically derived regression variables for the 30-minute time average.

Shear = 1.05 ,

Buoyancy = 1.41 ,

Mesoscale = 1.08 .

The σ_u/σ_v ratios shown above indicate consistency with previous results which indicated that puff growth due to various production mechanisms are greater in the downwind direction versus the crosswind direction.

C. RELATIONSHIP TO OTHER WORKS

It was found during the course of fitting the data that the results are very similar to those found by Schacher et al. (1986). In all three cases ($\sigma_{u,v,\theta}$), the short time average results are strongly dependent on the value of C_u while the long time averages are not. Both w_* ranges can not be fit without including shear, C_u. The conclusion is that shear production is not important for large averaging times since large scale processes dominate. Both the shear and buoyancy terms in Eq. (23) are functions of wind speed.

Shear production dominates at high wind speeds. As demonstrated previously in Table 6-1, the shear production contribution is greater than either buoyancy or mesoscale contributions at high wind speeds (>11 m/sec).

When using the results of this thesis to parameterize wind variablity one must first determine if the situation is stationary. In this context, stationarity means that there is a well established wind, that one is not in a land-sea-breeze transition period. If stationarity exists $C_{ms} = 0$, and if non-stationarity exists, the full Equation 23 should be used to calculate the appropriate σ^2.

Due to the nature of the collection methods, sampling location, and local conditions, these findings may be less than precise. Therefore, certain caveats are appropriate:

1. These results are only applicable to the coastal, overwater regime.
2. These results may be location specific since the data were from two cruises but at a single distance offshore.
3. The mesoscale production term was obtained by utilizing data obtained when the flow was driven by a sea-breeze cycle. This term may not be applicable to other conditions.
4. The mesoscale term must be set to zero, $C_{ms} = 0$, for stationary conditions.

Based on Schacher et al. (1986), there exists reasonable confidence that the buoyancy and shear production terms are transportable to other conditions and locations. There may be some difficulty with the buoyancy term since there exists the potential that not all the mesoscale influence was

absent when the values were determined but, for its current potential uses, there should be no significant error. The mesoscale term was a large effect which may be site specific; however, that limitation does not preclude the possibility that this effect may extend far out to sea.

The findings of this thesis are related to the results from Davidson (1974), where turbulence data were obtained over ocean waves during the BOMEX experiment of 1969, located 200 miles east-northeast of Barbados. Surface layer wind fluctuation and momentum transfer were shown to have been significantly influenced by both stability and wind wave coupling. The low frequency turbulence described by Davidson over the open ocean existed at low wind speeds and could have been due to any of several sources, including mesoscale production mechanisms. The similarity between the two sets of results is that low frequency turbulence at low wind speeds was observed in both near coast (Schacher et al. (1986)) and open ocean regimes (Davidson 1974). The implication is that this phenomenon may be generated by mesoscale production mechanisms, sensible heat flux, wind-wave coupling, Kelvin waves, or a combination of sources. The recommendation then, is to conduct further research to establish continuity between the findings of Davidson (1974), Schacher et al. (1986), and this study.

D. PUFF MODELING IMPLICATIONS

A final recommendation is to provide this work to the Naval Environmental Prediction Research Facility in Monterey, CA for incorporation into its Chemical Weapon Hazard Forecast (CHEMFO) model. Appendix F contains recommendations for the application of this thesis to modify CHEMFO such that it includes rudimentary puff modeling.

APPENDIX A

SCATTERPLOTS

The following are scatterplots of BLM data for $\sigma_{u,v}/U$ versus U.

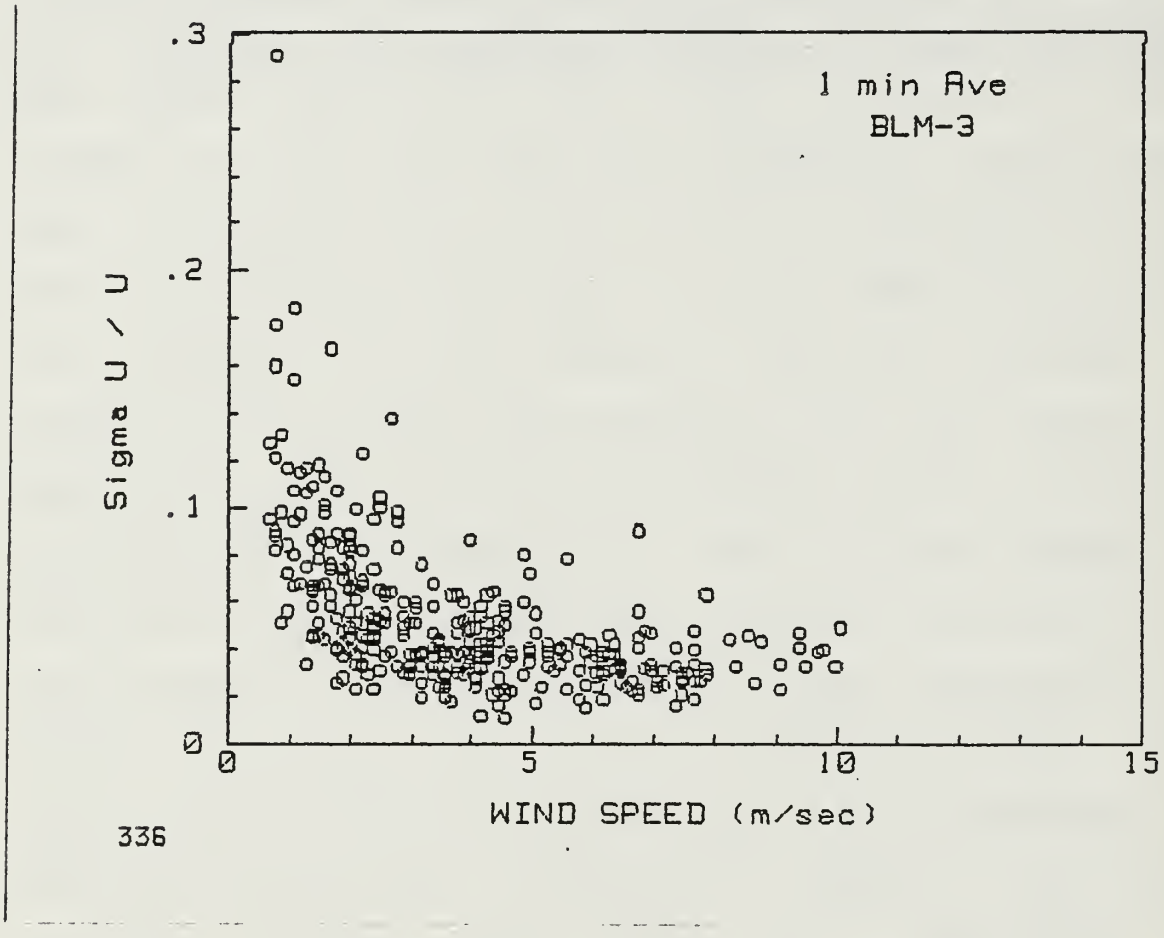

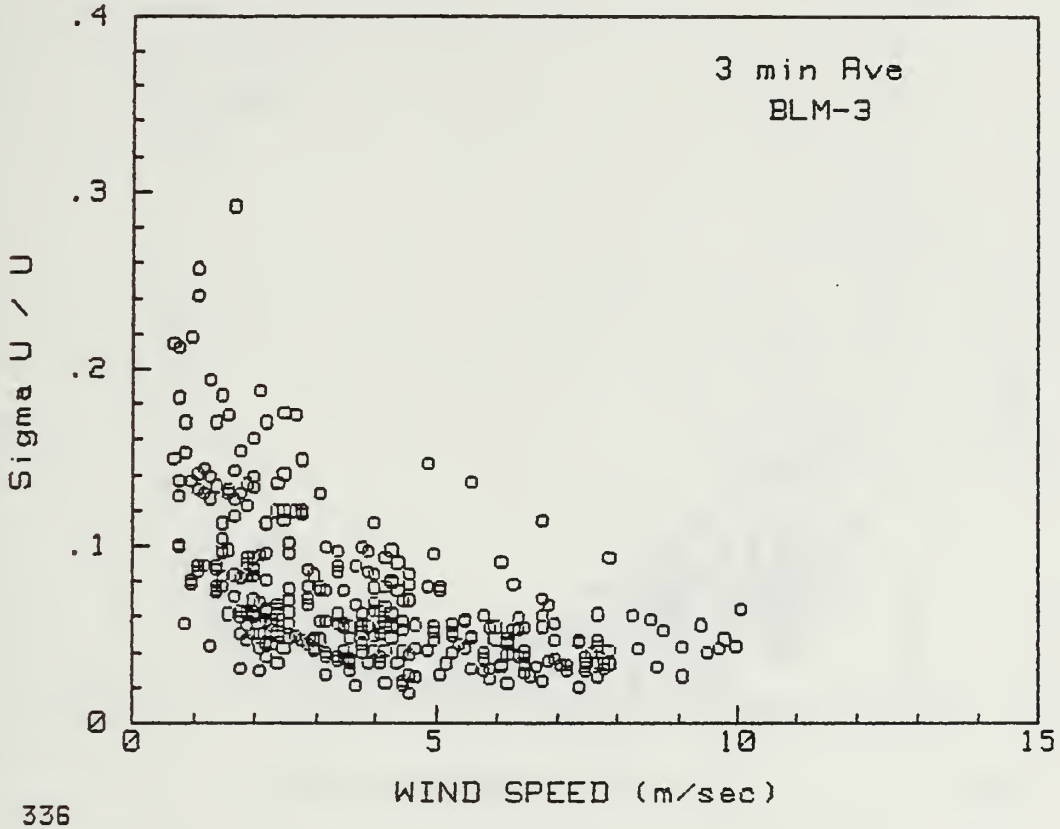

336

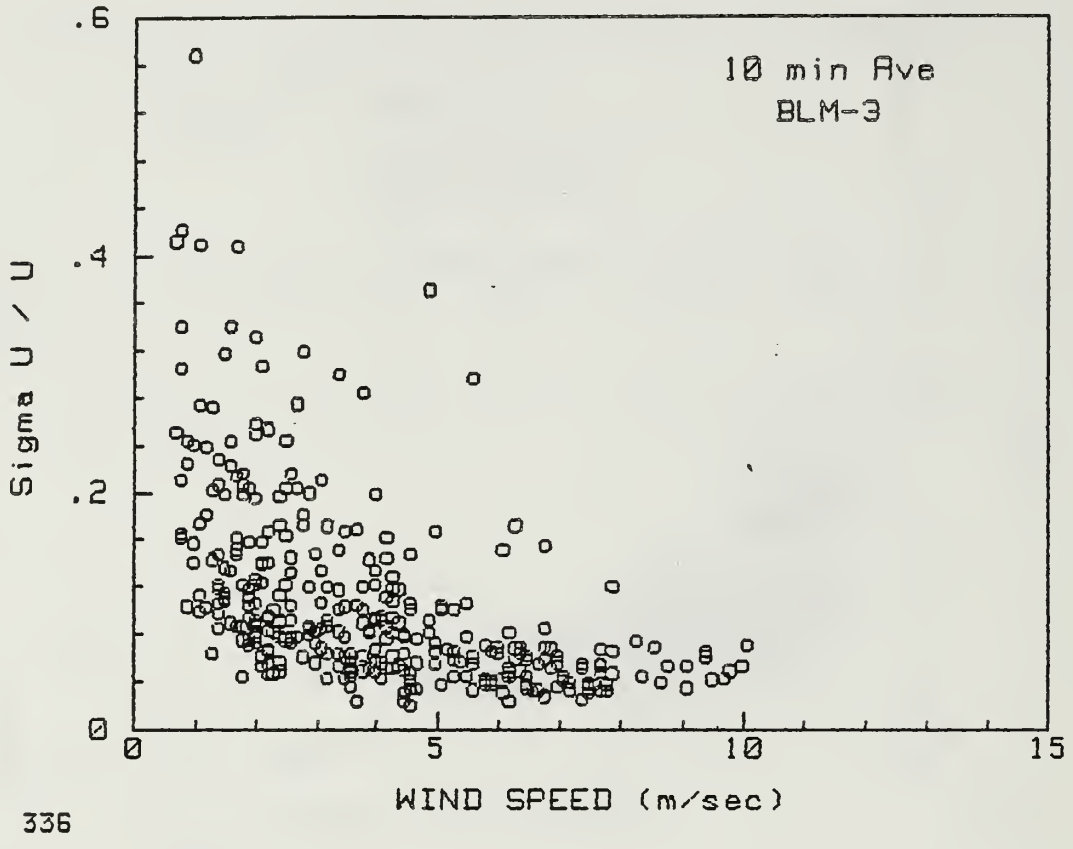
10 min Ave
BLM-3
Sigma U / U
.6
.4
.2
0
0
5
10
15
WIND SPEED (m/sec)
336

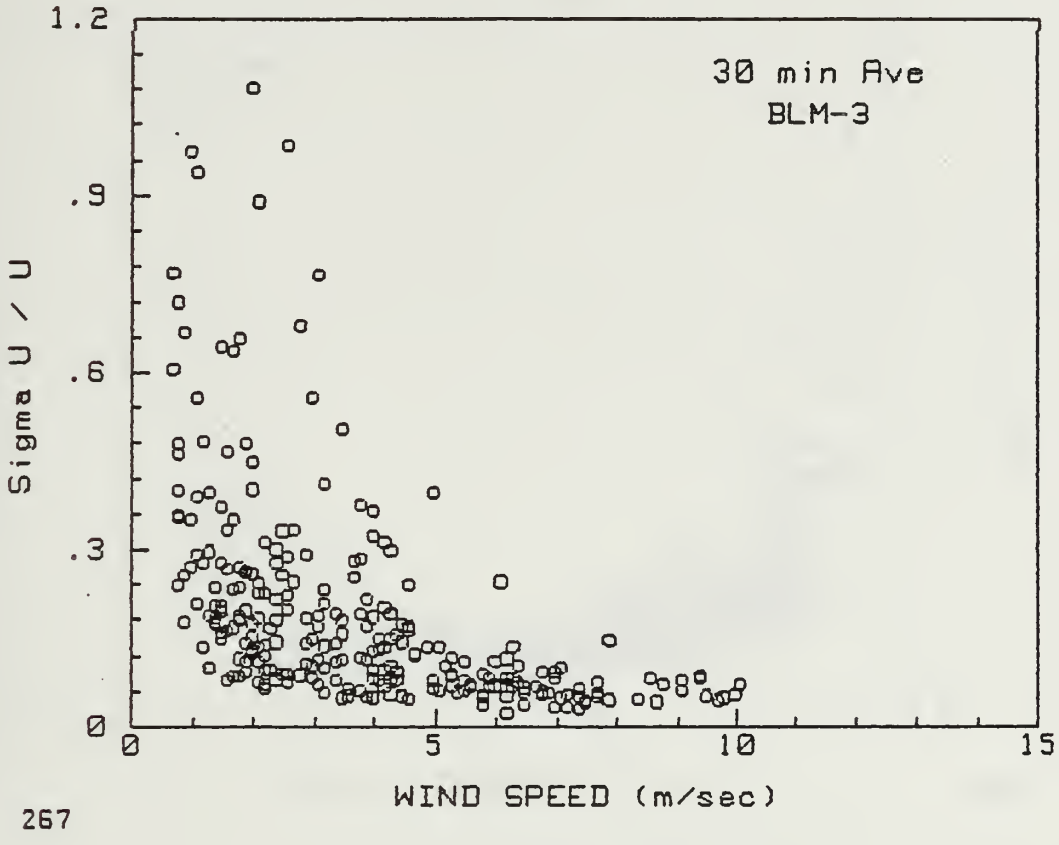
30 min Ave
BLM-3
Sigma U / U
1.2
.9
.6
.3
0
0
5
10
15
WIND SPEED (m/sec)
267

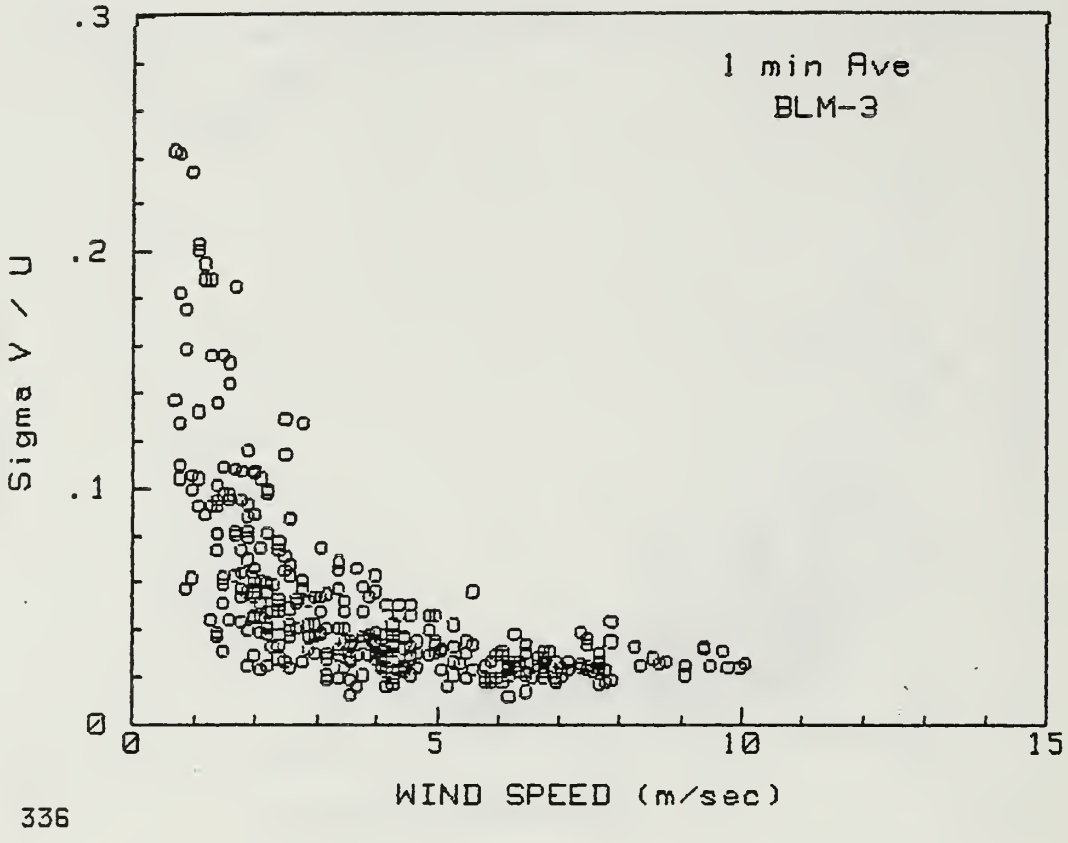
1 min Ave
BLM-3
Sigma V / U
.3
.2
.1
0
0
5
10
15
WIND SPEED (m/sec)
336

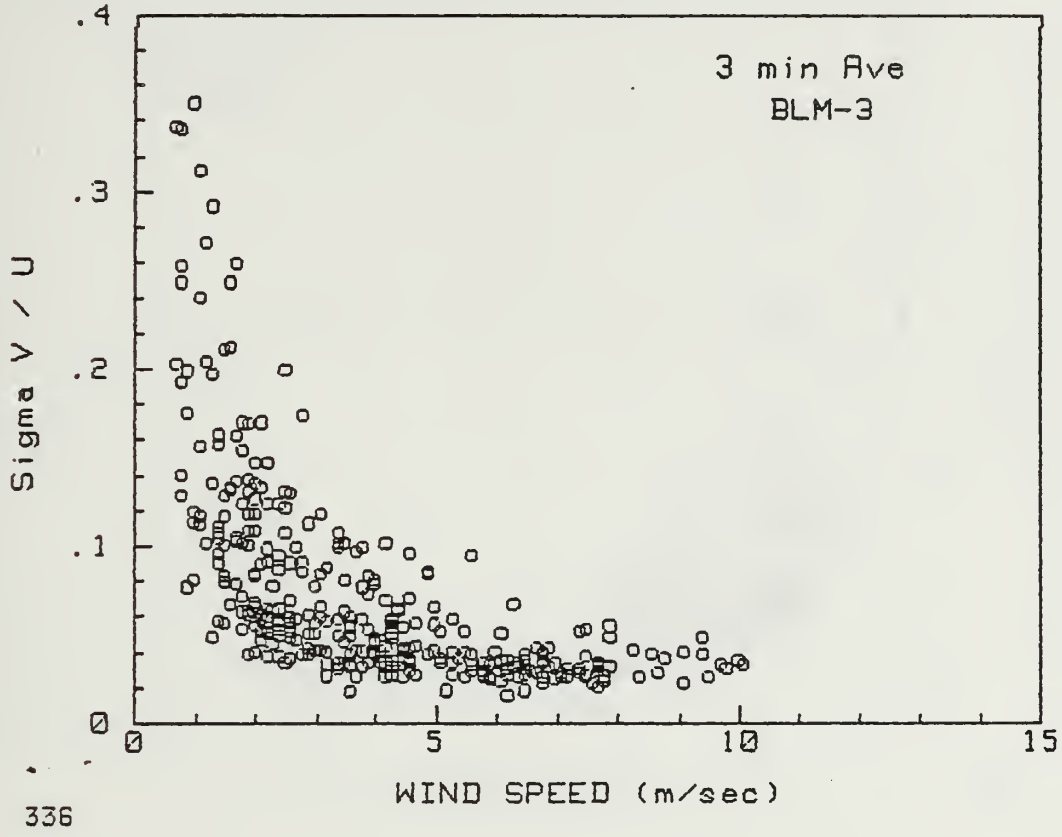

336

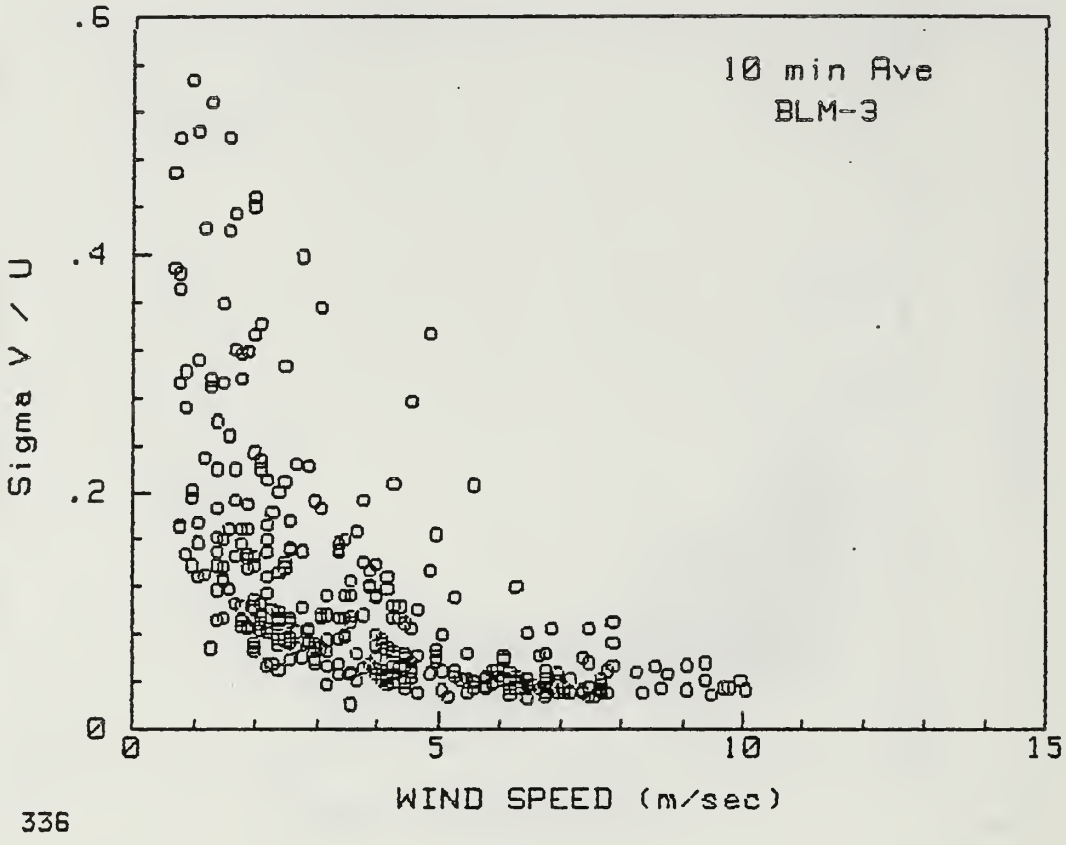
10 min Ave
BLM-3
Sigma V / U
.6
.4
.2
0
0
5
10
15
WIND SPEED (m/sec)
336

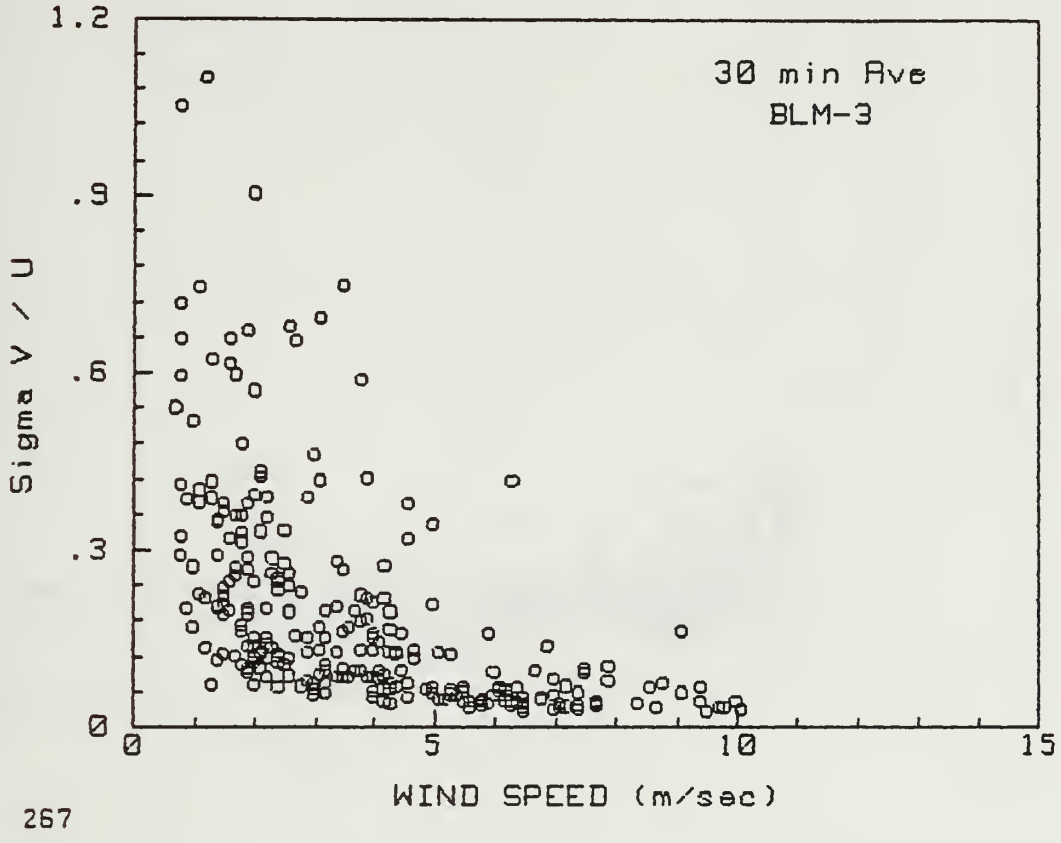
30 min Ave
BLM-3
Sigma V / U
1.2
.9
.6
.3
0
0
5
10
15
WIND SPEED (m/sec)
267

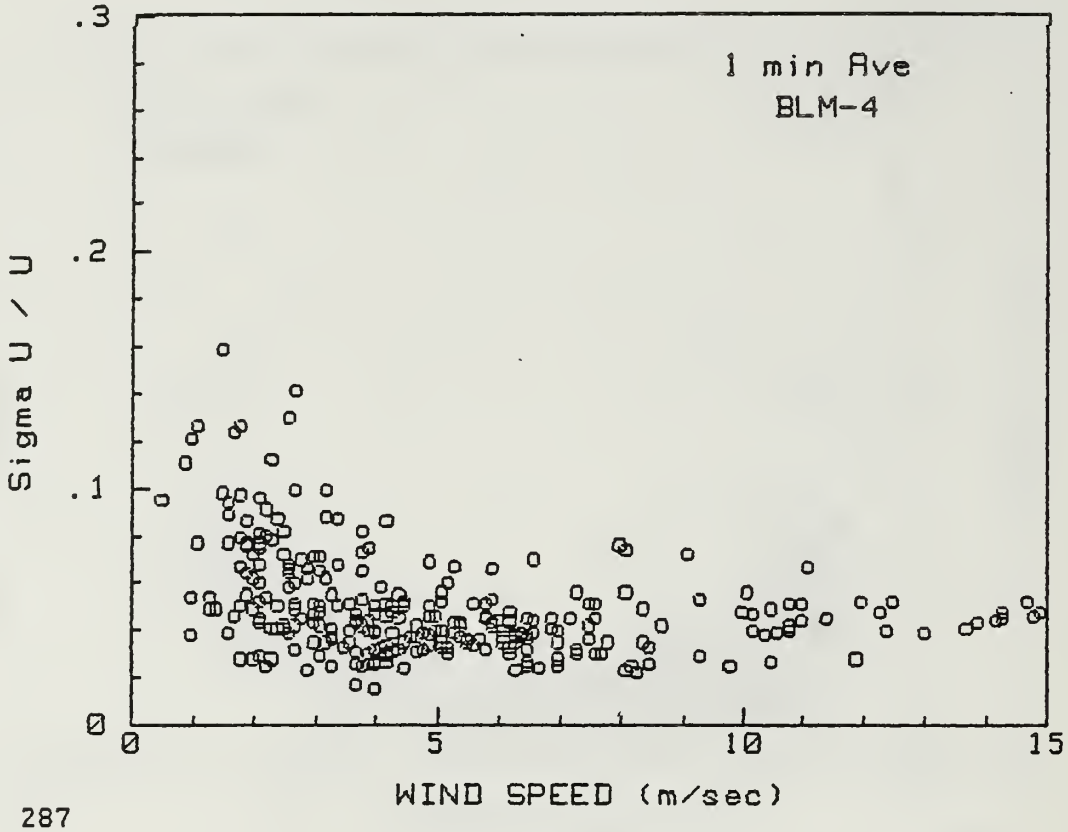

287

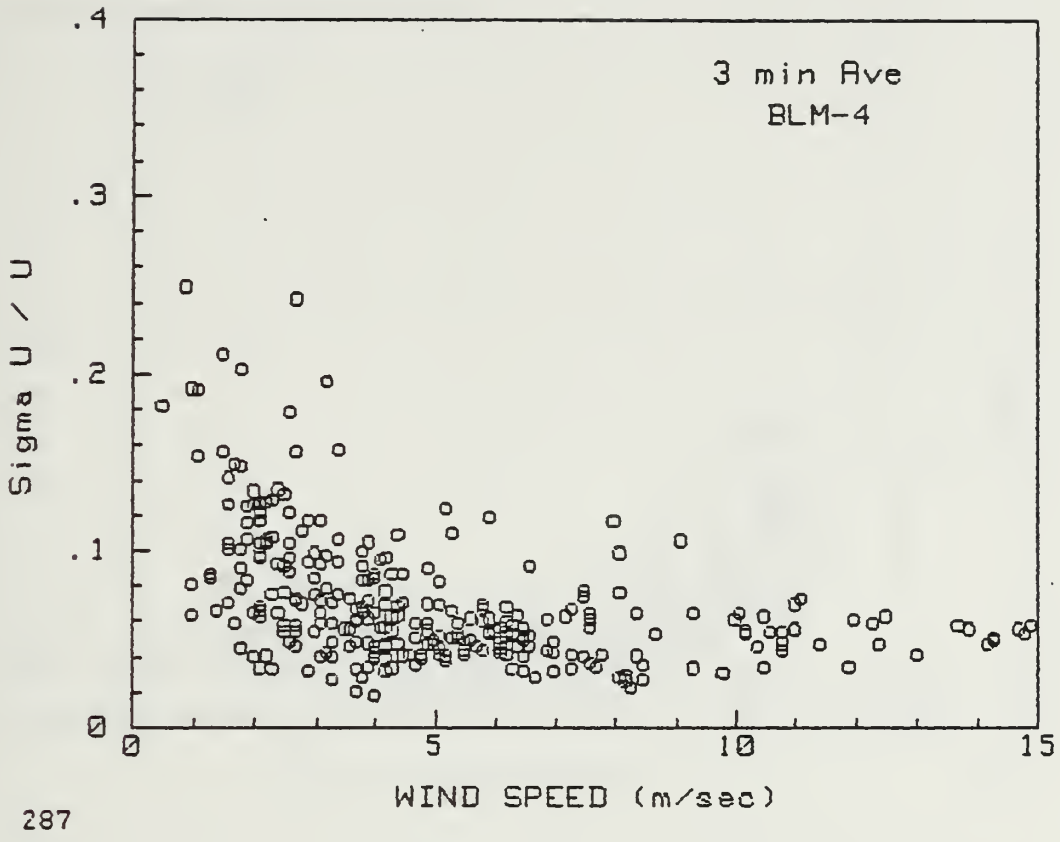

287

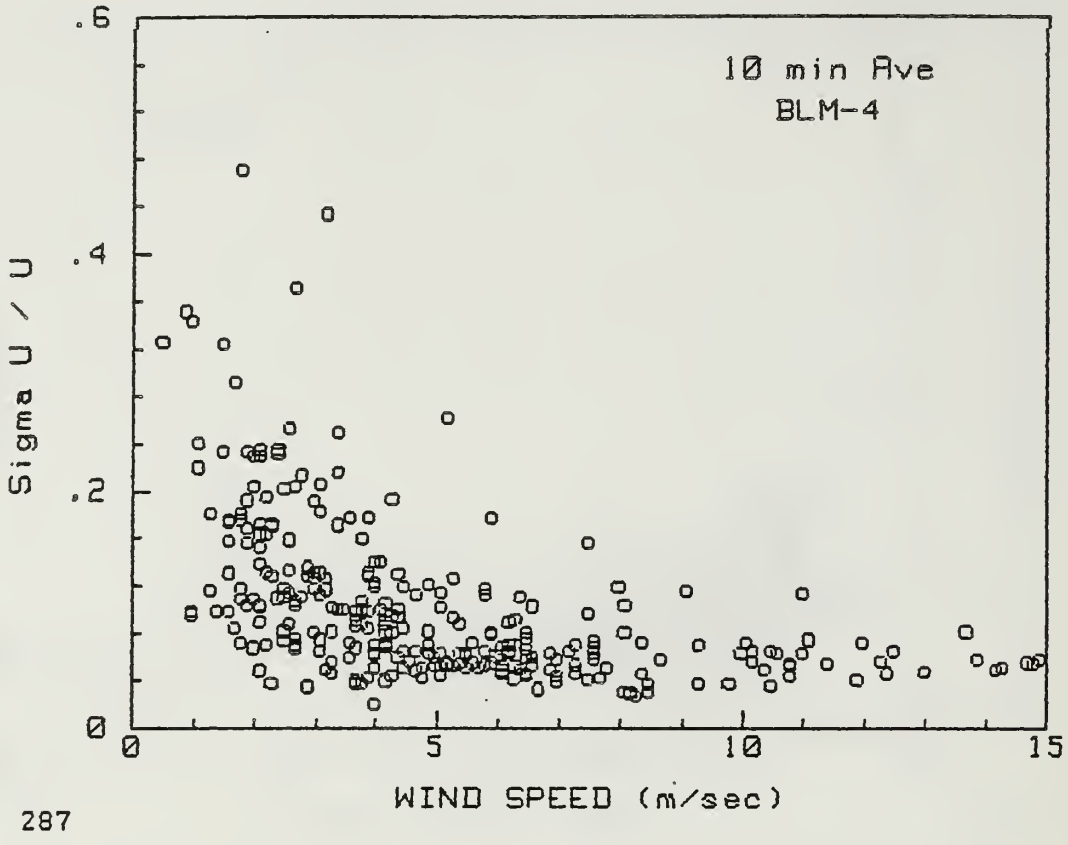
10 min Ave
BLM-4
Sigma U / U
.6
.4
.2
0
0
5
10
15
WIND SPEED (m/sec)
287

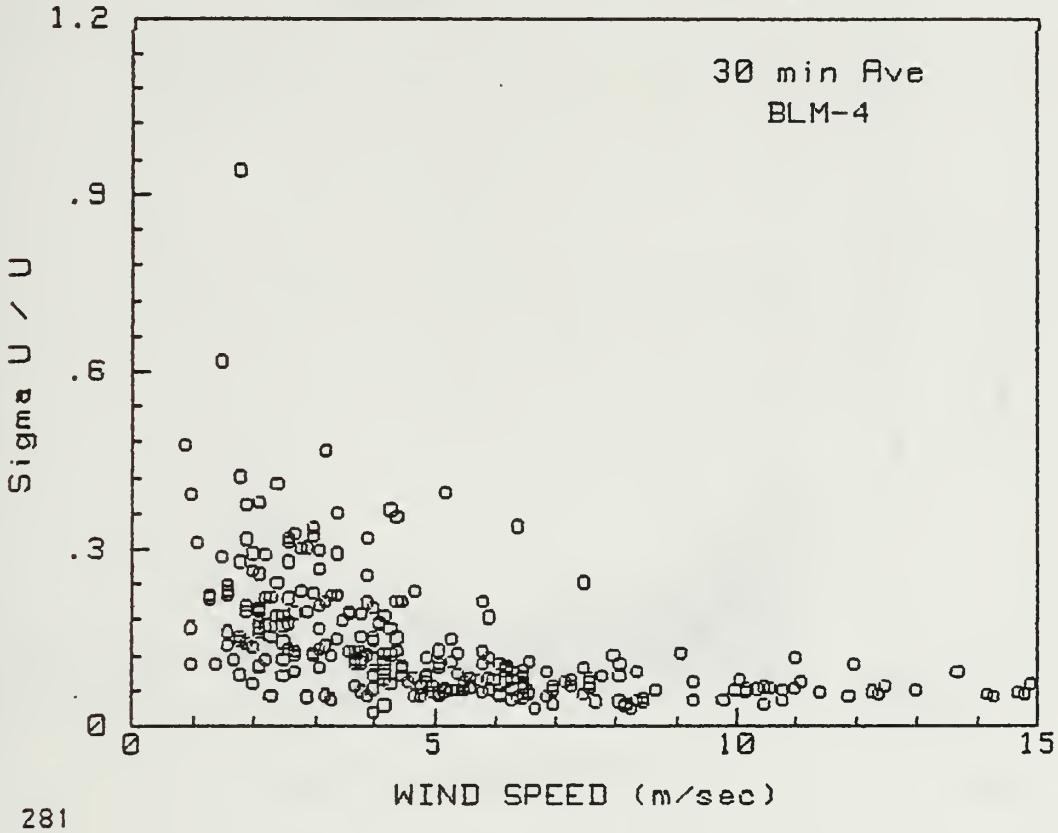
30 min Ave
BLM-4
Sigma U / U
1.2
.9
.6
.3
0
0
5
10
15
WIND SPEED (m/sec)
281

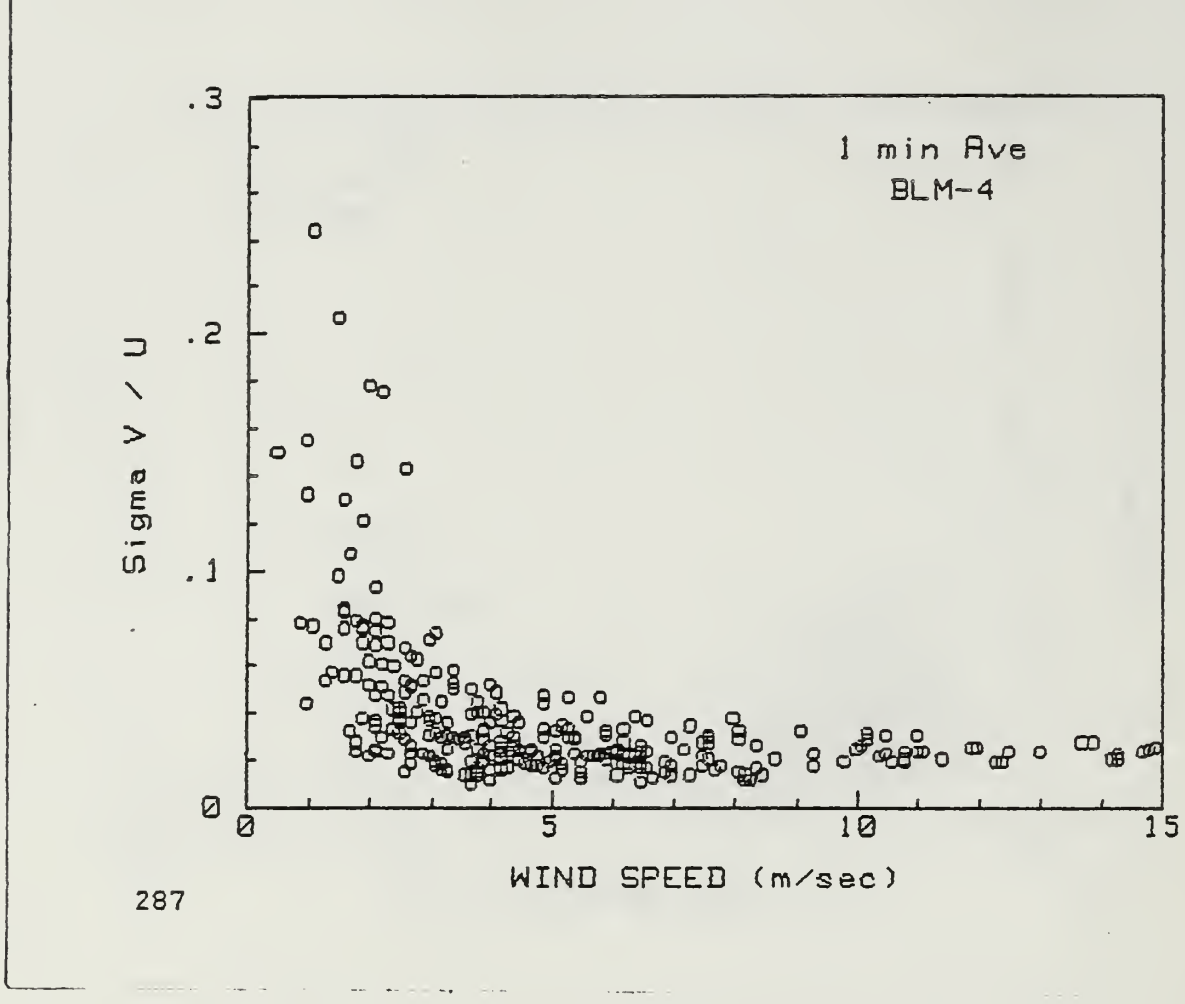
1 min Ave
BLM-4
Sigma V / U
.3
.2
.1
0
0
5
10
15
WIND SPEED (m/sec)
287

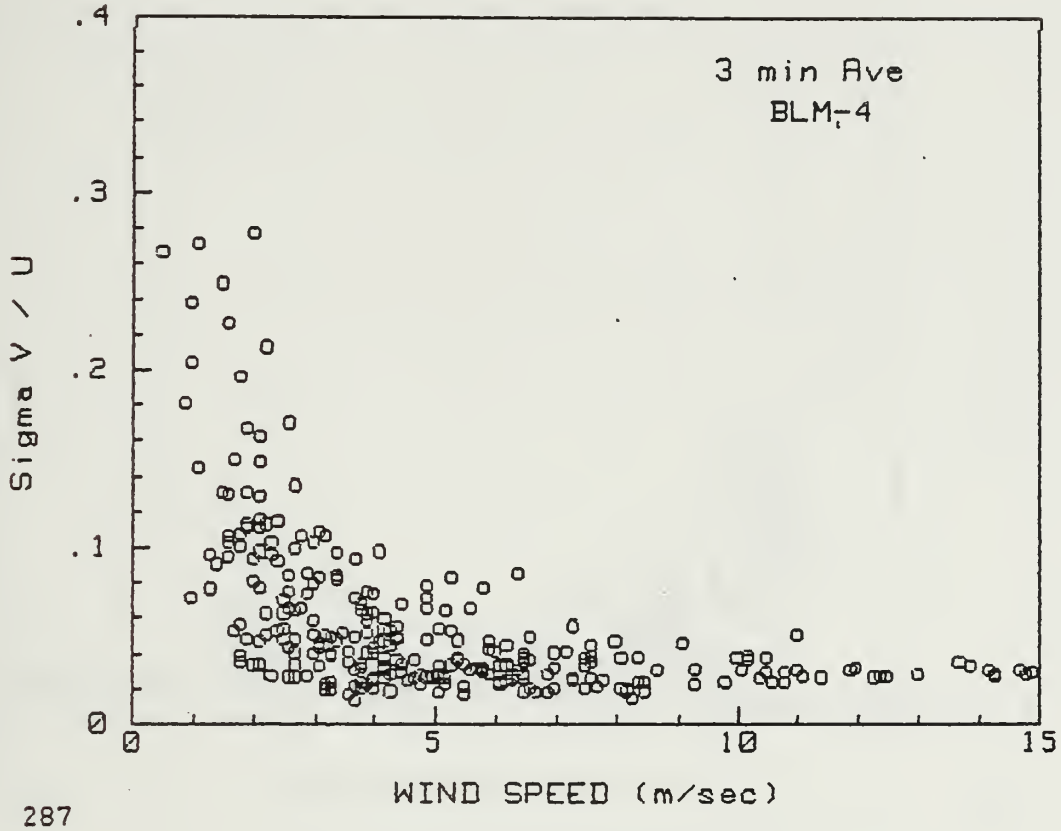

287

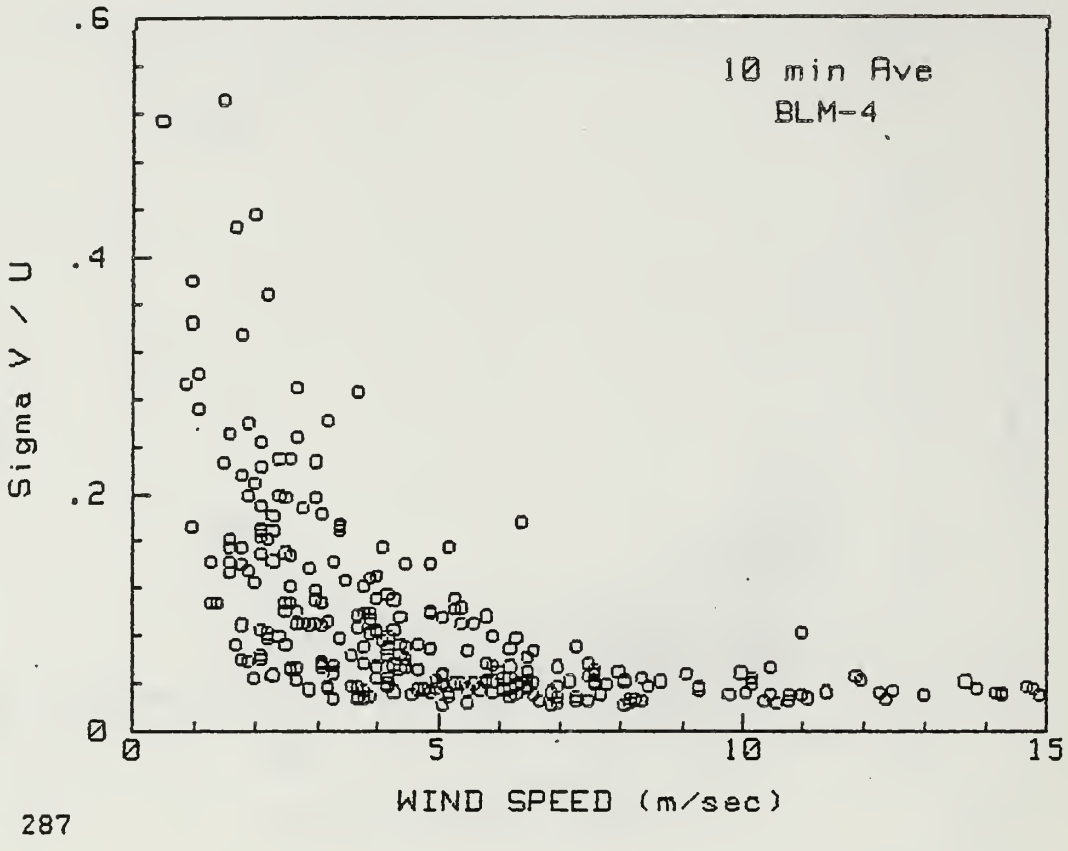
10 min Ave
BLM-4
Sigma V / U
.6
.4
.2
0
0
5
10
15
WIND SPEED (m/sec)
287

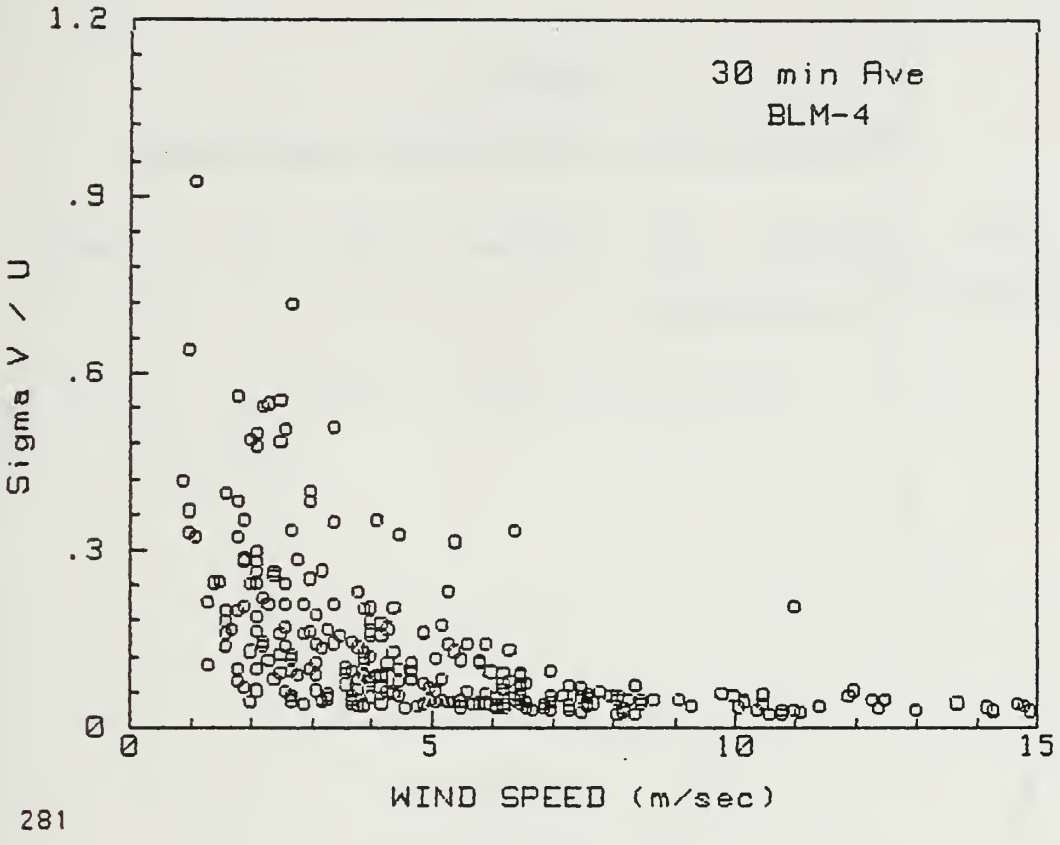
30 min Ave
BLM-4
Sigma V / U
1.2
.9
.6
.3
0
0
5
10
15
WIND SPEED (m/sec)
281

APPENDIX B

AVERAGED PLOTS, UNRESTRICTED CONDITIONS

The following are averaged BLM-3 and 4 data for unrestricted conditions.

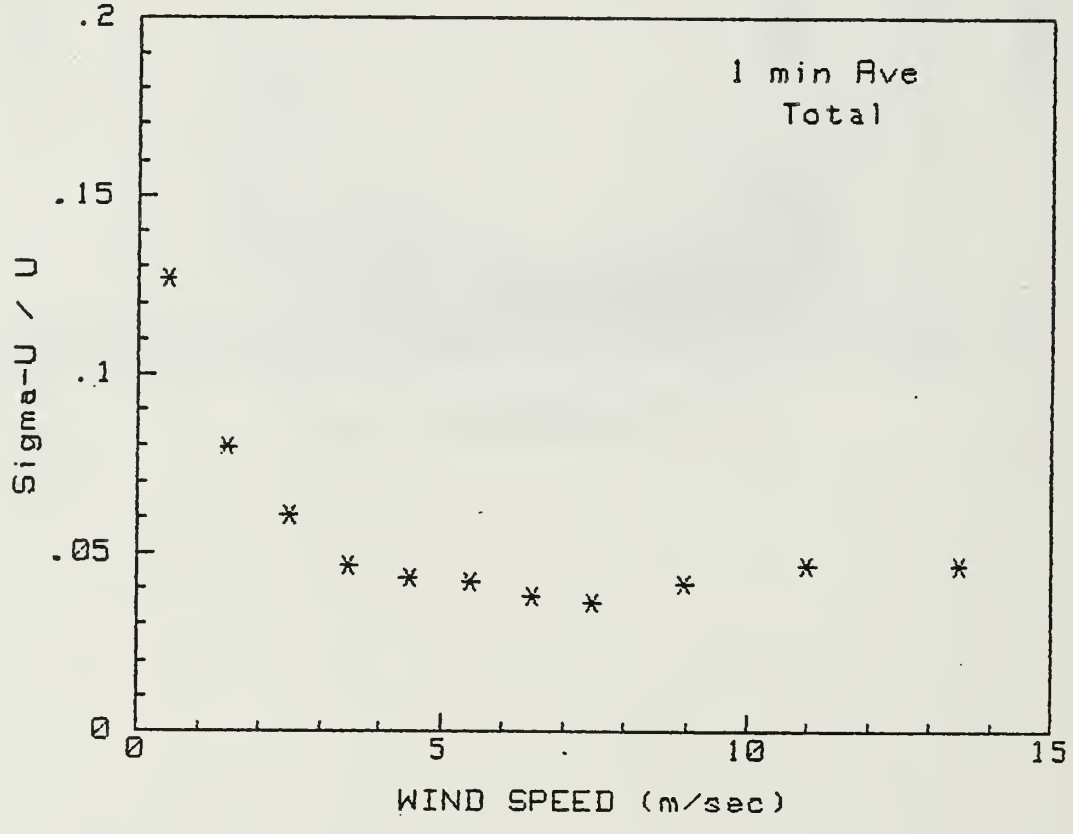

U	#	SIGMA	Std Dev
.5	10	.126	.006
1.5	77	.080	.001
2.5	102	.060	0.000
3.5	91	.046	0.000
4.5	89	.043	0.000
5.5	56	.041	0.000
6.5	60	.038	0.000
7.5	43	.036	0.000
9.0	30	.041	0.000
11.0	17	.046	.001
13.5	14	.046	.001

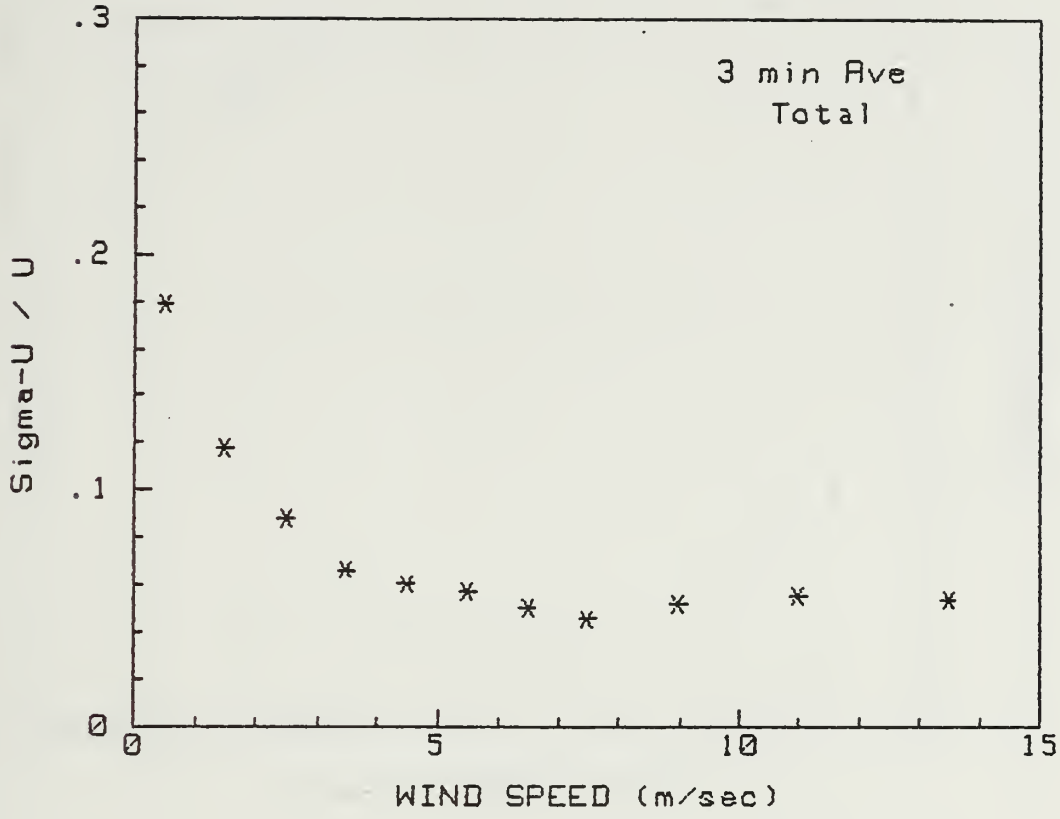

U	#	SIGMA	Std Dev
.5	10	.178	.012
1.5	77	.117	.002
2.5	102	.088	.001
3.5	91	.066	.001
4.5	89	.060	0.000
5.5	56	.057	0.000
6.5	60	.050	0.000
7.5	43	.045	0.000
9.0	30	.052	.001
11.0	17	.055	.001
13.5	14	.054	.001

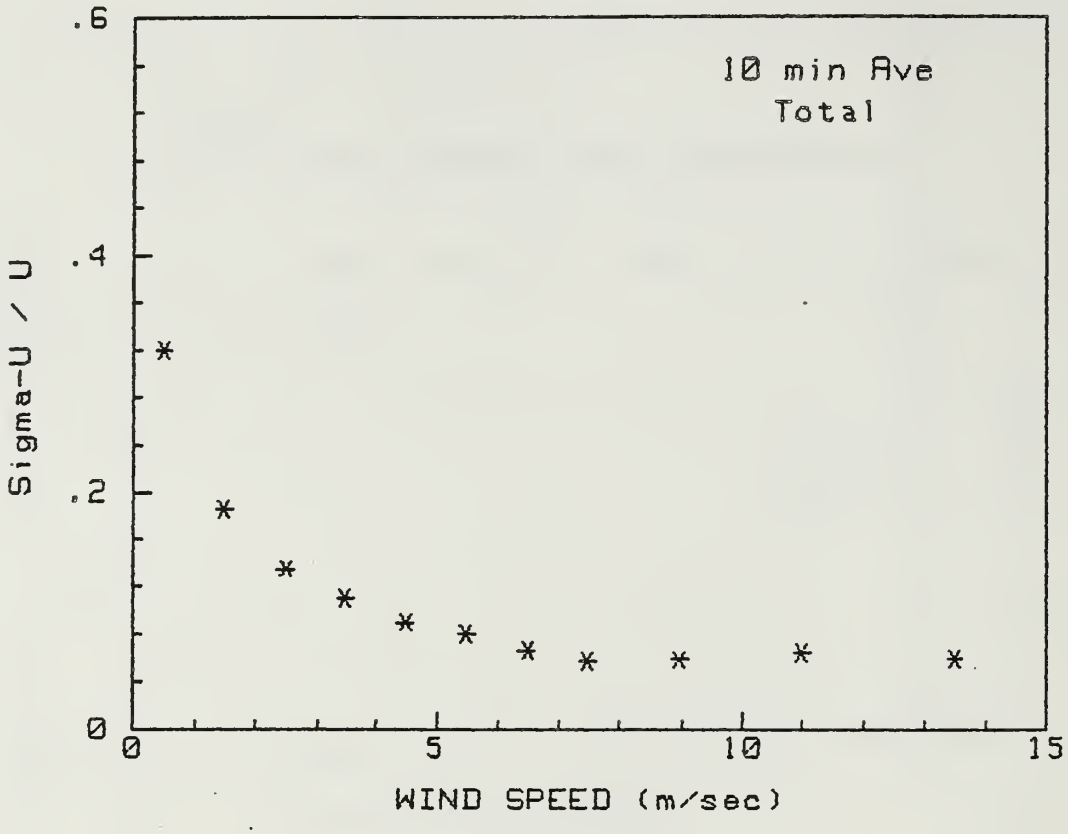

U	#	SIGMA	Std Dev
.5	10	.319	.038
1.5	77	.184	.004
2.5	102	.134	.002
3.5	91	.109	.001
4.5	89	.089	.001
5.5	56	.079	.001
6.5	60	.065	.001
7.5	43	.056	.001
9.0	30	.058	.001
11.0	17	.064	.001
13.5	14	.058	.001

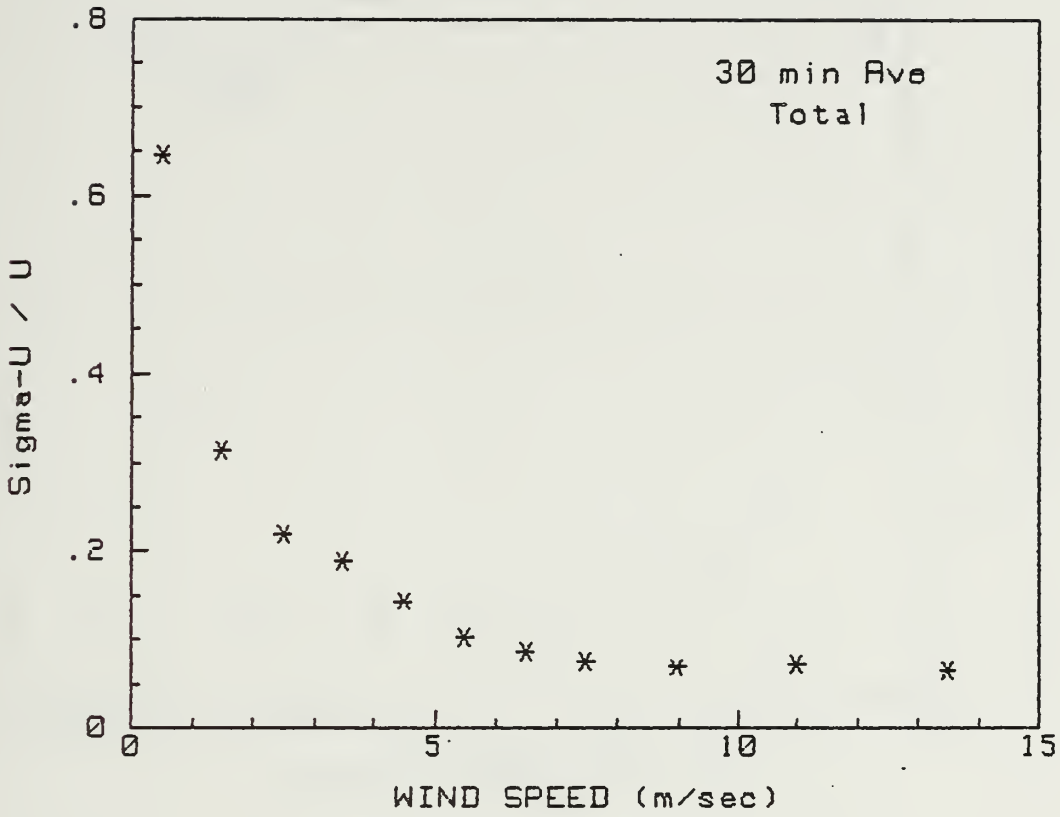

U	#	SIGMA	Std Dev
.5	10	.645	.187
1.5	71	.312	.016
2.5	86	.218	.006
3.5	79	.187	.005
4.5	71	.141	.003
5.5	52	.100	.002
6.5	52	.085	.001
7.5	36	.073	.001
9.0	29	.067	.001
11.0	17	.071	.001
13.5	13	.064	.001

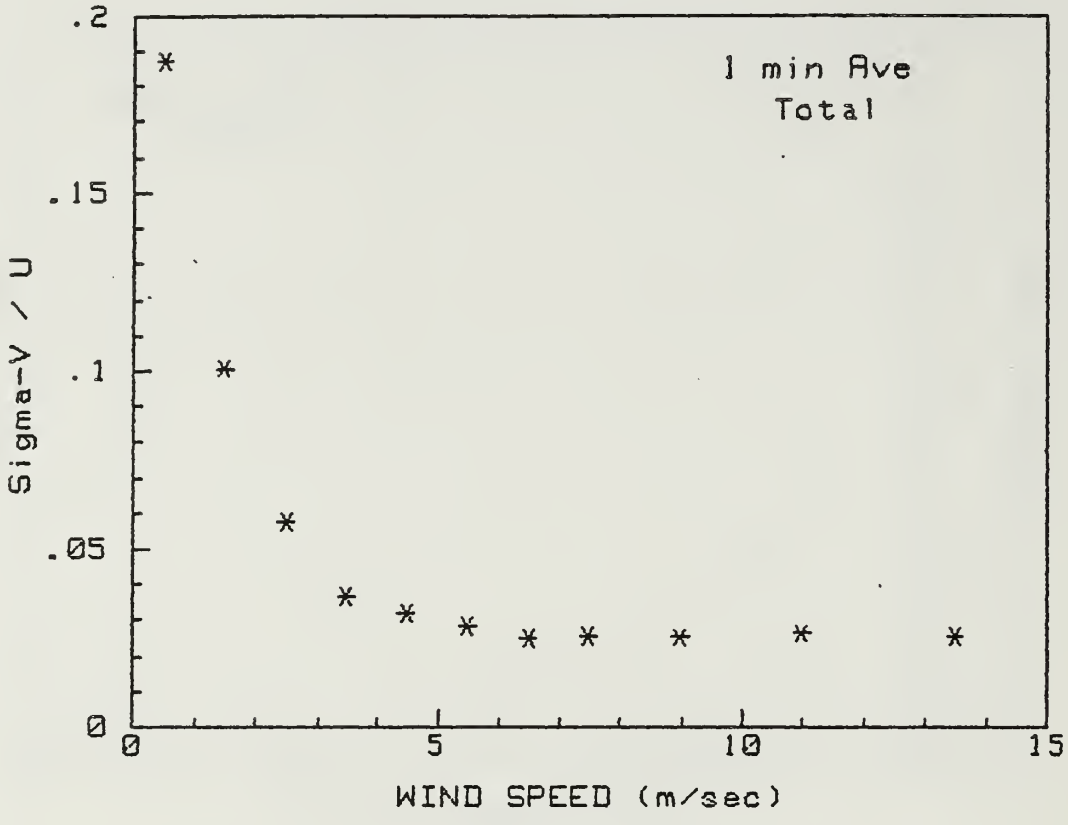

U	#	SIGMA	Std Dev
.5	10	.187	.013
1.5	77	.100	.001
2.5	102	.057	0.000
3.5	91	.036	0.000
4.5	89	.032	0.000
5.5	56	.028	0.000
6.5	60	.025	0.000
7.5	43	.025	0.000
9.0	30	.025	0.000
11.0	17	.026	0.000
13.5	14	.025	0.000

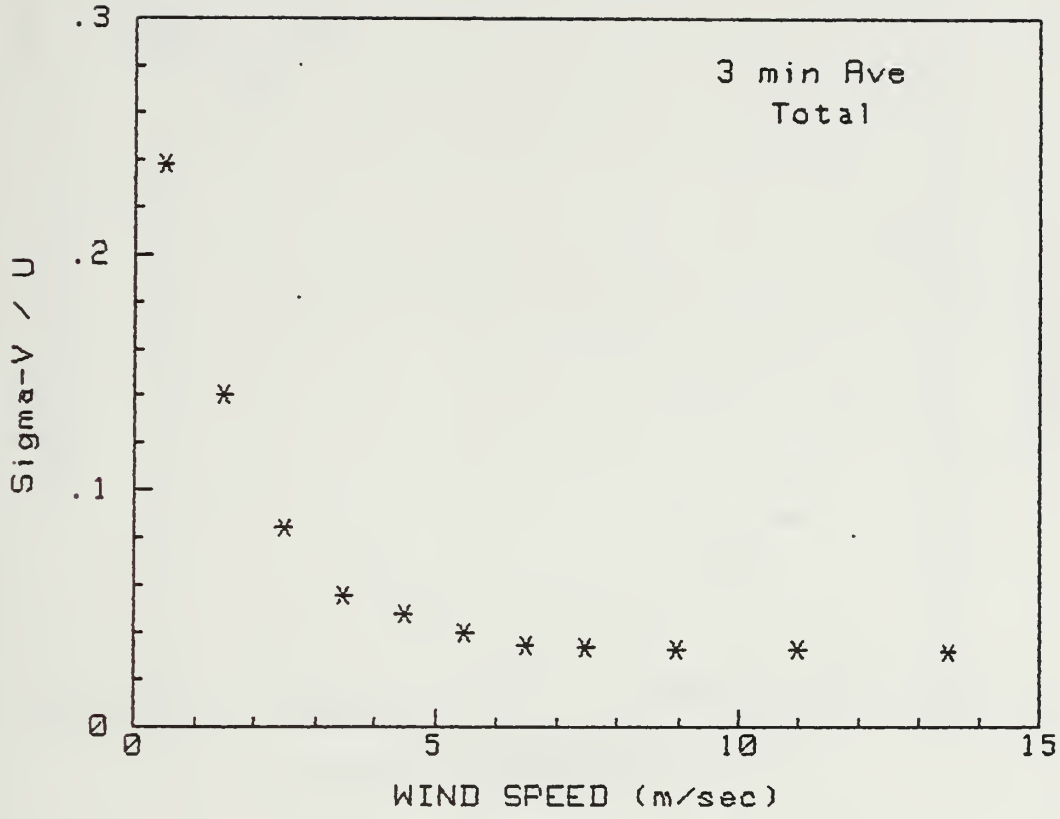

U	#	SIGMA	Std Dev
.5	10	.237	.021
1.5	77	.140	.003
2.5	102	.084	.001
3.5	91	.056	0.000
4.5	89	.048	0.000
5.5	56	.040	0.000
6.5	60	.034	0.000
7.5	43	.034	0.000
9.0	30	.033	0.000
11.0	17	.033	0.000
13.5	14	.031	0.000

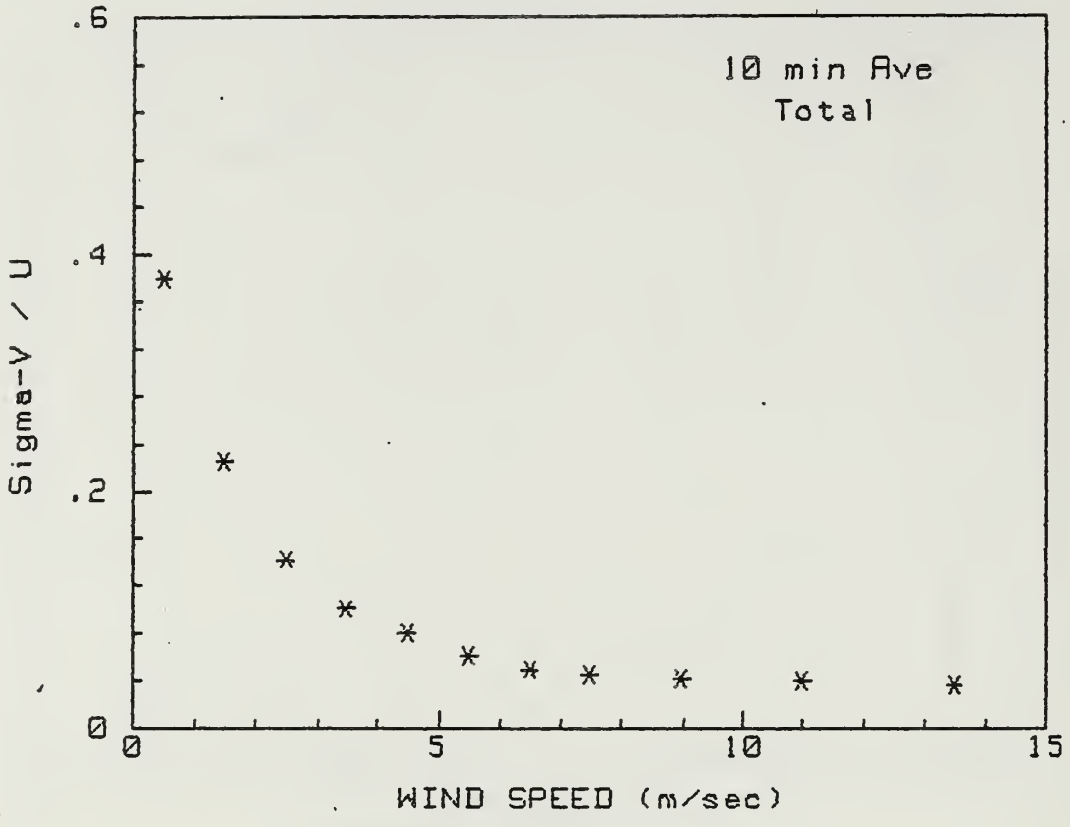

U	#	SIGMA	Std Dev
.5	10	.377	.055
1.5	77	.224	.007
2.5	102	.141	.002
3.5	91	.100	.001
4.5	89	.079	.001
5.5	56	.061	.001
6.5	60	.049	0.000
7.5	43	.044	0.000
9.0	30	.041	0.000
11.0	17	.039	0.000
13.5	14	.035	0.000

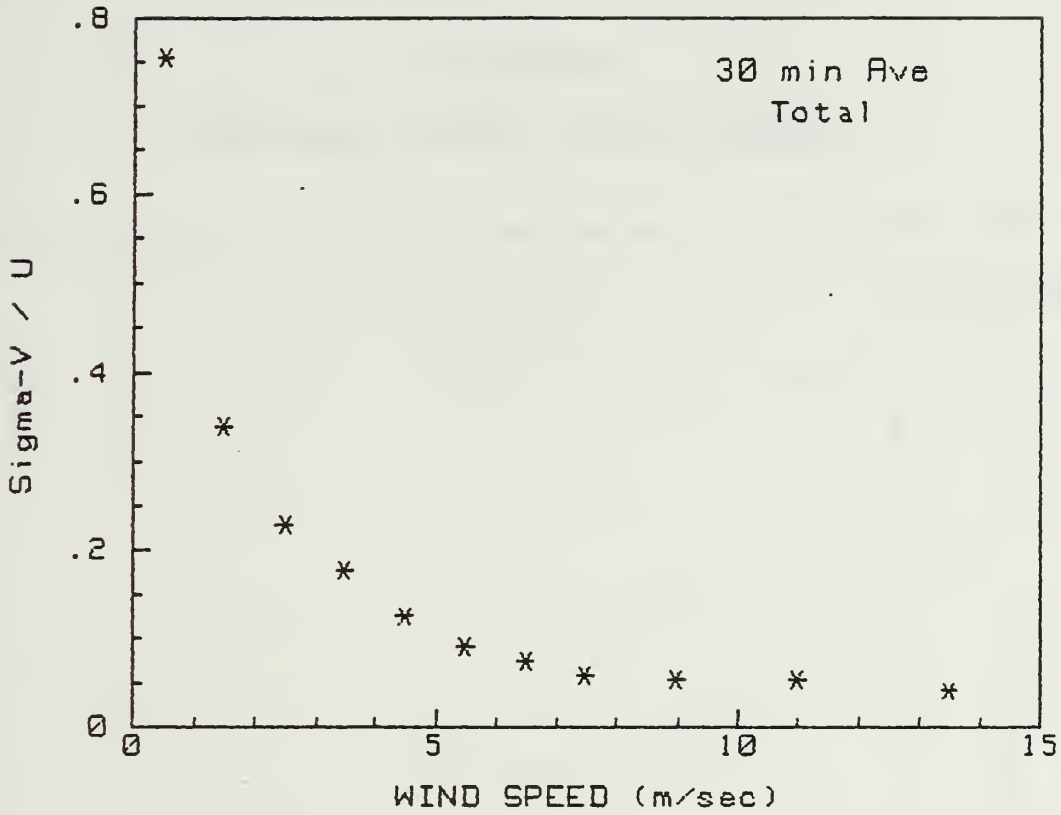

U	#	SIGMA	Std Dev
.5	10	.754	.237
1.5	71	.339	.017
2.5	86	.227	.007
3.5	79	.175	.004
4.5	71	.123	.002
5.5	52	.090	.001
6.5	52	.074	.001
7.5	36	.056	.001
9.0	29	.053	.001
11.0	17	.051	.001
13.5	13	.040	0.000

APPENDIX C

AVERAGED PLOTS, STABLE CONDITIONS

The following are averaged BLM data during only stable conditions.

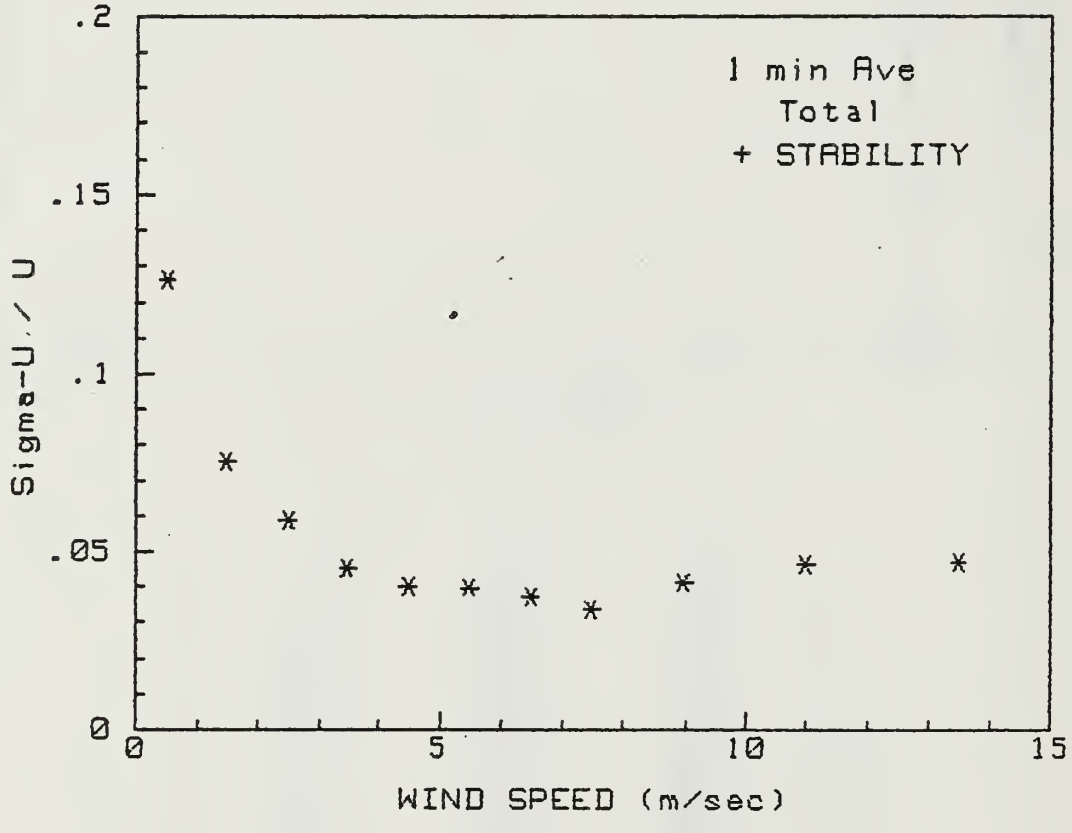

U	#	SIGMA	Std Dev
.5	7	.126	.007
1.5	40	.075	.001
2.5	60	.058	0.000
3.5	60	.045	0.000
4.5	61	.040	0.000
5.5	38	.039	0.000
6.5	52	.037	0.000
7.5	31	.033	0.000
9.0	23	.041	0.000
11.0	15	.046	.001
13.5	13	.047	.001

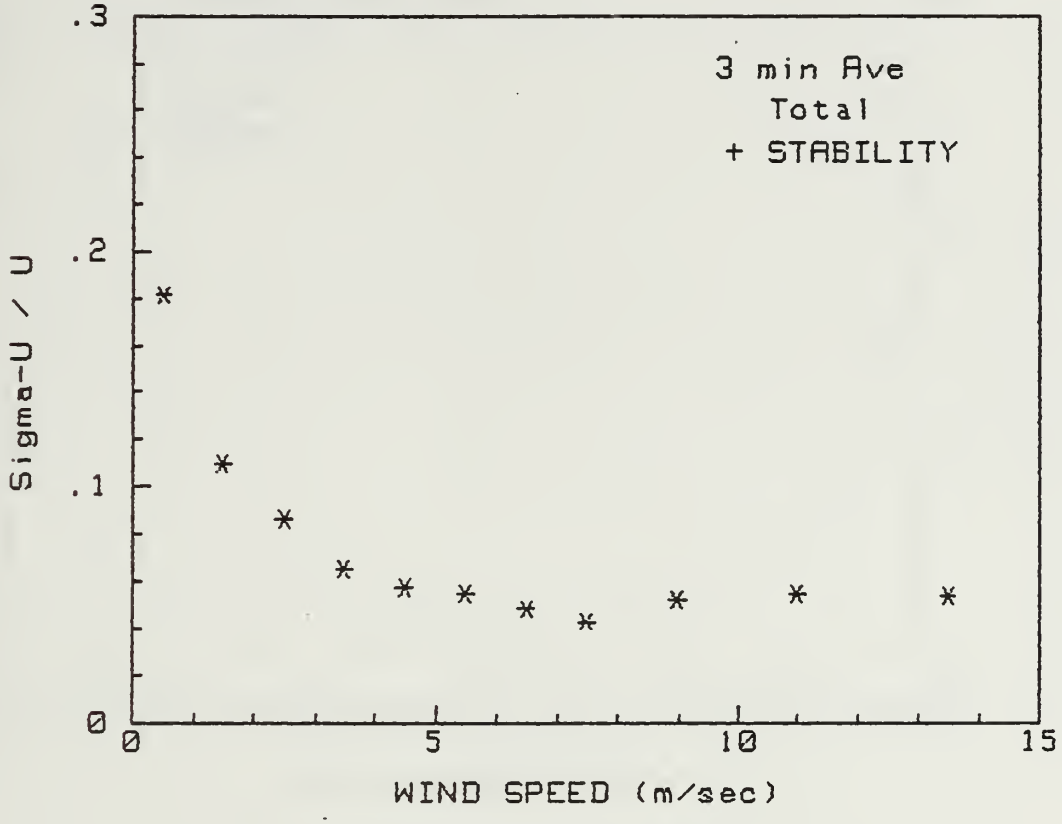

U	#	SIGMA	Std Dev
.5	7	.180	.016
1.5	40	.109	.002
2.5	60	.086	.001
3.5	60	.065	.001
4.5	61	.057	0.000
5.5	38	.054	.001
6.5	52	.048	0.000
7.5	31	.043	0.000
9.0	23	.052	.001
11.0	15	.055	.001
13.5	13	.053	.001

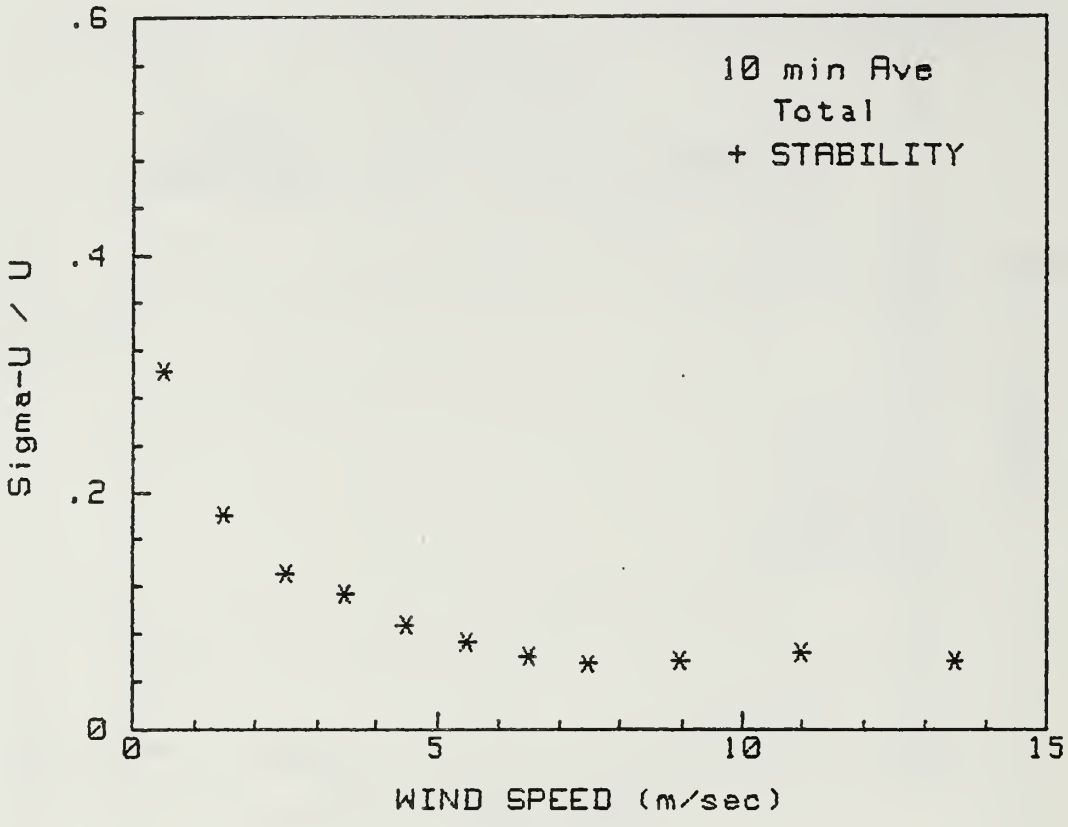

U	#	SIGMA	Std Dev
.5	7	.301	.044
1.5	40	.180	.006
2.5	60	.130	.002
3.5	60	.113	.002
4.5	61	.086	.001
5.5	38	.073	.001
6.5	52	.061	.001
7.5	31	.054	.001
9.0	23	.057	.001
11.0	15	.063	.001
13.5	13	.056	.001

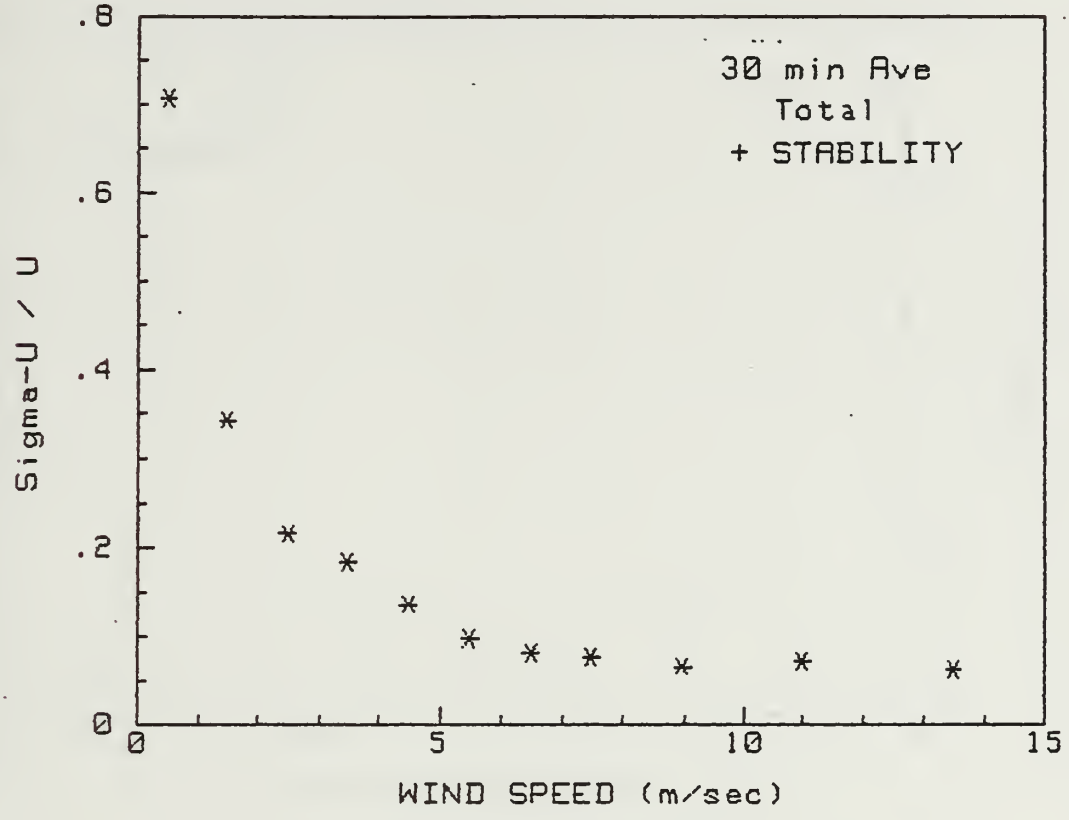

U	#	SIGMA	Std Dev
.5	7	.705	.281
1.5	36	.341	.029
2.5	46	.214	.008
3.5	48	.182	.005
4.5	45	.135	.003
5.5	35	.096	.002
6.5	44	.080	.001
7.5	24	.076	.001
9.0	22	.065	.001
11.0	15	.071	.001
13.5	12	.062	.001

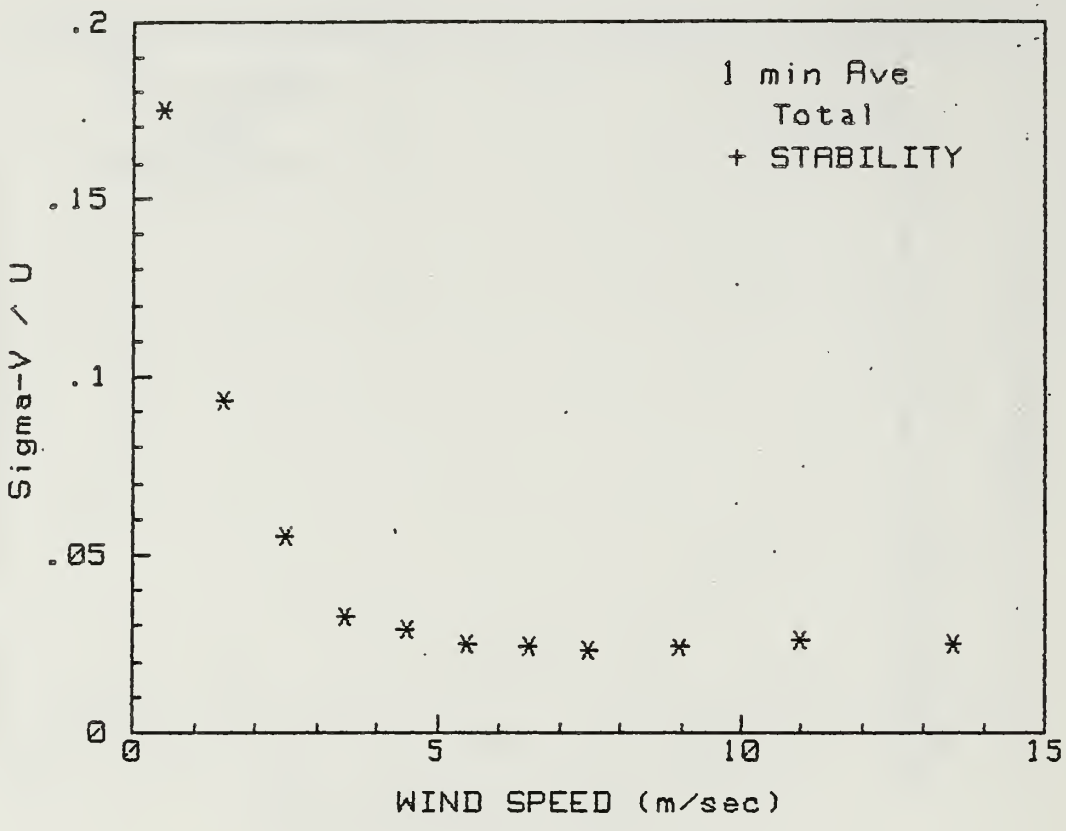

U	#	SIGMA	Std Dev
.5	7	.175	.015
1.5	40	.093	.002
2.5	60	.055	0.000
3.5	60	.032	0.000
4.5	61	.029	0.000
5.5	38	.025	0.000
6.5	52	.024	0.000
7.5	31	.023	0.000
9.0	23	.024	0.000
11.0	15	.026	0.000
13.5	13	.025	0.000

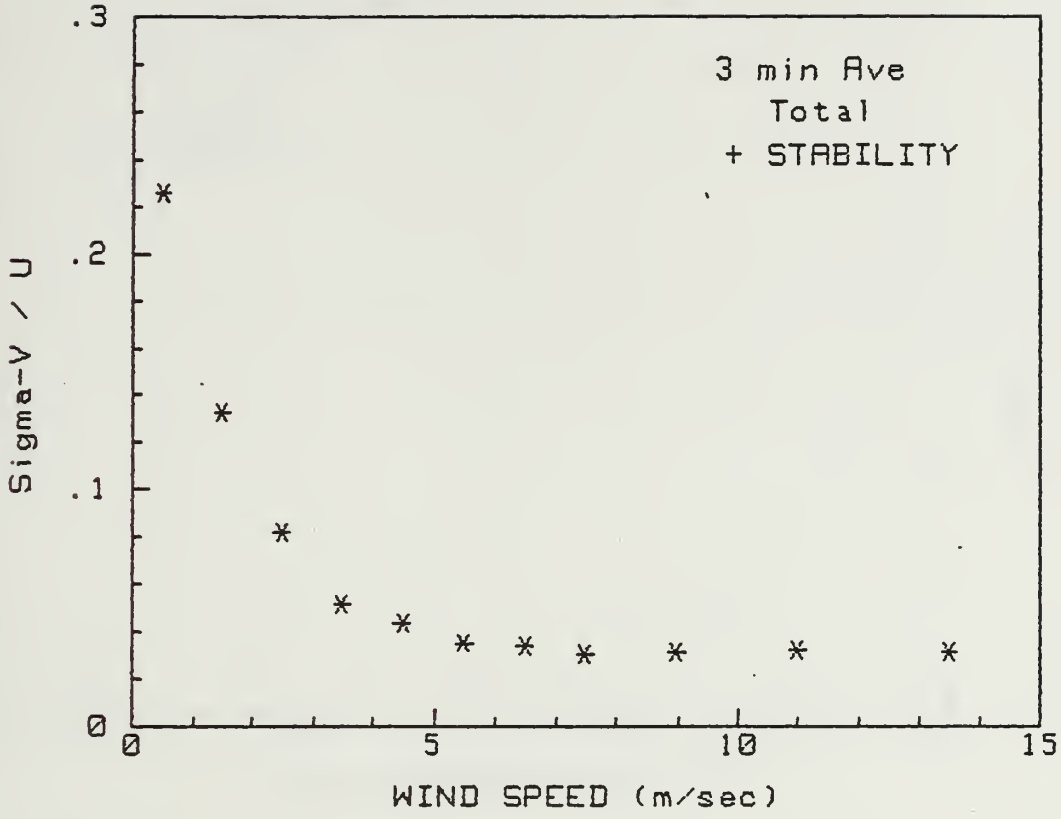

U	#	SIGMA	Std Dev
.5	7	.225	.024
1.5	40	.132	.003
2.5	60	.082	.001
3.5	60	.051	0.000
4.5	61	.043	0.000
5.5	38	.035	0.000
6.5	52	.033	0.000
7.5	31	.030	0.000
9.0	23	.031	0.000
11.0	15	.032	0.000
13.5	13	.031	0.000

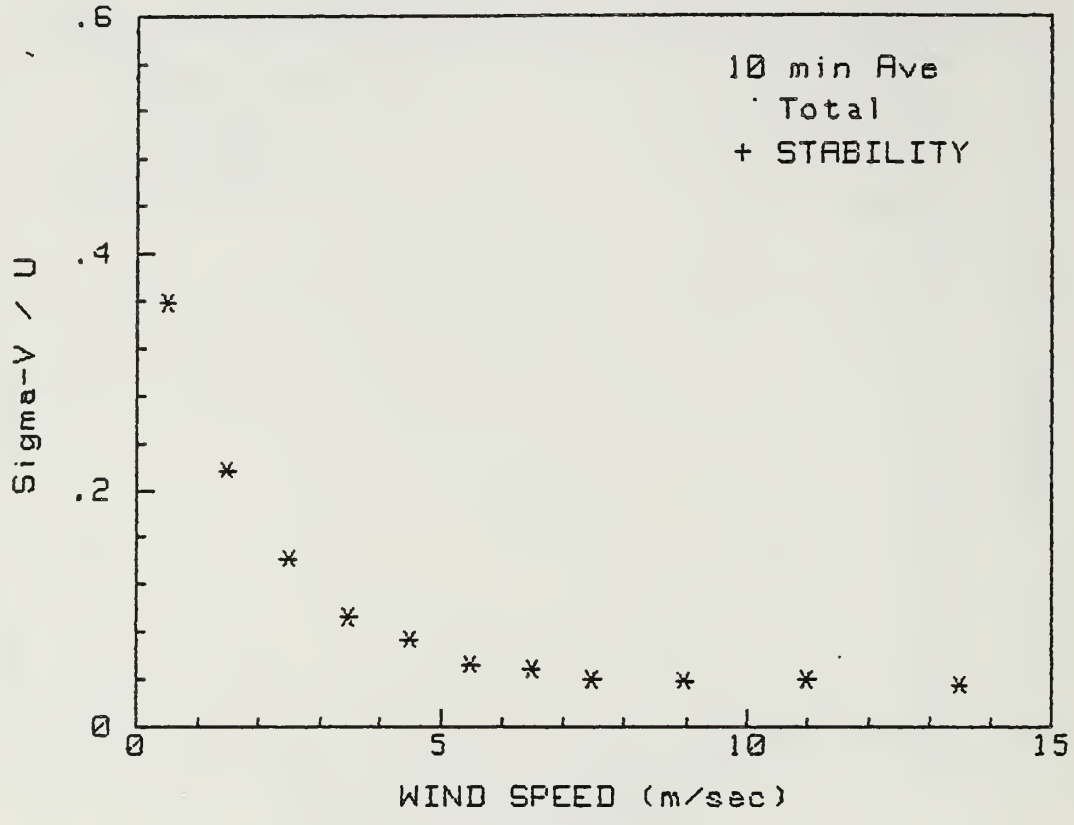

U	#	SIGMA	Std Dev
.5	7	.357	.064
1.5	40	.216	.009
2.5	60	.141	.003
3.5	60	.092	.001
4.5	61	.073	.001
5.5	38	.052	.001
6.5	52	.048	0.000
7.5	31	.040	0.000
9.0	23	.038	0.000
11.0	15	.039	0.000
13.5	13	.035	0.000

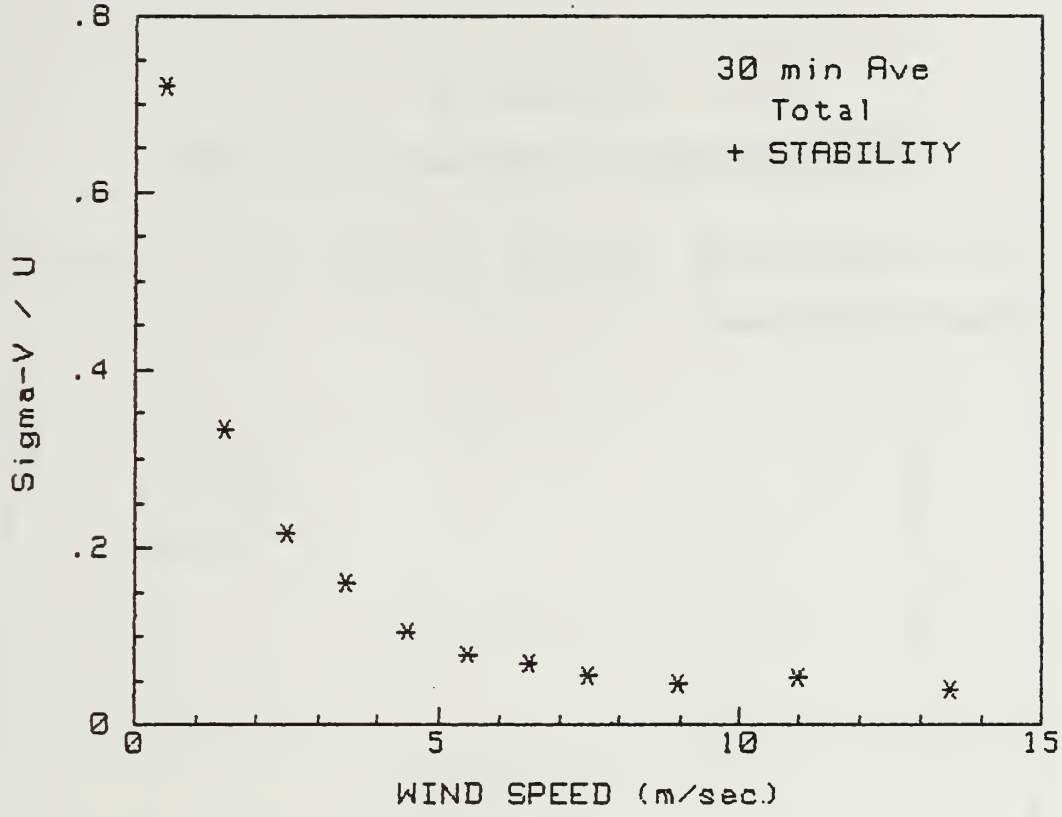

U	#	SIGMA	Std Dev
.5	7	.719	.276
1.5	36	.330	.022
2.5	46	.215	.008
3.5	48	.160	.005
4.5	45	.104	.002
5.5	35	.079	.001
6.5	44	.069	.001
7.5	24	.054	.001
9.0	22	.046	0.000
11.0	15	.053	.001
13.5	12	.039	0.000

APPENDIX D

AVERAGED PLOTS, STATIONARY CONDITIONS

The following are averaged BLM data plots during only stationary conditions.

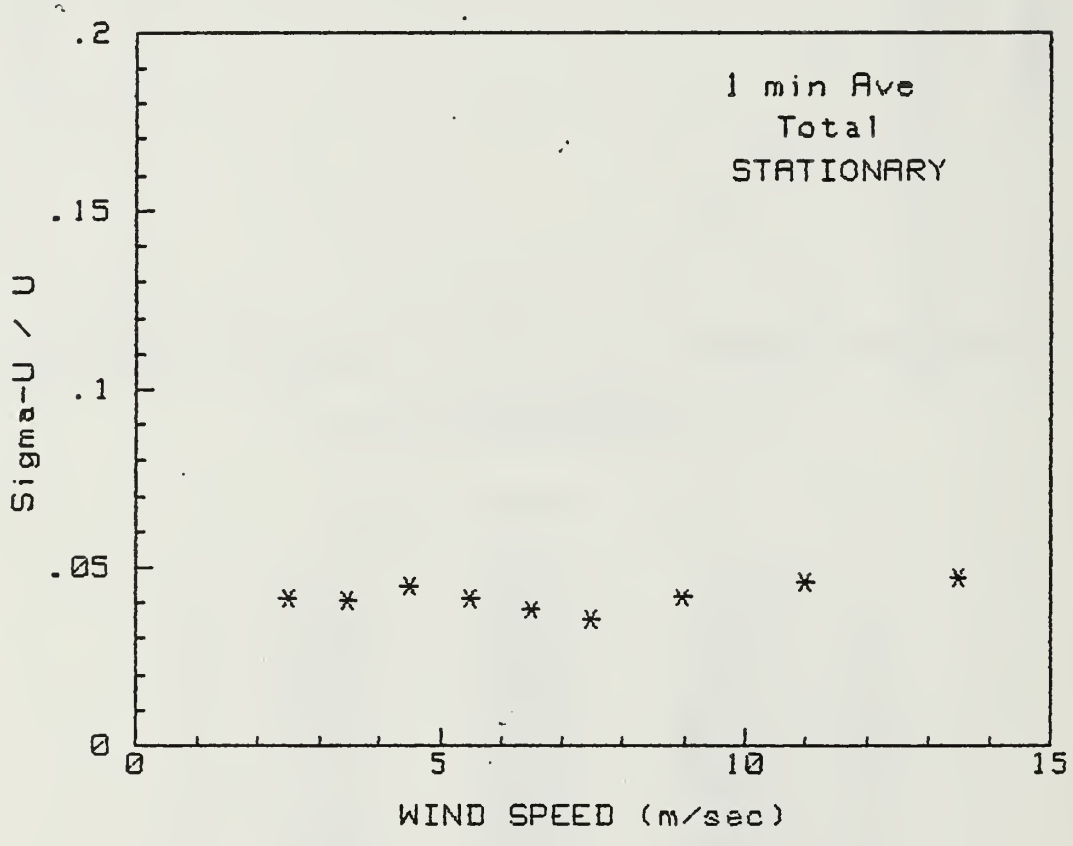

U	#	SIGMA	Std Dev
.5	0	0.000	0.000
1.5	0	0.000	0.000
2.5	2	.041	.002
3.5	7	.041	.001
4.5	17	.045	.001
5.5	20	.041	0.000
6.5	39	.038	0.000
7.5	30	.035	0.000
9.0	27	.041	0.000
11.0	15	.045	.001
13.5	13	.047	.001

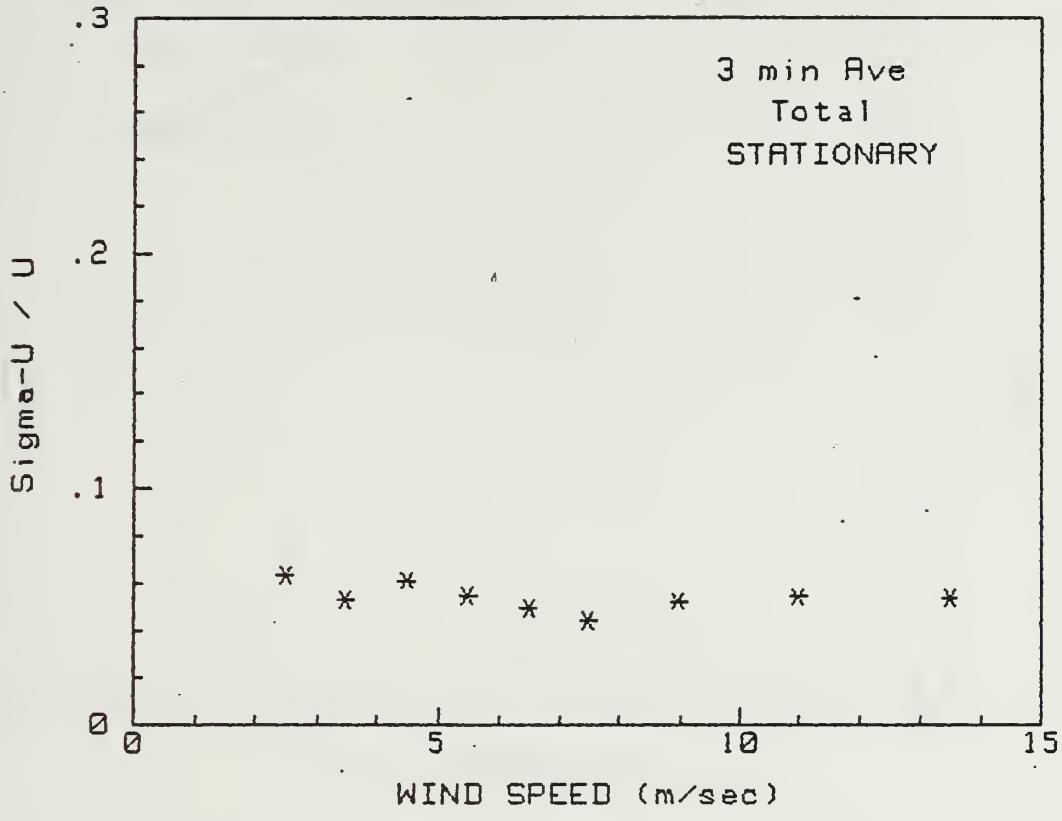

U	#	SIGMA	Std Dev
.5	0	0.000	0.000
1.5	0	0.000	0.000
2.5	2	.063	.004
3.5	7	.052	.001
4.5	17	.061	.001
5.5	20	.055	.001
6.5	39	.049	0.000
7.5	30	.044	0.000
9.0	27	.052	.001
11.0	15	.054	.001
13.5	13	.053	.001

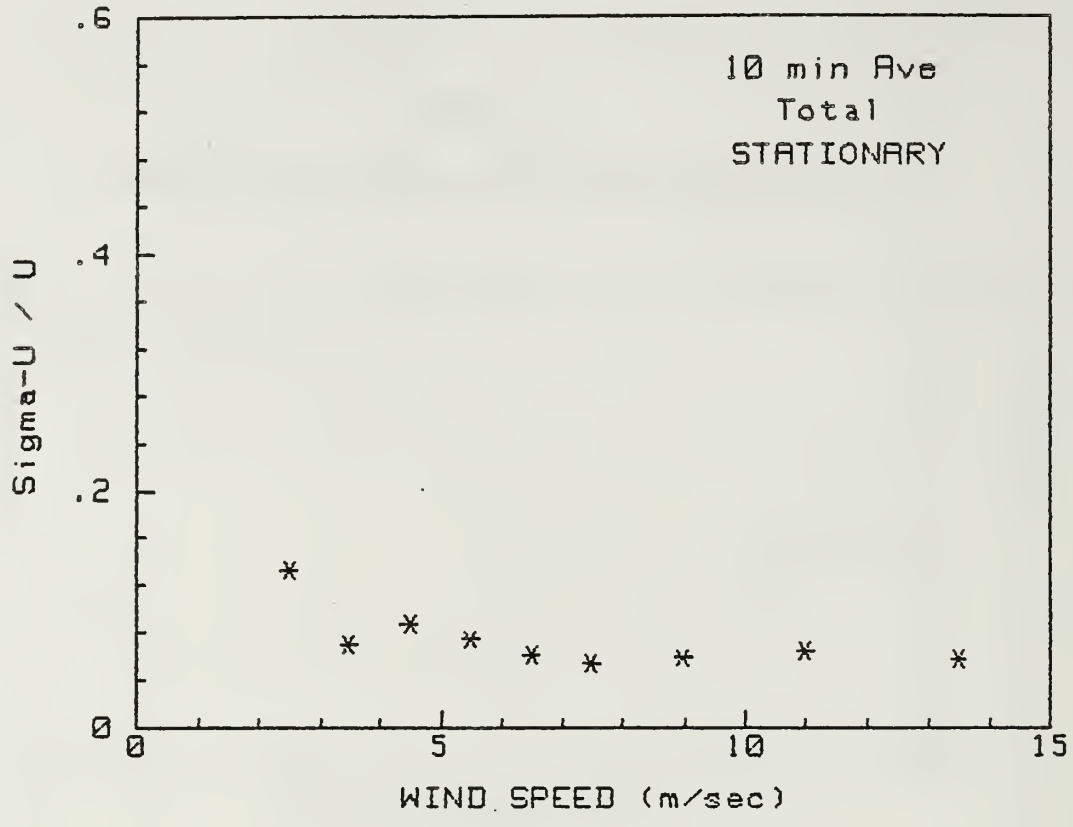

U	#	SIGMA	Std Dev
.5	0	0.000	0.000
1.5	0	0.000	0.000
2.5	2	.132	.018
3.5	7	.069	.002
4.5	17	.087	.002
5.5	20	.073	.001
6.5	39	.060	.001
7.5	30	.053	.001
9.0	27	.058	.001
11.0	15	.063	.001
13.5	13	.056	.001

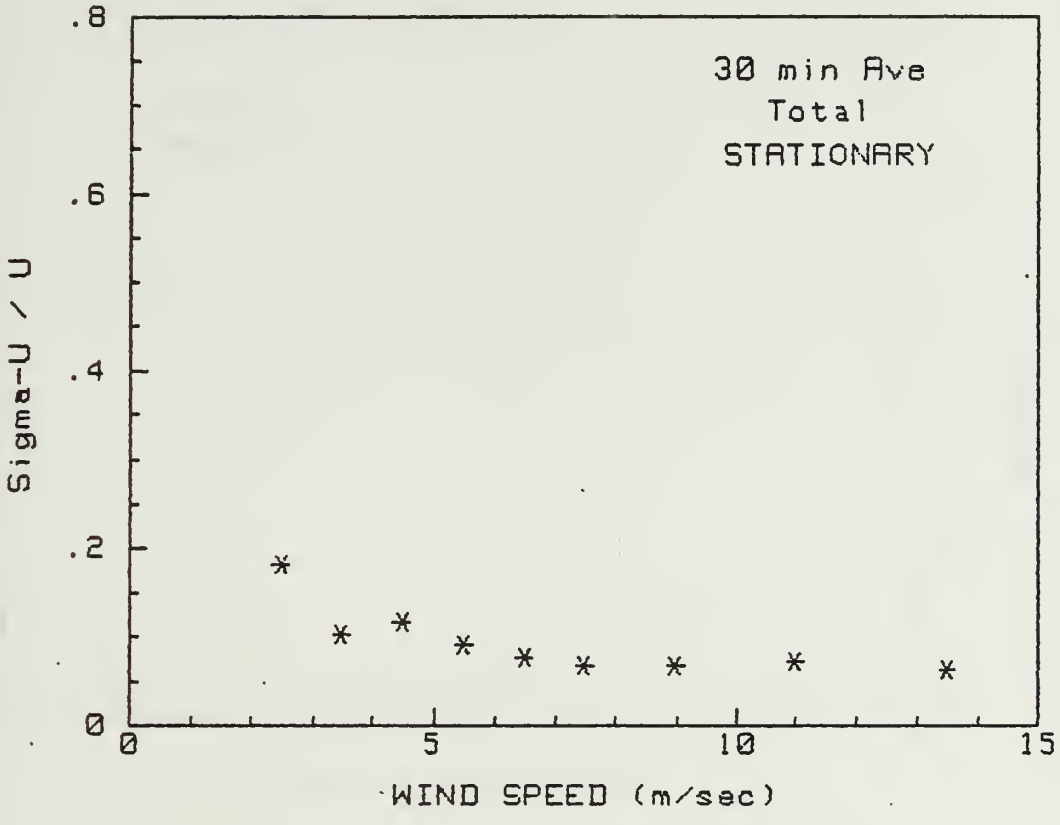

U	#	SIGMA	Std Dev
.5	0	0.000	0.000
1.5	0	0.000	0.000
2.5	2	.179	.033
3.5	6	.101	.005
4.5	15	.115	.004
5.5	20	.089	.002
6.5	38	.075	.001
7.5	27	.066	.001
9.0	27	.067	.001
11.0	15	.070	.001
13.5	12	.062	.001

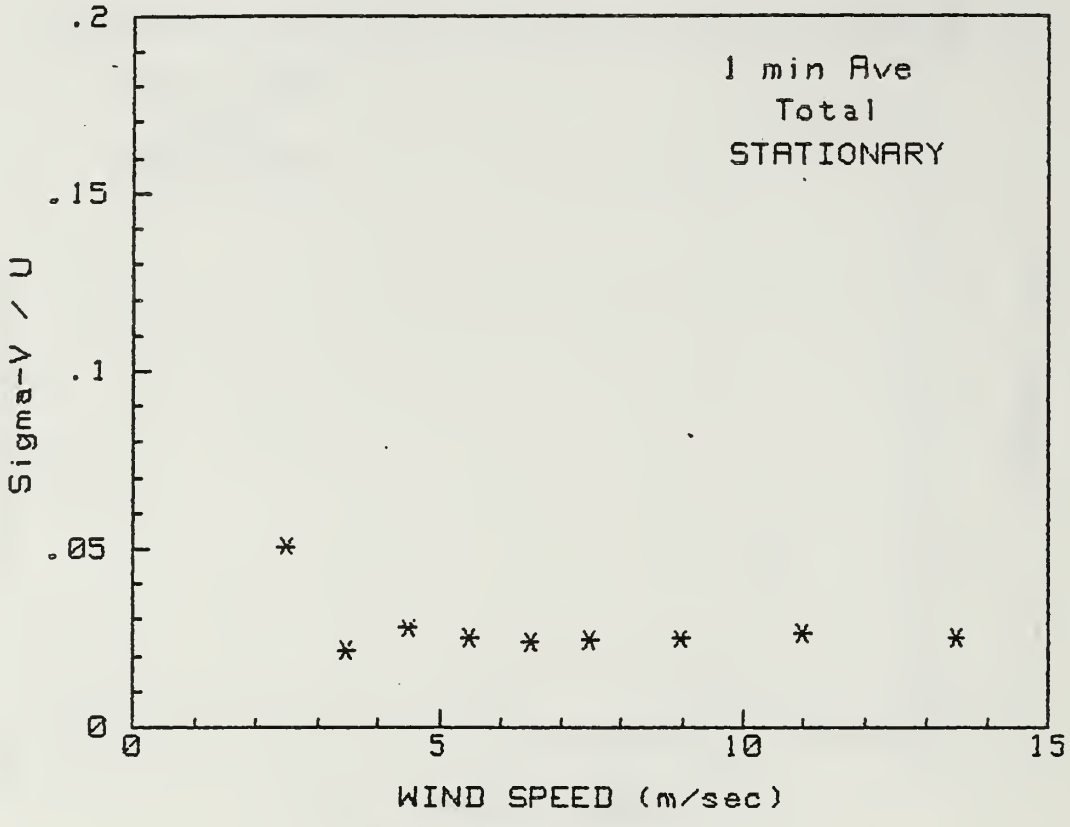

U	#	SIGMA	Std Dev
.5	0	0.000	0.000
1.5	0	0.000	0.000
2.5	2	.051	.003
3.5	7	.021	0.000
4.5	17	.027	0.000
5.5	20	.024	0.000
6.5	39	.024	0.000
7.5	30	.024	0.000
9.0	27	.024	0.000
11.0	15	.026	0.000
13.5	13	.025	0.000

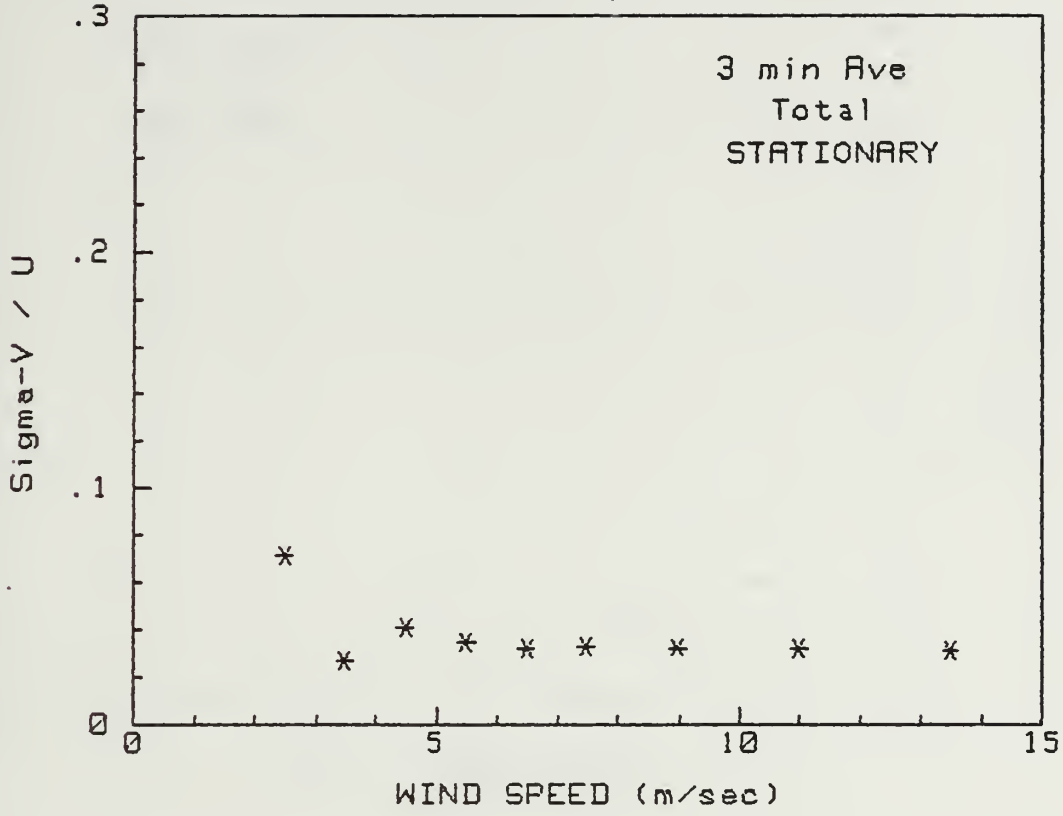

U	#	SIGMA	Std Dev
.5	0	0.000	0.000
1.5	0	0.000	0.000
2.5	2	.071	.005
3.5	7	.026	0.000
4.5	17	.040	0.000
5.5	20	.034	0.000
6.5	39	.032	0.000
7.5	30	.033	0.000
9.0	27	.032	0.000
11.0	15	.032	0.000
13.5	13	.031	0.000

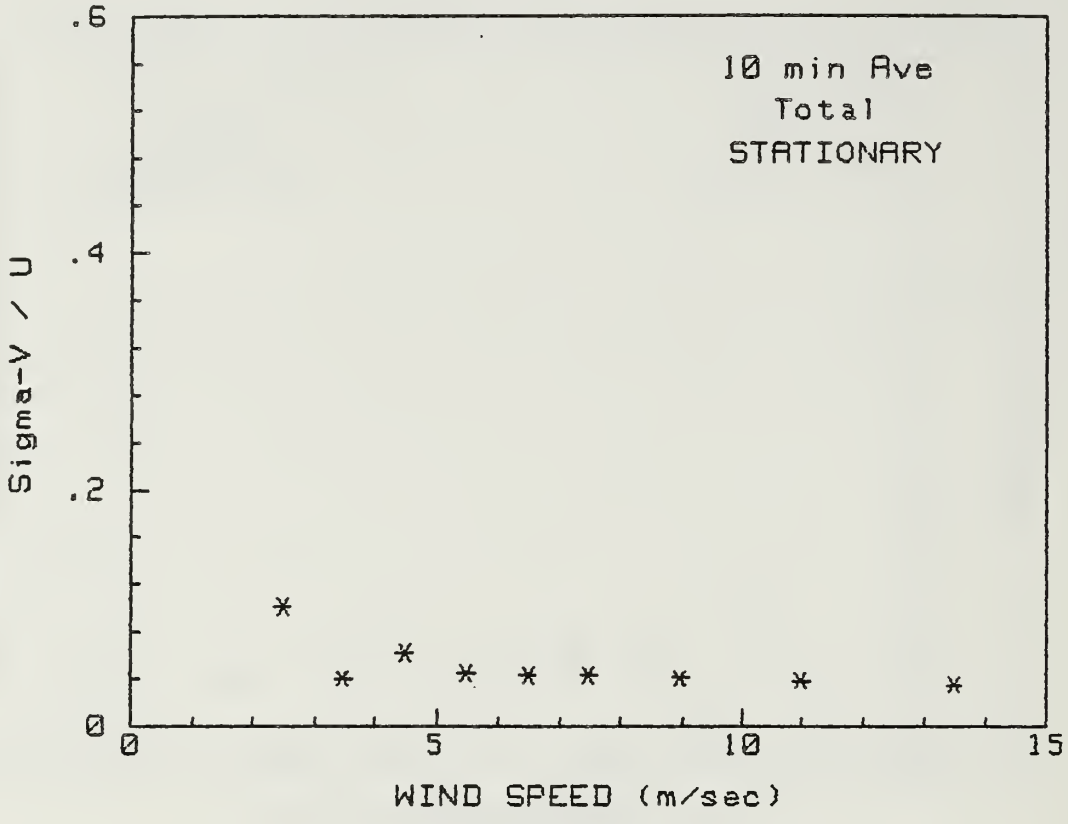

U	#	SIGMA	Std Dev
.5	0	0.000	0.000
1.5	0	0.000	0.000
2.5	2	.100	.011
3.5	7	.040	.001
4.5	17	.062	.001
5.5	20	.045	0.000
6.5	39	.043	0.000
7.5	30	.043	0.000
9.0	27	.040	0.000
11.0	15	.038	0.000
13.5	13	.035	0.000

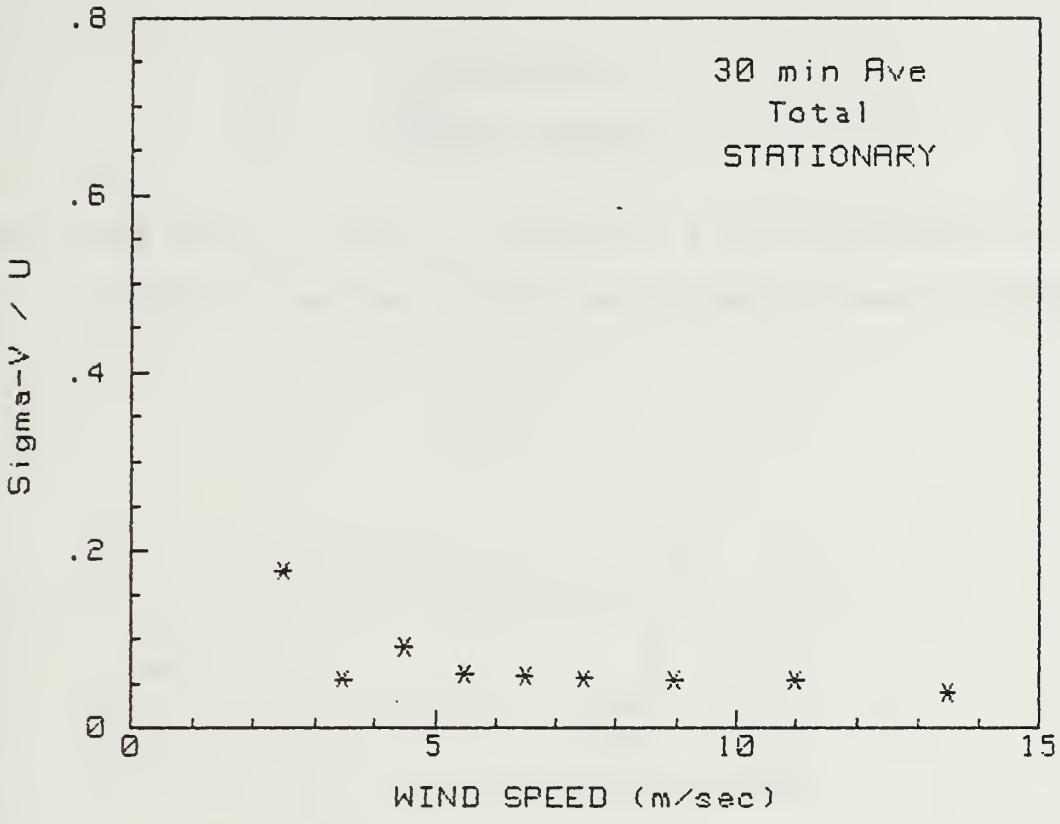

U	#	SIGMA	Std Dev
.5	0	0.000	0.000
1.5	0	0.000	0.000
2.5	2	.175	.031
3.5	6	.053	.001
4.5	15	.090	.002
5.5	20	.059	.001
6.5	38	.057	.001
7.5	27	.054	.001
9.0	27	.053	.001
11.0	15	.052	.001
13.5	12	.039	0.000

APPENDIX E

FITTING CURVES

The following are empirical fitting curves for stable, stationary and unrestricted conditions for BLM data.

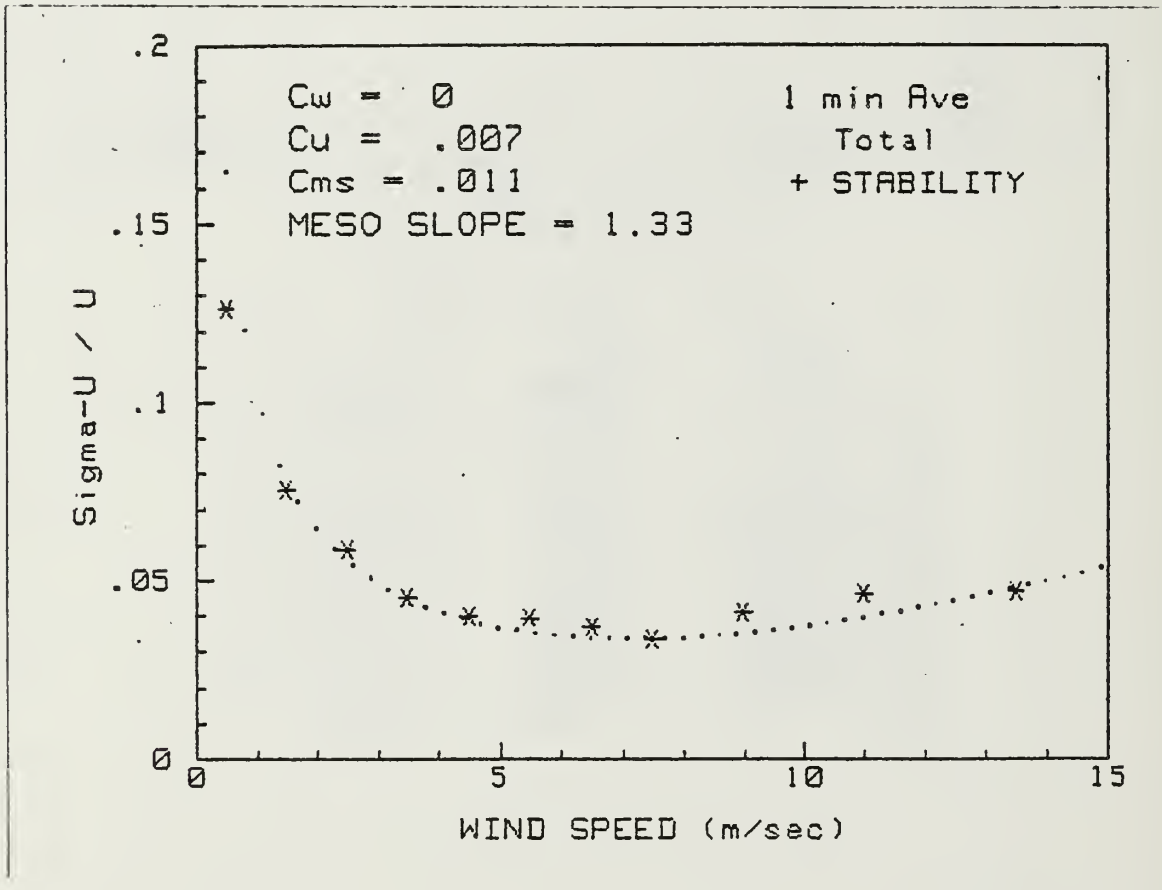

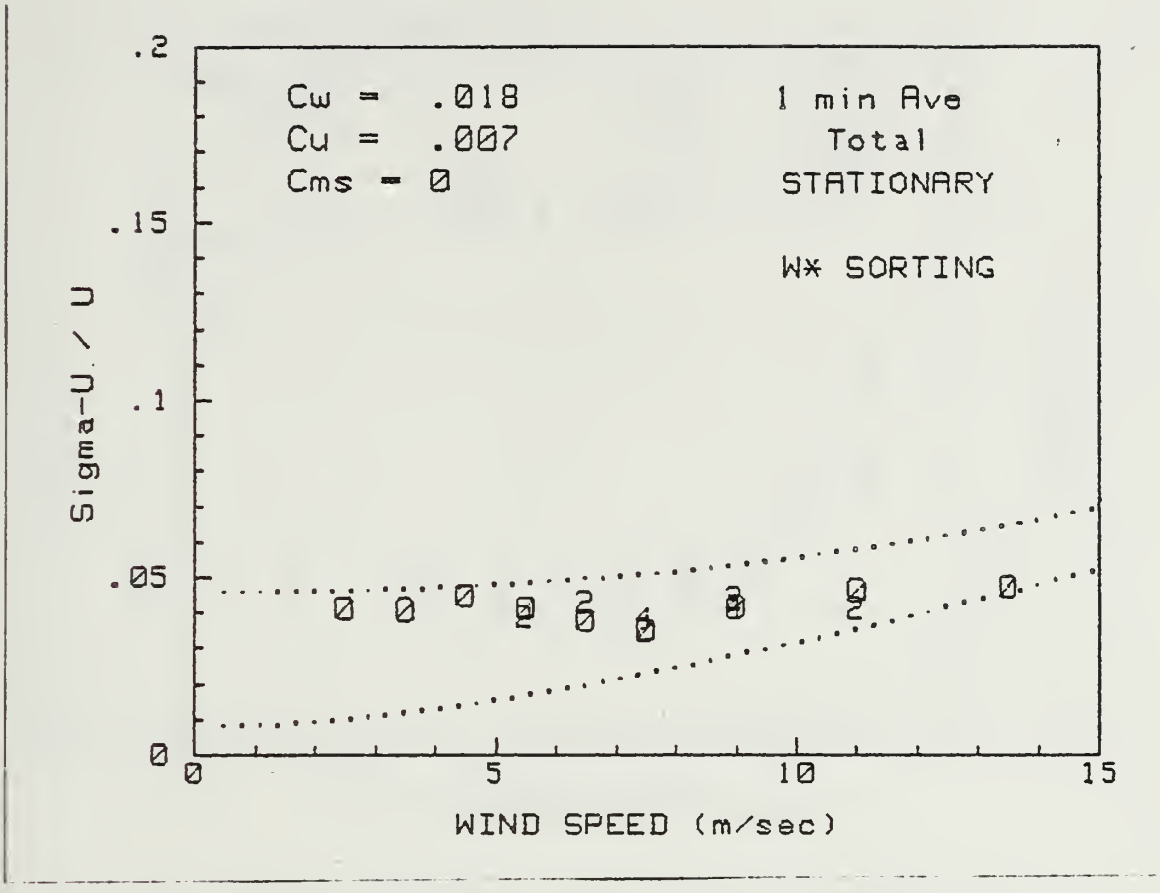
Cw = .018
Cu = .007
Cms = 0
1 min Ave
Total
STATIONARY
W* SORTING
Sigma-U / U
.2
.15
.1
.05
0
0
5
10
15
WIND SPEED (m/sec)

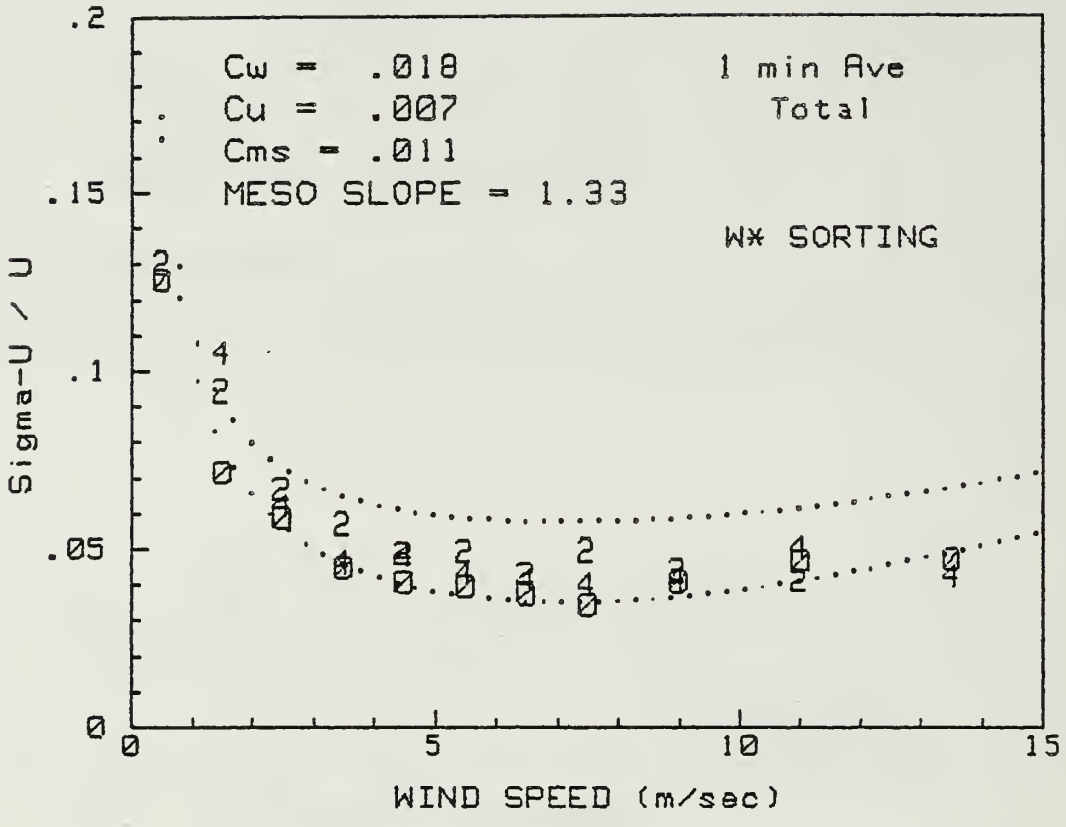
Cw = .018
Cu = .007
Cms = .011
MESO SLOPE = 1.33
1 min Ave
Total
W* SORTING
Sigma-U / U
WIND SPEED (m/sec)
0
.05
.1
.15
.2
5
10
15

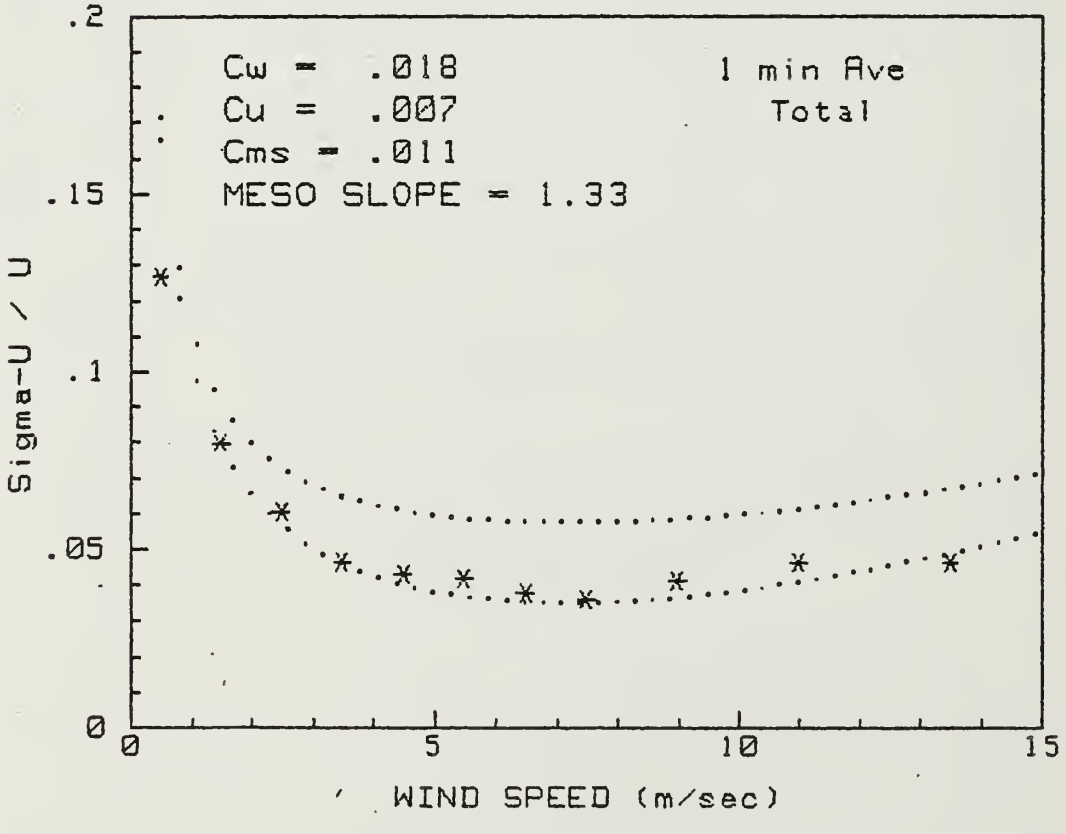
Cw = .018
Cu = .007
Cms = .011
MESO SLOPE = 1.33
1 min Ave
Total
Sigma-U / U
WIND SPEED (m/sec)
0
.05
.1
.15
.2
5
10
15

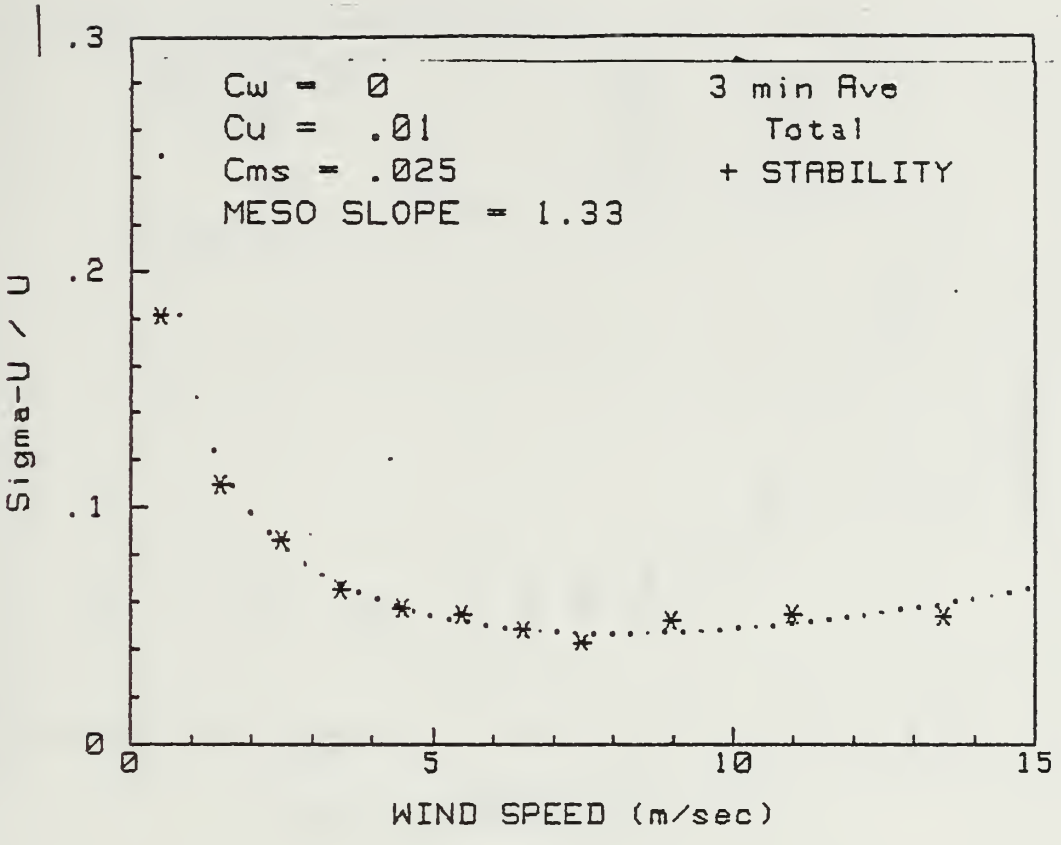
Cw = 0
Cu = .01
Cms = .025
MESO SLOPE = 1.33
3 min Ave
Total
+ STABILITY
Sigma-U / U
.3
.2
.1
0
0
5
10
15
WIND SPEED (m/sec)

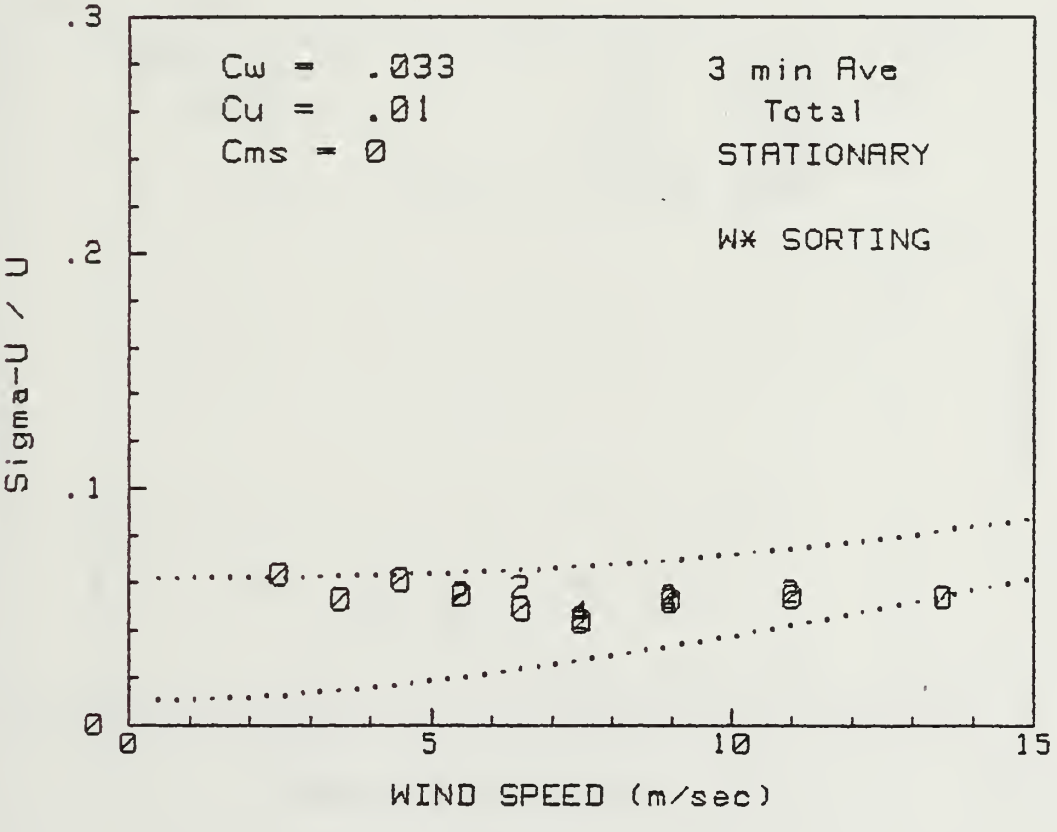
Cw = .033
Cu = .01
Cms = 0
3 min Ave
Total
STATIONARY
W* SORTING
Sigma-U / U
.3
.2
.1
0
0
5
10
15
WIND SPEED (m/sec)

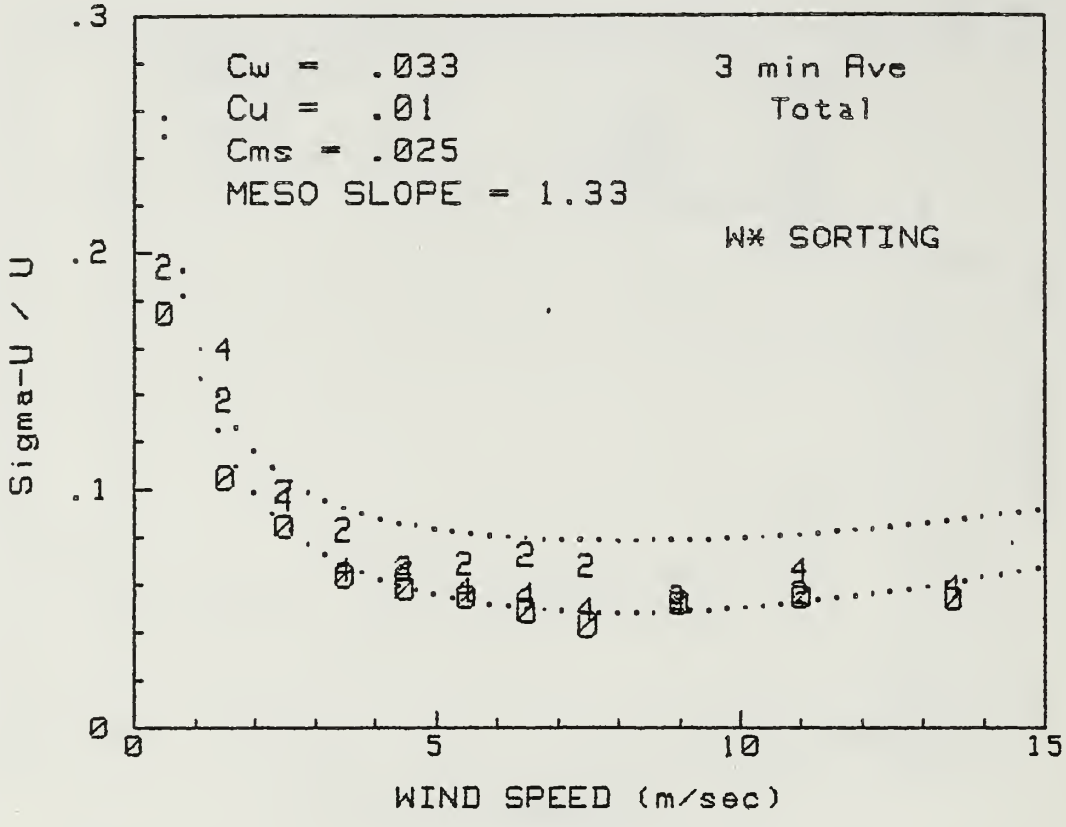
Cw = .033
Cu = .01
Cms = .025
MESO SLOPE = 1.33
3 min Ave
Total
W* SORTING
Sigma-U / U
WIND SPEED (m/sec)
0
.1
.2
.3
5
10
15

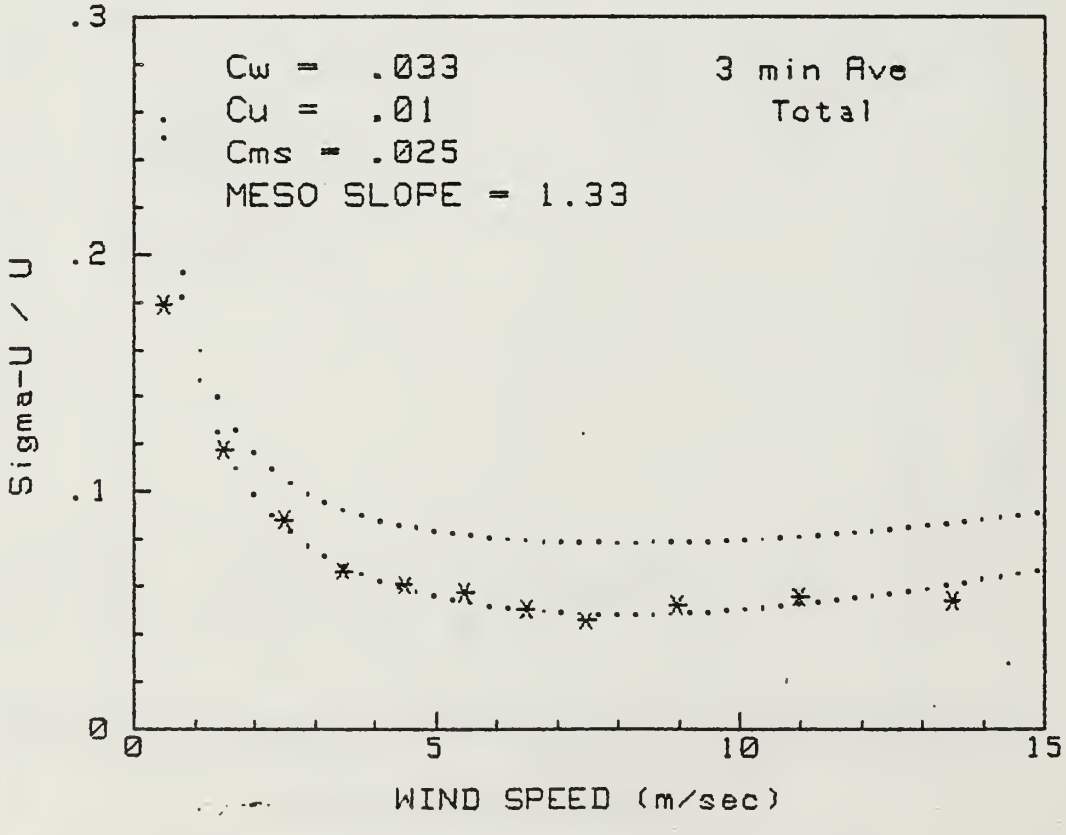
Cw = .033
Cu = .01
Cms = .025
MESO SLOPE = 1.33
3 min Ave
Total
Sigma-U / U
WIND SPEED (m/sec)
0
.1
.2
.3
5
10
15

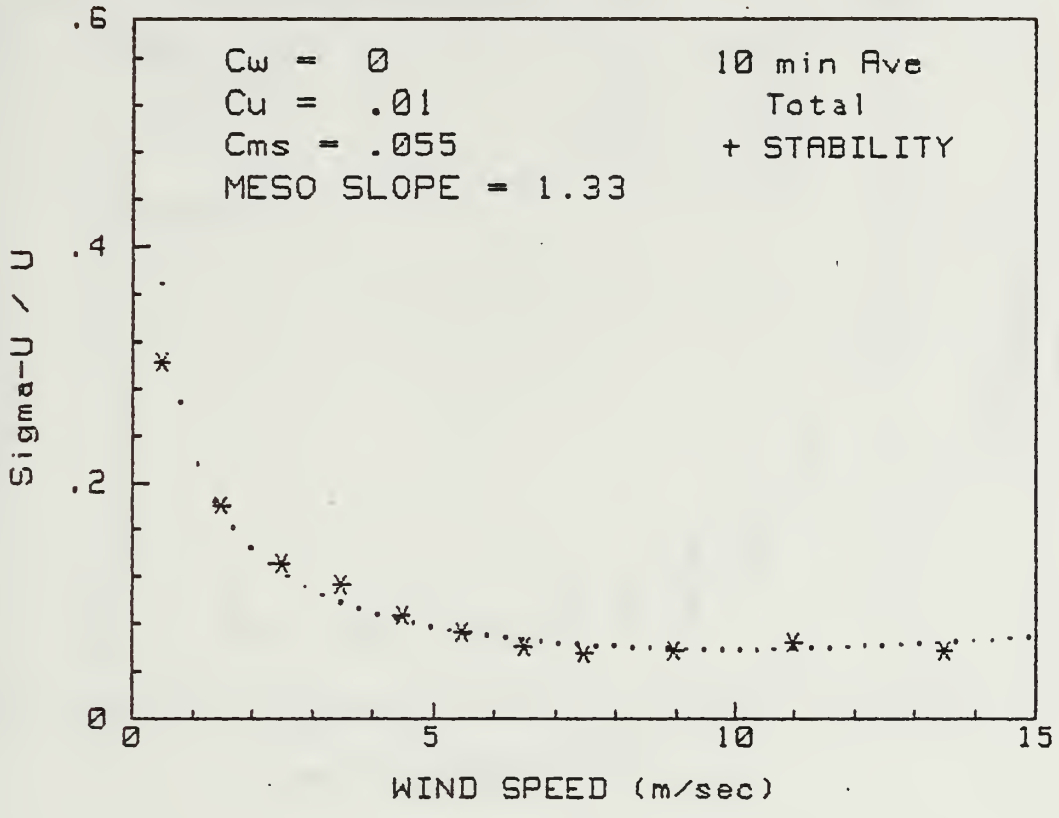
Cw = 0
Cu = .01
Cms = .055
MESO SLOPE = 1.33
10 min Ave
Total
+ STABILITY
Sigma-U / U
.6
.4
.2
0
0
5
10
15
WIND SPEED (m/sec)

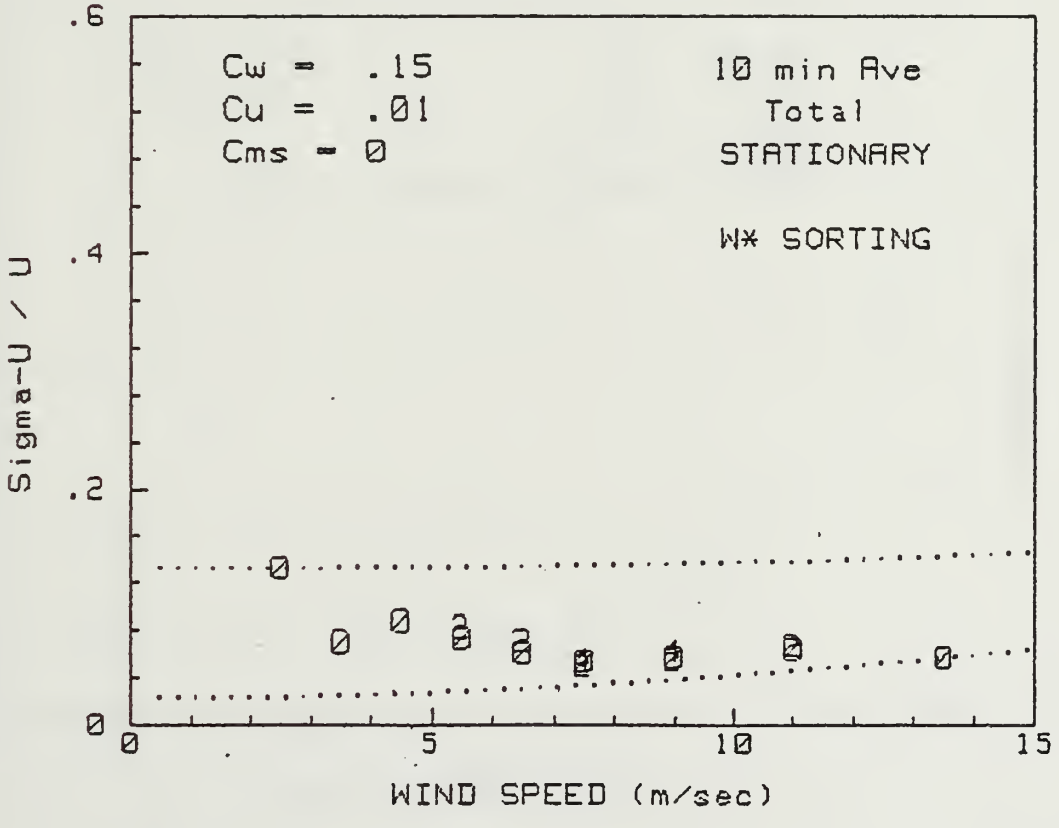
Cw = .15
Cu = .01
Cms = 0
10 min Ave
Total
STATIONARY
W* SORTING
Sigma-U / U
.6
.4
.2
0
0
5
10
15
WIND SPEED (m/sec)

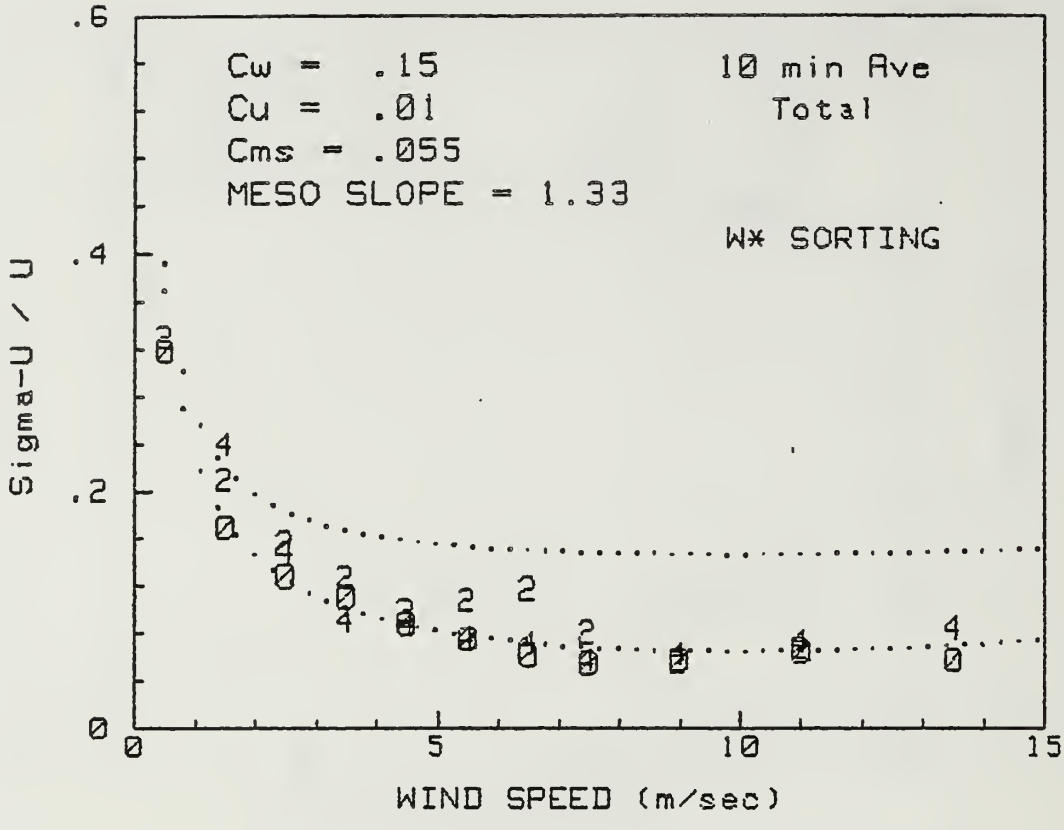
Cw = .15
Cu = .01
Cms = .055
MESO SLOPE = 1.33
10 min Ave
Total
W* SORTING
Sigma-U / U
WIND SPEED (m/sec)
0
.2
.4
.6
5
10
15

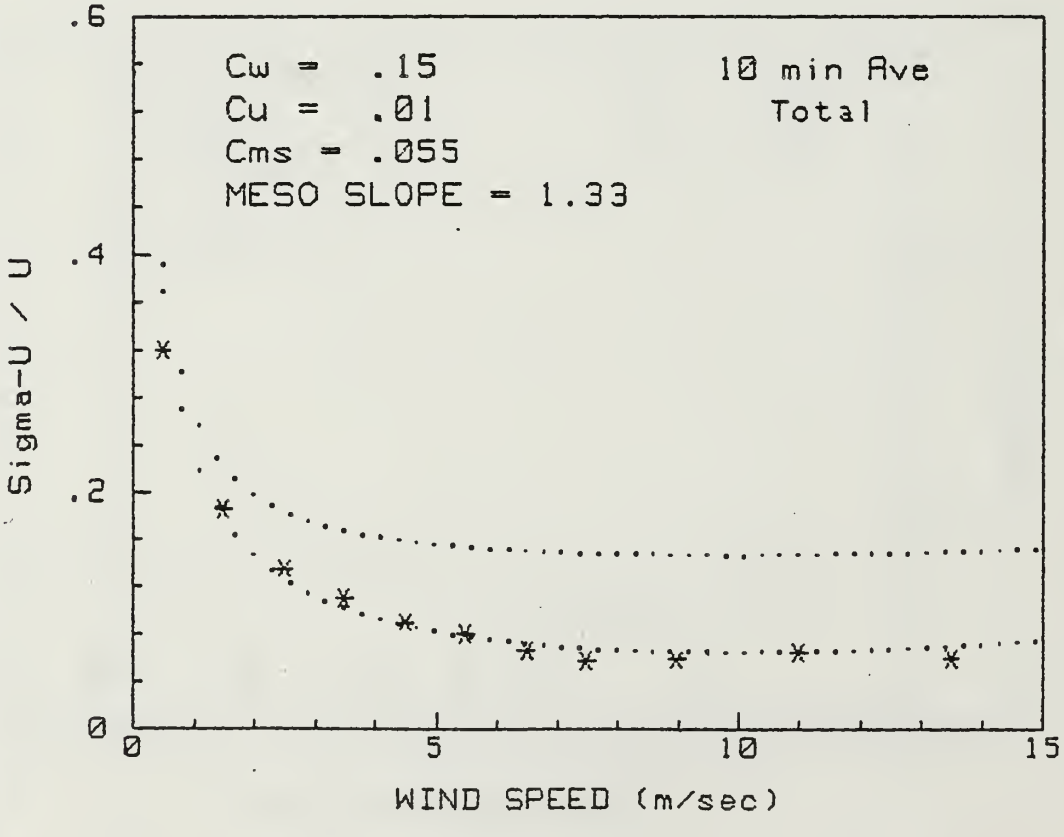
Cw = .15
Cu = .01
Cms = .055
MESO SLOPE = 1.33
10 min Ave
Total
Sigma-U / U
WIND SPEED (m/sec)
0
.2
.4
.6
5
10
15

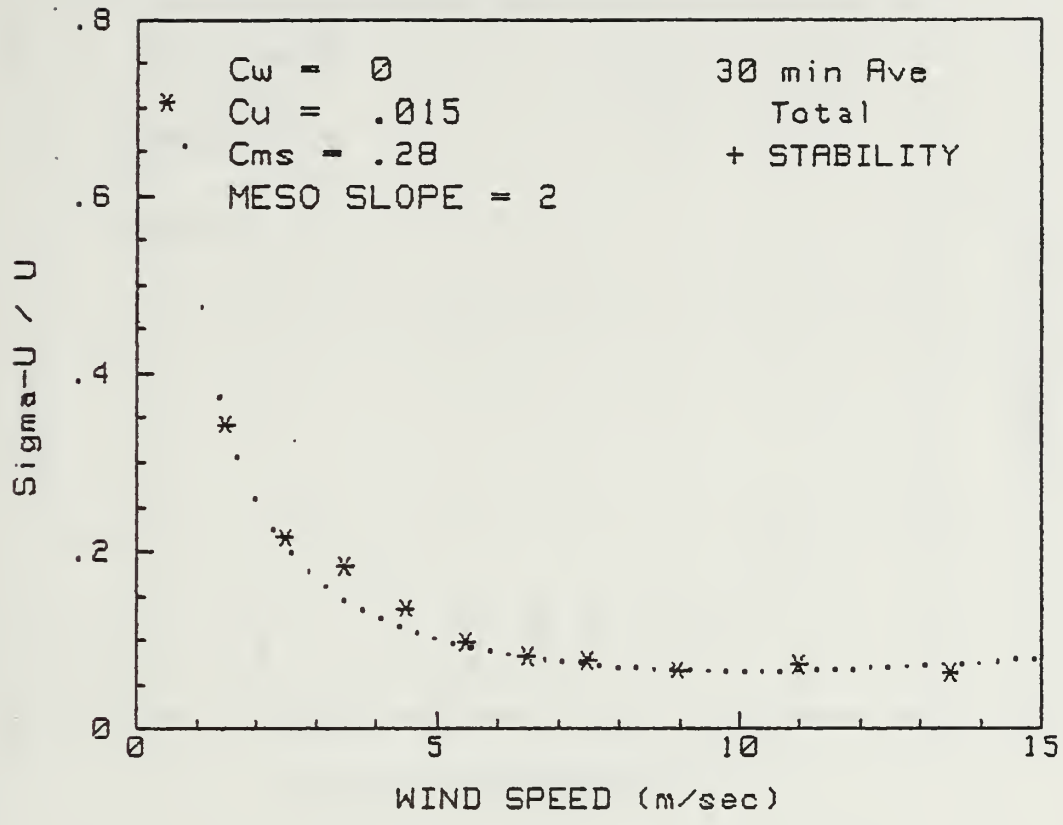
Cw = 0
Cu = .015
Cms = .28
MESO SLOPE = 2
30 min Ave
Total
+ STABILITY
Sigma-U / U
WIND SPEED (m/sec)
.8
.6
.4
.2
0
0
5
10
15

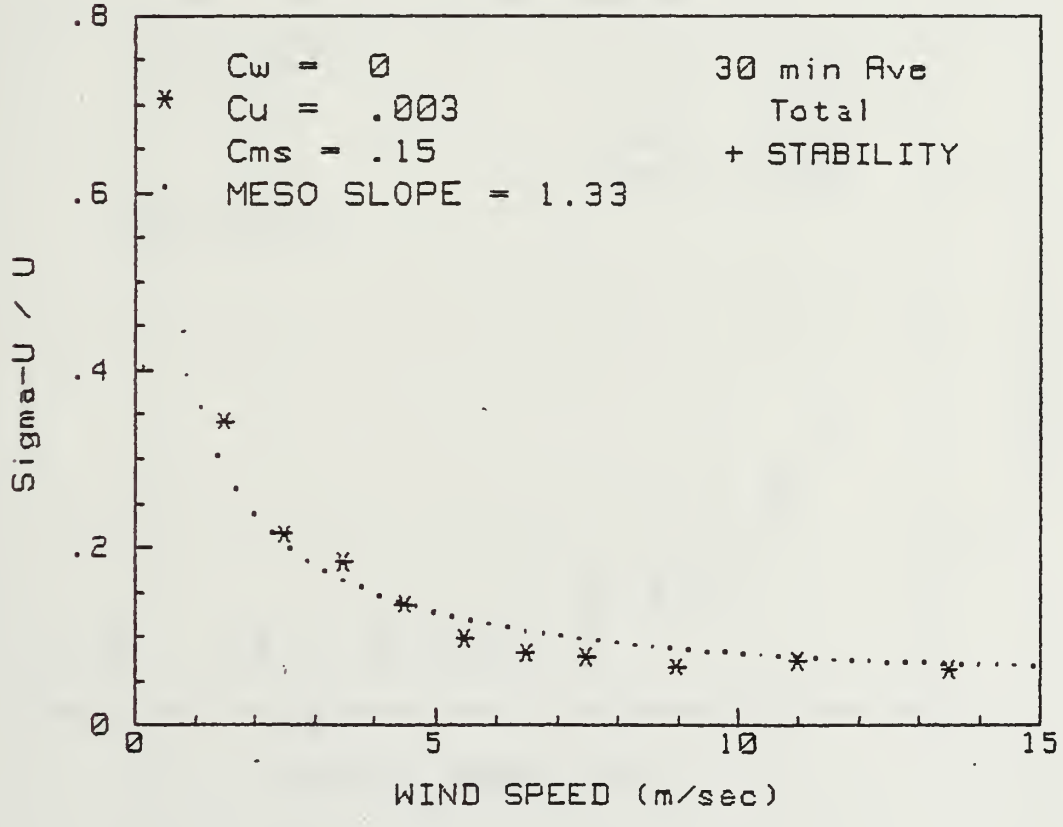
Cw = 0
Cu = .003
Cms = .15
MESO SLOPE = 1.33
30 min Ave
Total
+ STABILITY
Sigma-U / U
WIND SPEED (m/sec)
.8
.6
.4
.2
0
0
5
10
15

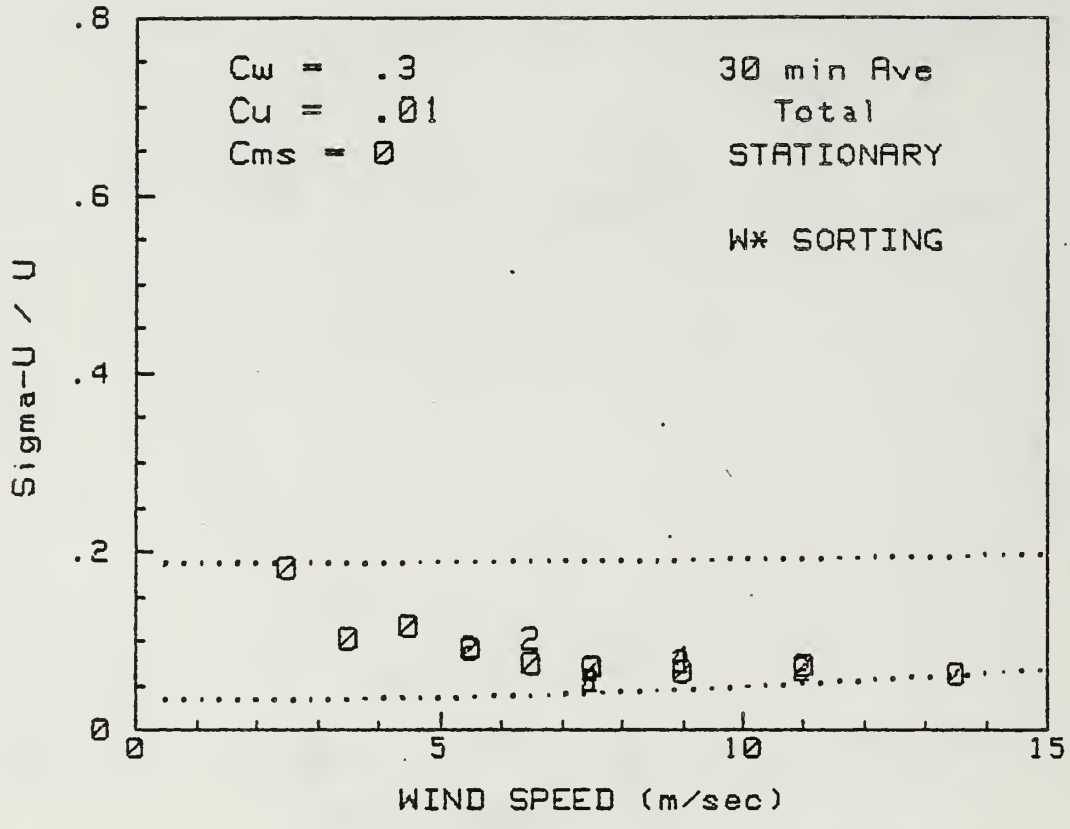
Cw = .3
Cu = .01
Cms = 0
30 min Ave
Total
STATIONARY
W* SORTING
Sigma-U / U
WIND SPEED (m/sec)

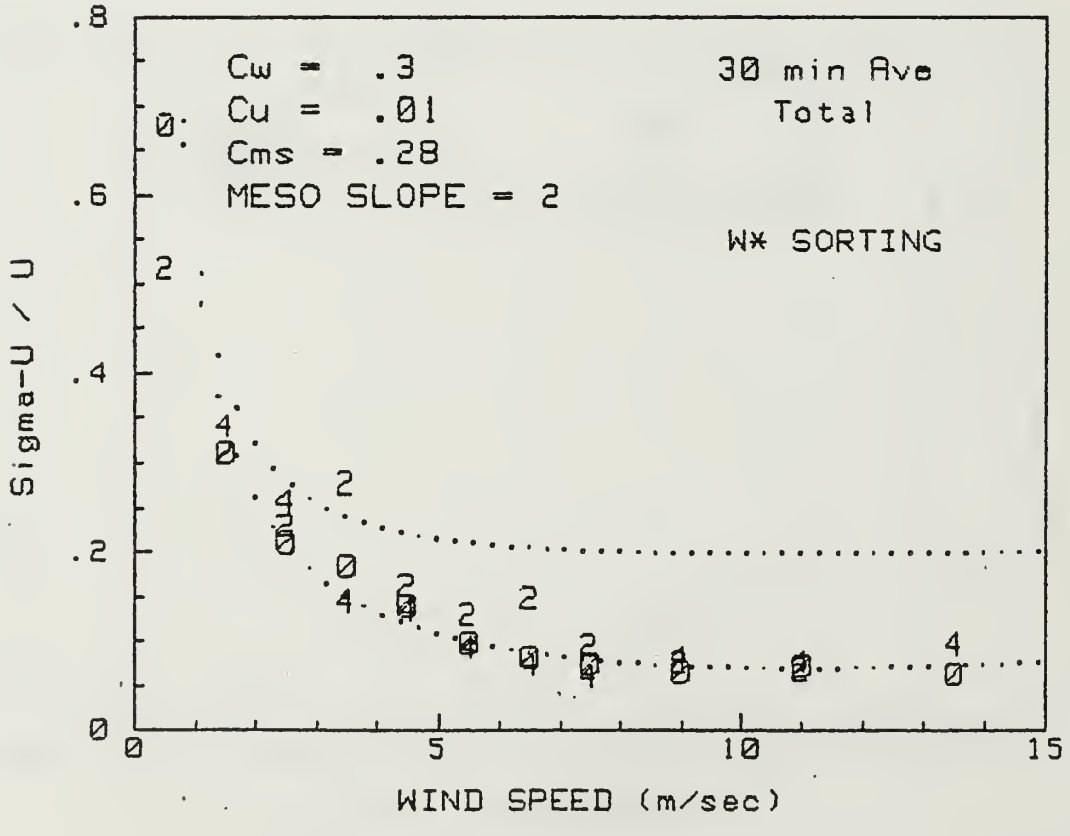
Cw = .3
Cu = .01
Cms = .28
MESO SLOPE = 2
30 min Ave
Total
W* SORTING
Sigma-U / U
WIND SPEED (m/sec)

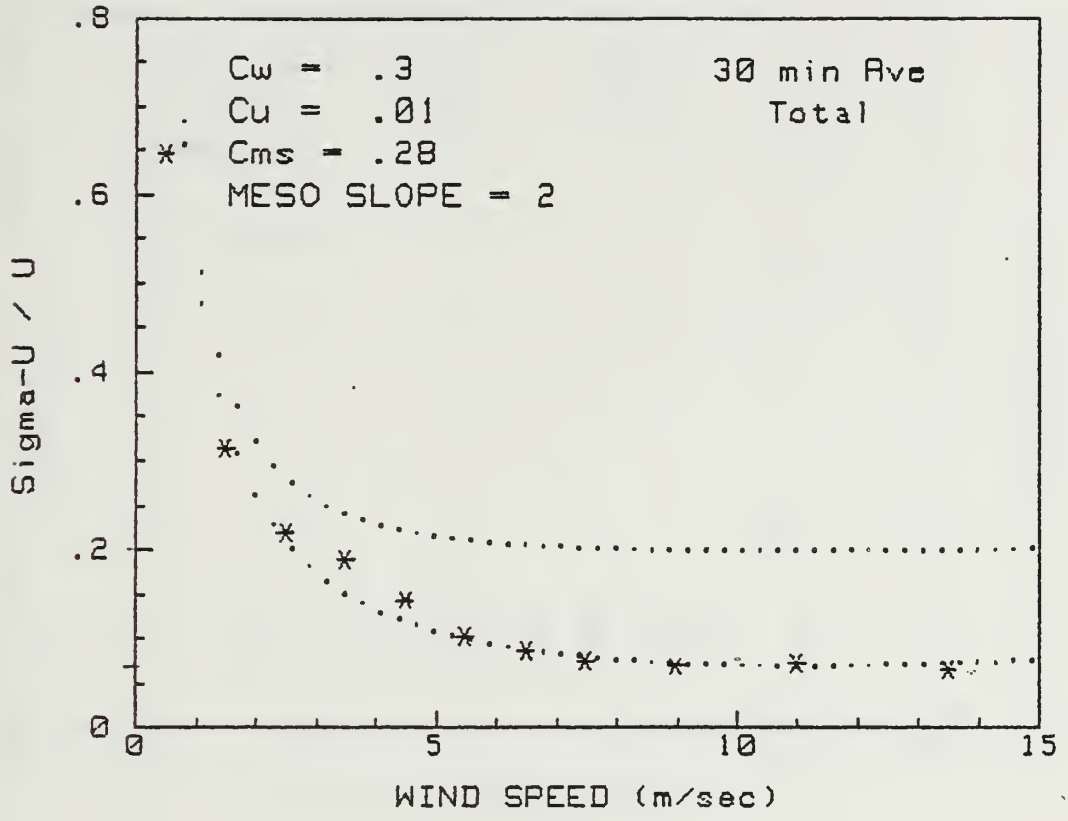
Cw = .3
Cu = .01
Cms = .28
MESO SLOPE = 2
30 min Ave
Total
Sigma-U / U
WIND SPEED (m/sec)
.8
.6
.4
.2
0
0
5
10
15

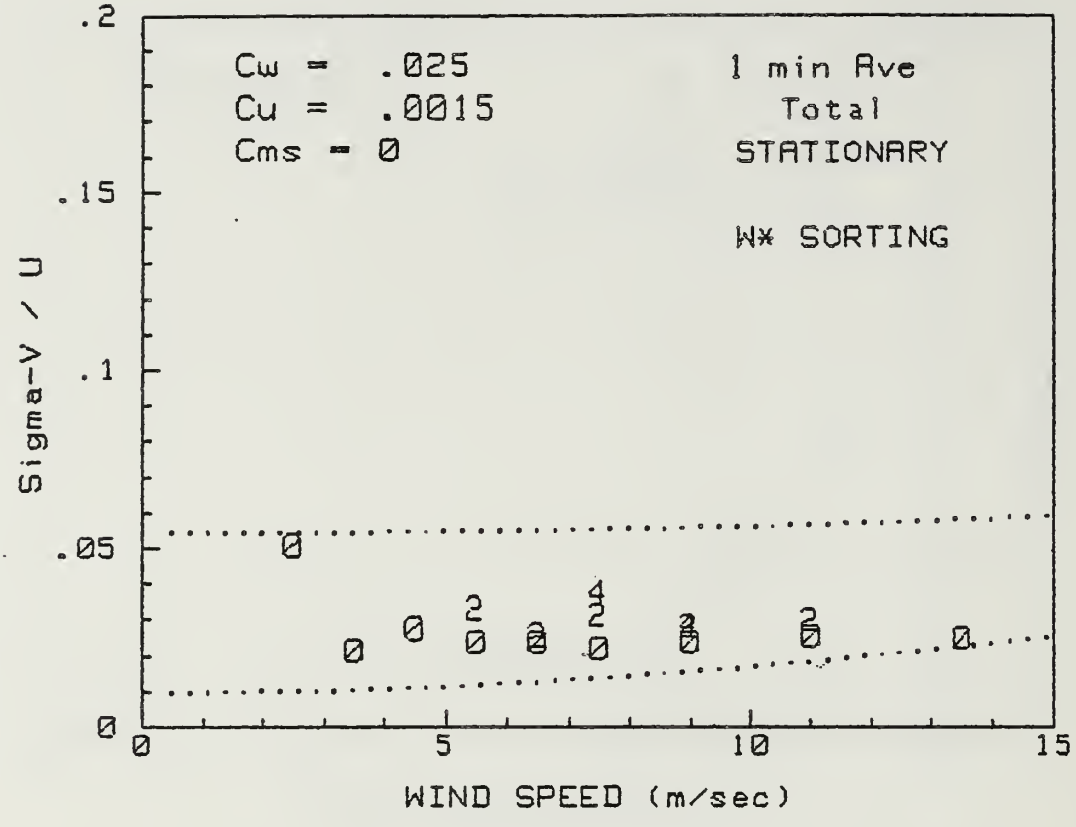
Cw = .025
Cu = .0015
Cms = 0
1 min Ave
Total
STATIONARY
W* SORTING
Sigma-V / U
.2
.15
.1
.05
0
0
5
10
15
WIND SPEED (m/sec)

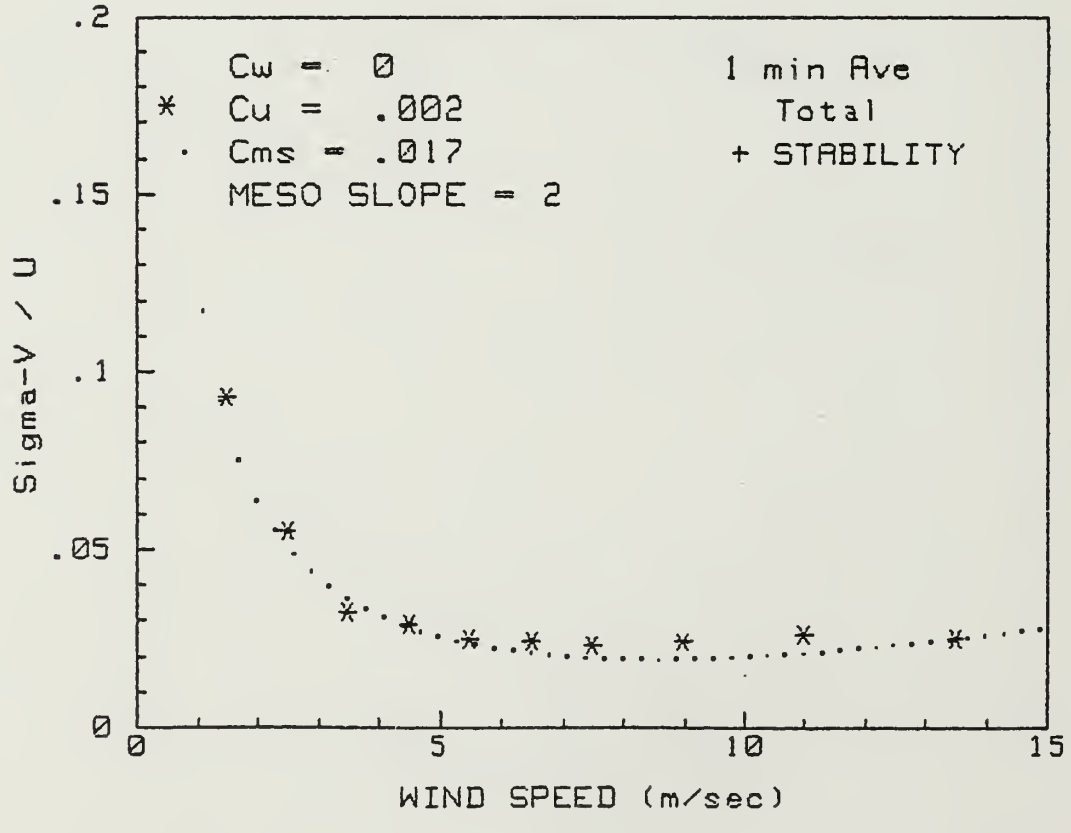
Cw = 0
Cu = .002
Cms = .017
MESO SLOPE = 2
1 min Ave
Total
+ STABILITY
Sigma-V / U
.2
.15
.1
.05
0
0
5
10
15
WIND SPEED (m/sec)

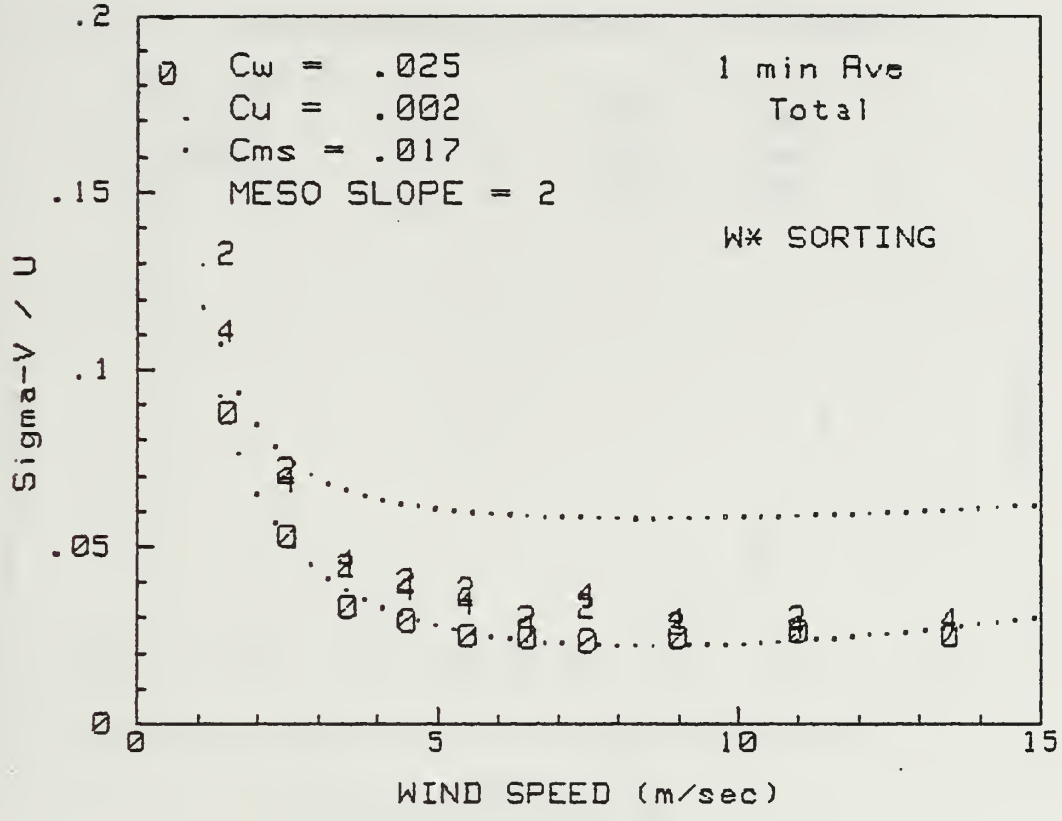
Cw = .025
Cu = .002
Cms = .017
MESO SLOPE = 2
1 min Ave
Total
W* SORTING
Sigma-V / U
WIND SPEED (m/sec)
0
.05
.1
.15
.2
5
10
15

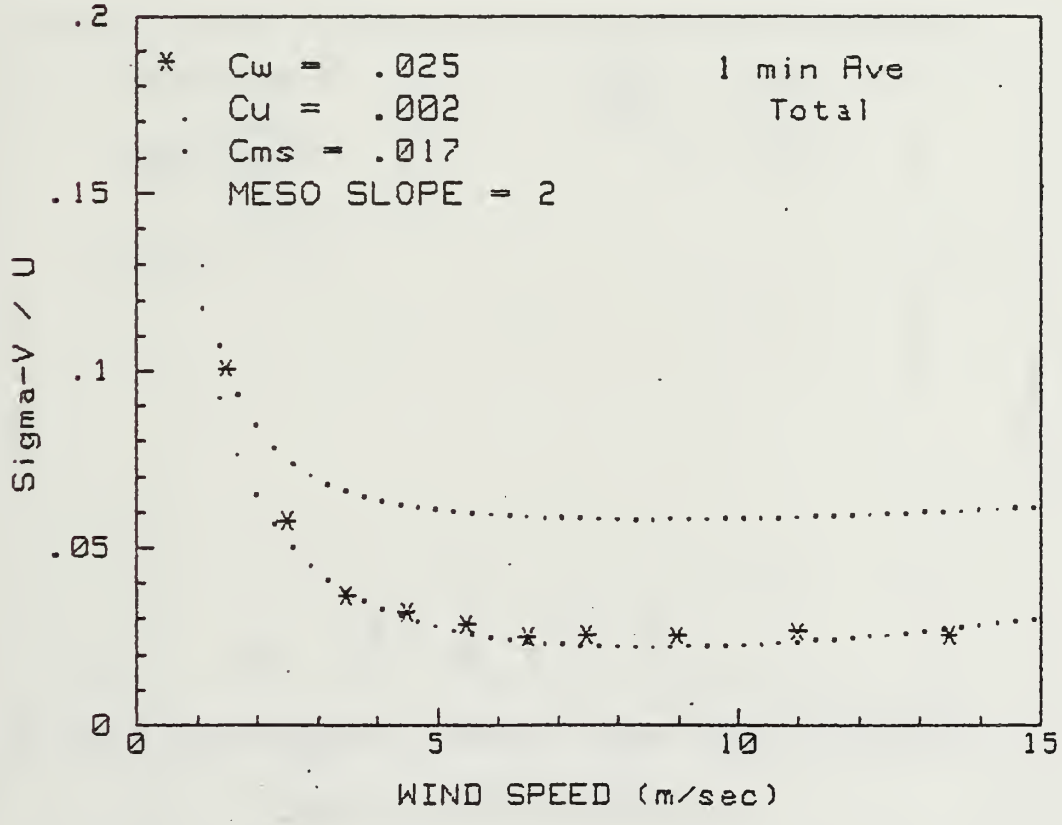
Cw = .025
Cu = .002
Cms = .017
MESO SLOPE = 2
1 min Ave
Total
Sigma-V / U
WIND SPEED (m/sec)
0
.05
.1
.15
.2
5
10
15

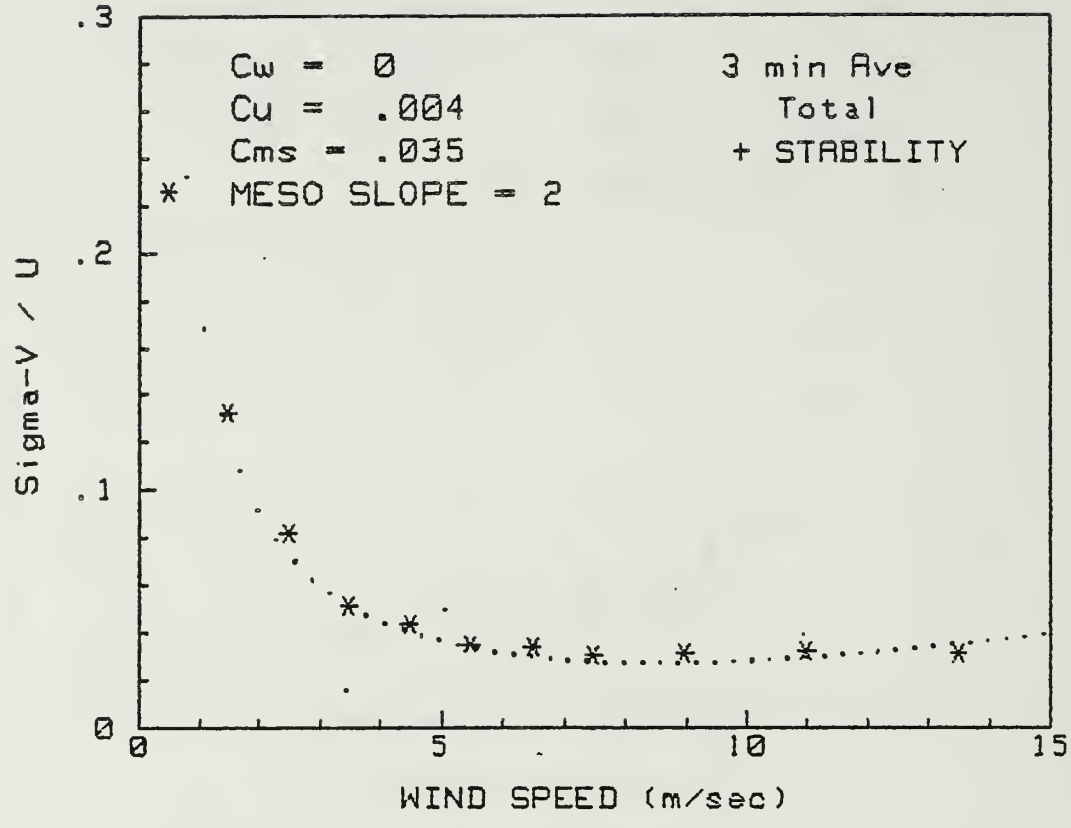
Cw = 0
Cu = .004
Cms = .035
MESO SLOPE = 2
3 min Ave
Total
+ STABILITY
Sigma-V / U
.3
.2
.1
0
0
5
10
15
WIND SPEED (m/sec)

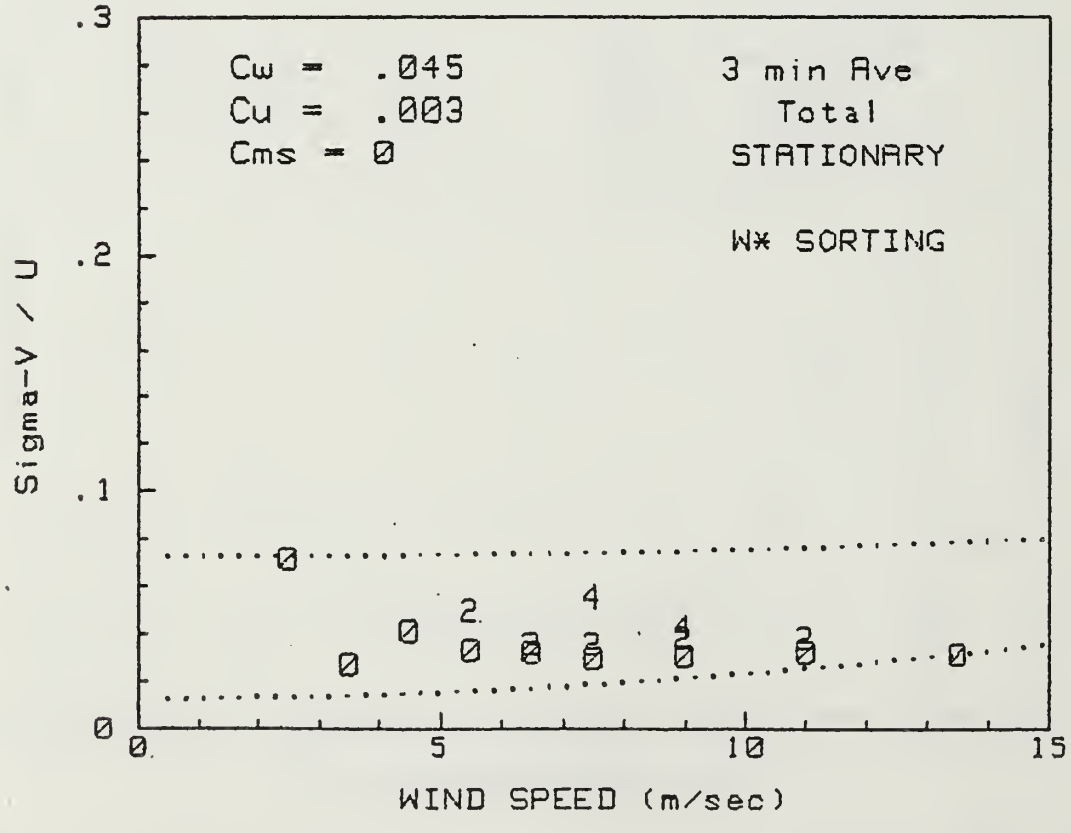
Cw = .045
Cu = .003
Cms = 0
3 min Ave
Total
STATIONARY
W* SORTING
Sigma-V / U
.3
.2
.1
0
0
5
10
15
WIND SPEED (m/sec)

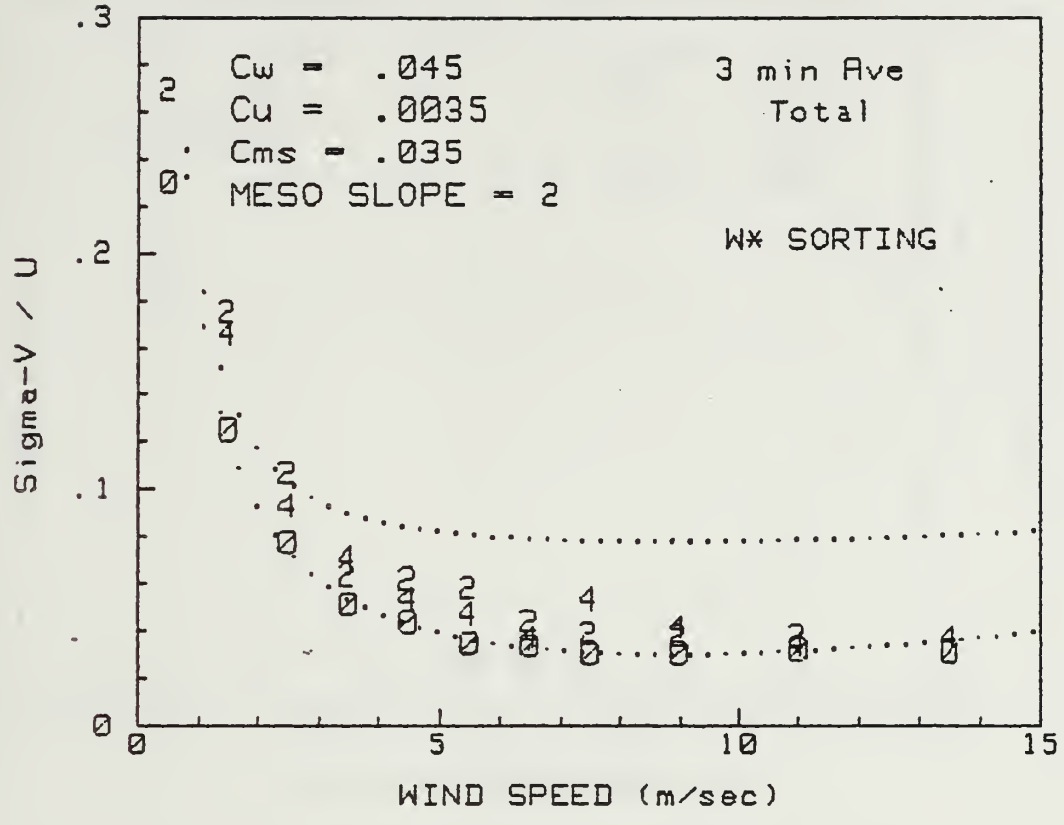
Cw = .045
Cu = .0035
Cms = .035
MESO SLOPE = 2
3 min Ave
Total
W* SORTING
Sigma-V / U
WIND SPEED (m/sec)
0
.1
.2
.3
5
10
15

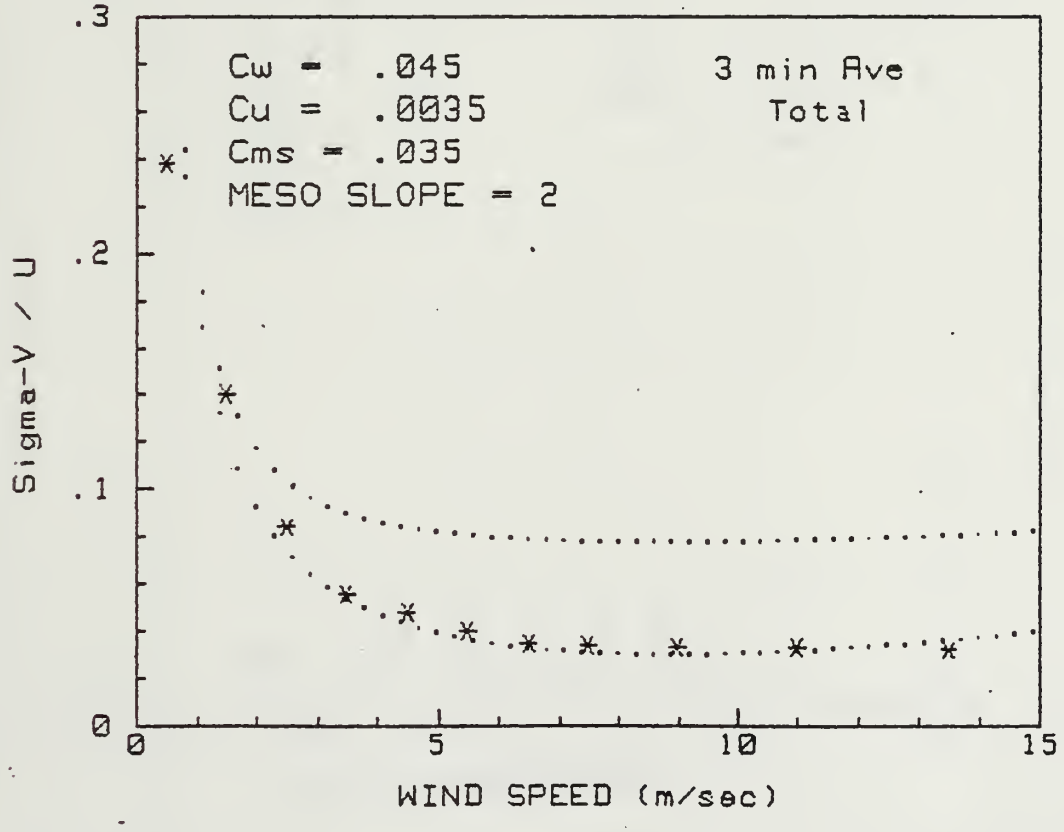
Cw = .045
Cu = .0035
Cms = .035
MESO SLOPE = 2
3 min Ave
Total
Sigma-V / U
WIND SPEED (m/sec)
0
.1
.2
.3
5
10
15

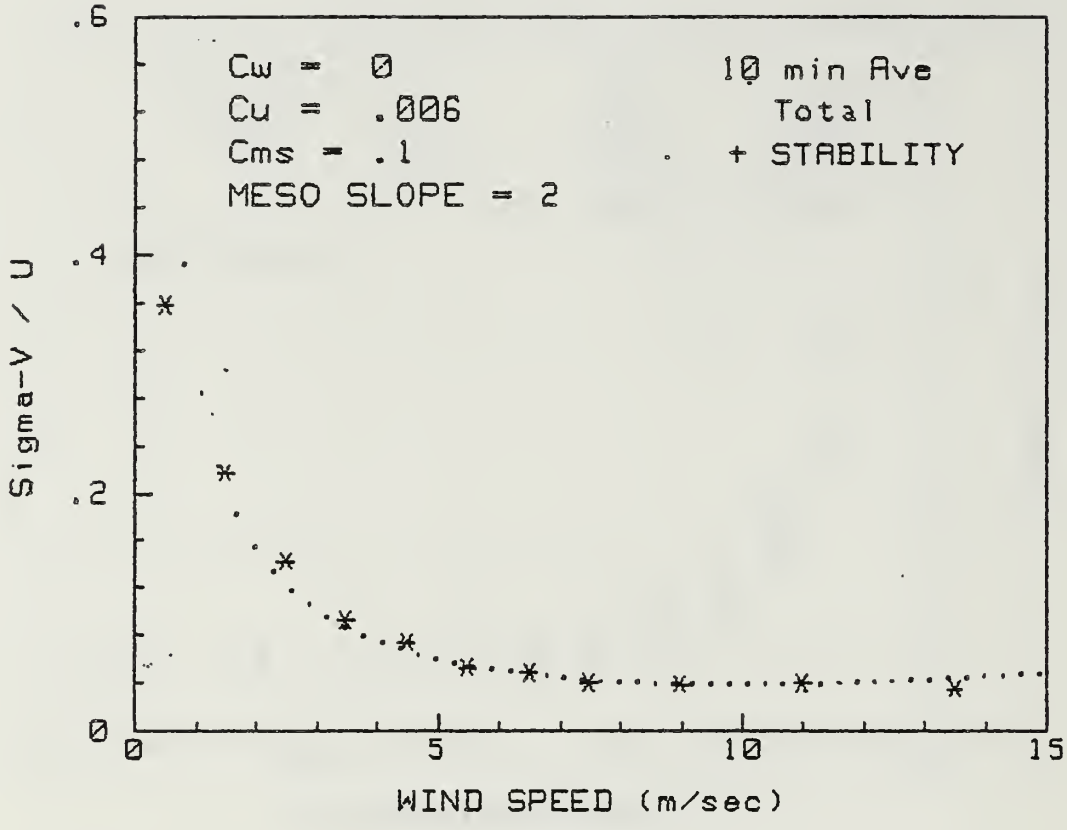
Cw = 0
Cu = .006
Cms = .1
MESO SLOPE = 2
10 min Ave
Total
+ STABILITY
Sigma-V / U
.6
.4
.2
0
0
5
10
15
WIND SPEED (m/sec)

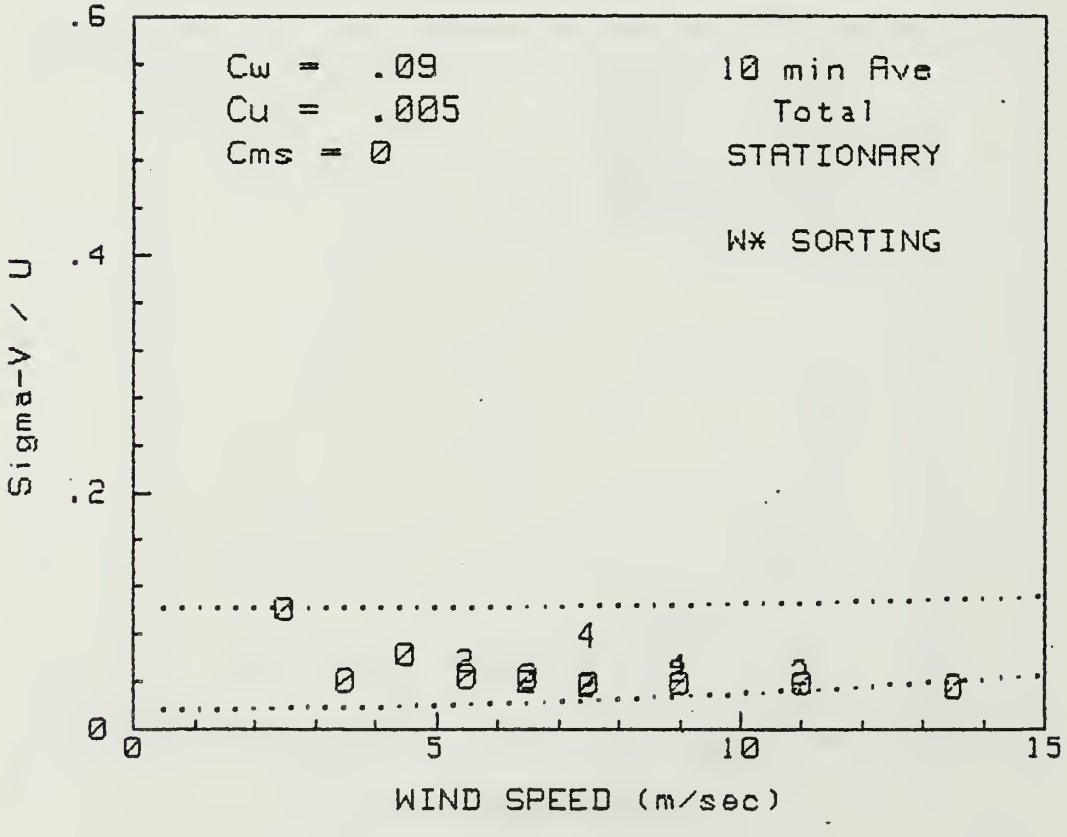
Cw = .09
Cu = .005
Cms = 0
10 min Ave
Total
STATIONARY
W* SORTING
Sigma-V / U
.6
.4
.2
0
0
5
10
15
WIND SPEED (m/sec)

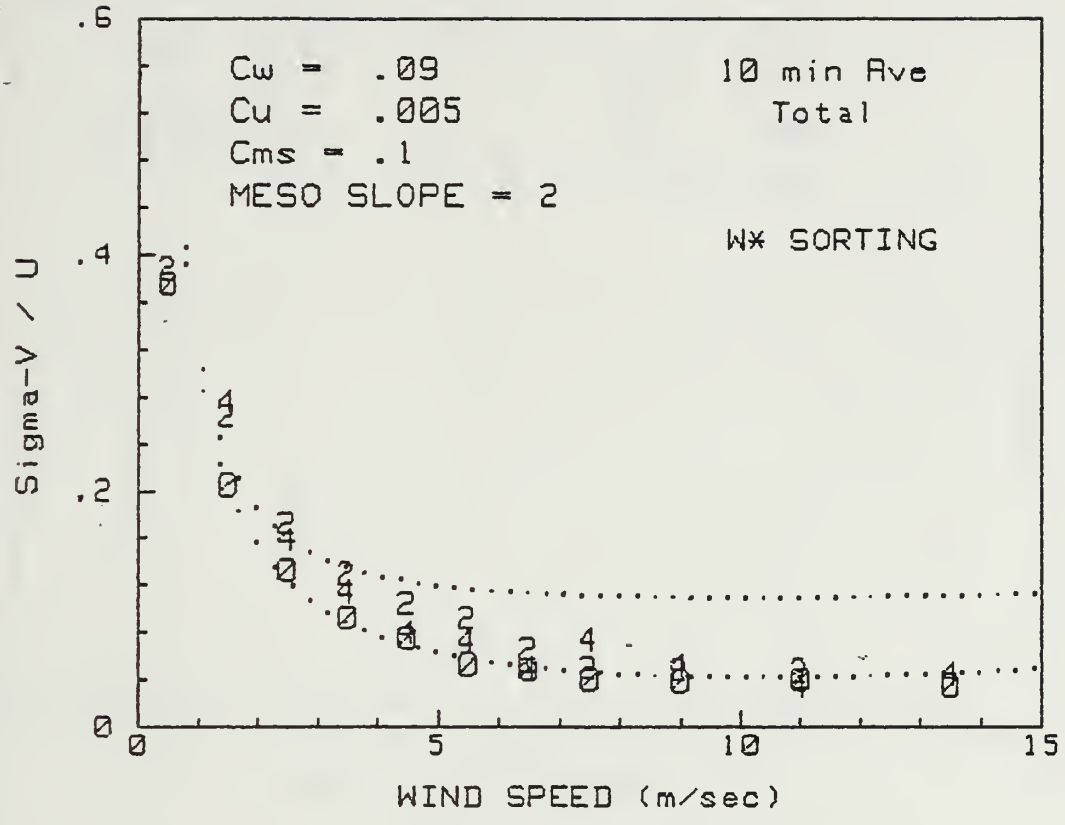
Cw = .09
Cu = .005
Cms = .1
MESO SLOPE = 2
10 min Ave
Total
W* SORTING
Sigma-V / U
WIND SPEED (m/sec)
0
.2
.4
.6
5
10
15

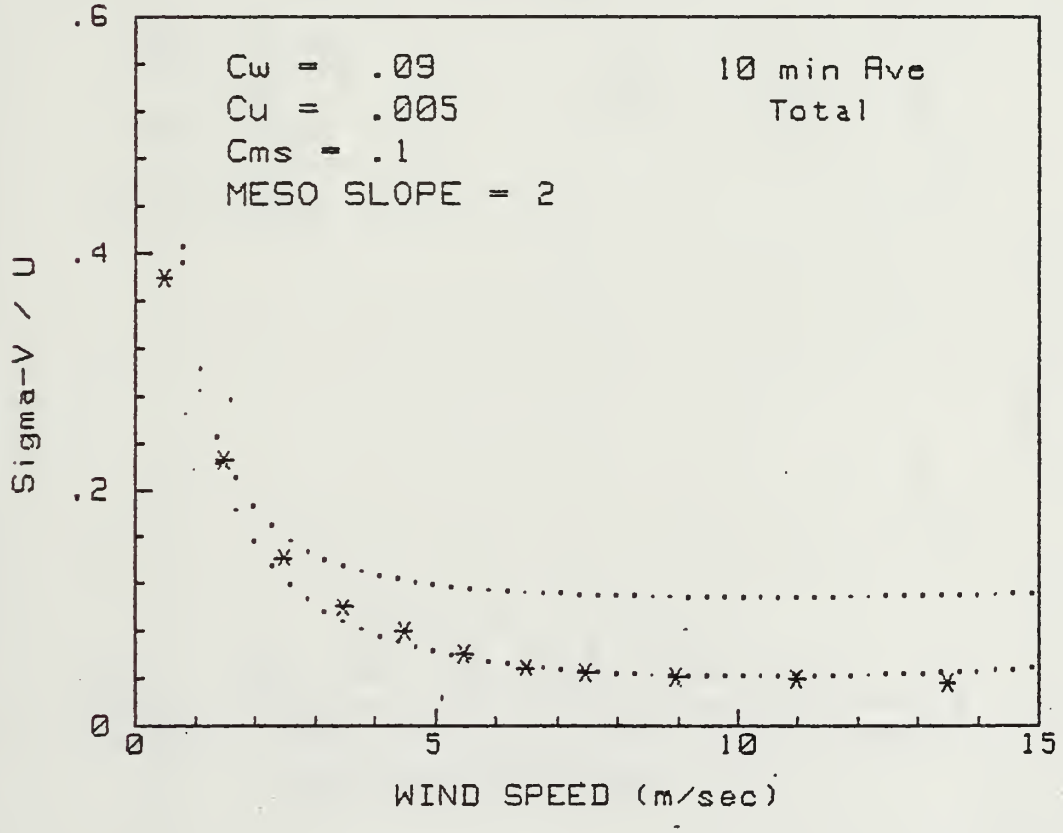
Cw = .09
Cu = .005
Cms = .1
MESO SLOPE = 2
10 min Ave
Total
Sigma-V / U
WIND SPEED (m/sec)
0
.2
.4
.6
5
10
15

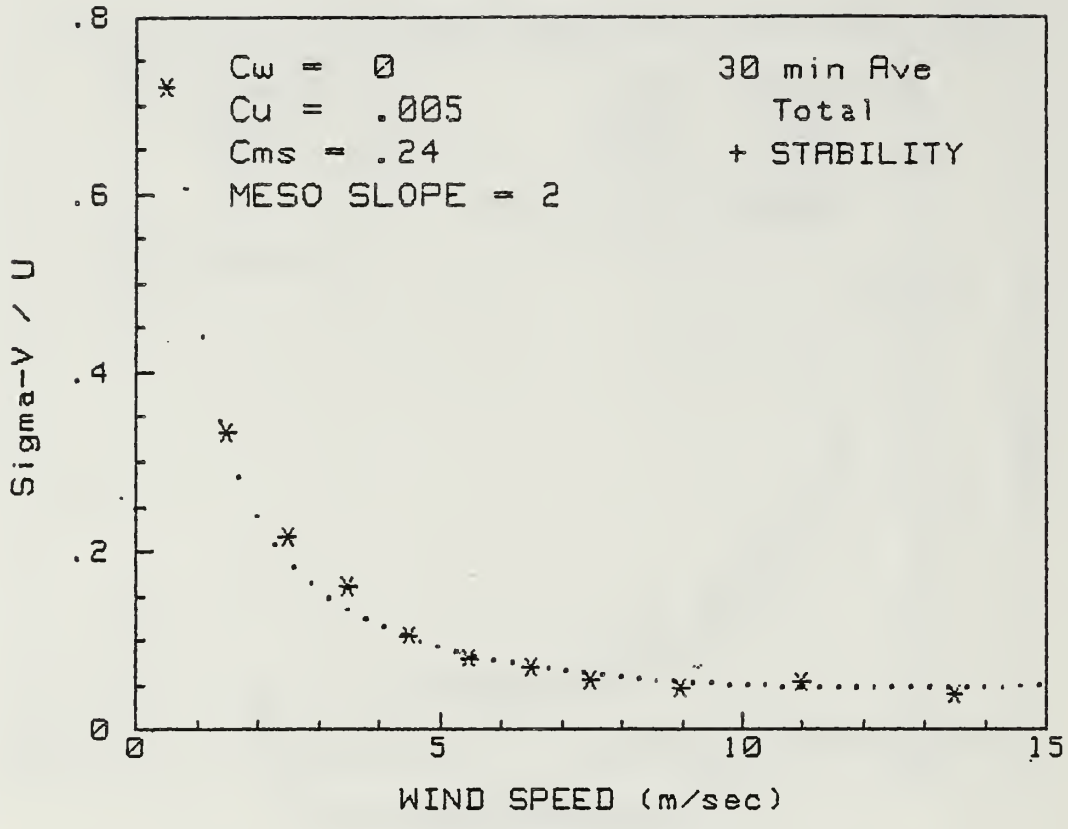
Cw = 0
Cu = .005
Cms = .24
MESO SLOPE = 2
30 min Ave
Total
+ STABILITY
Sigma-V / U
WIND SPEED (m/sec)
0
.2
.4
.6
.8
5
10
15

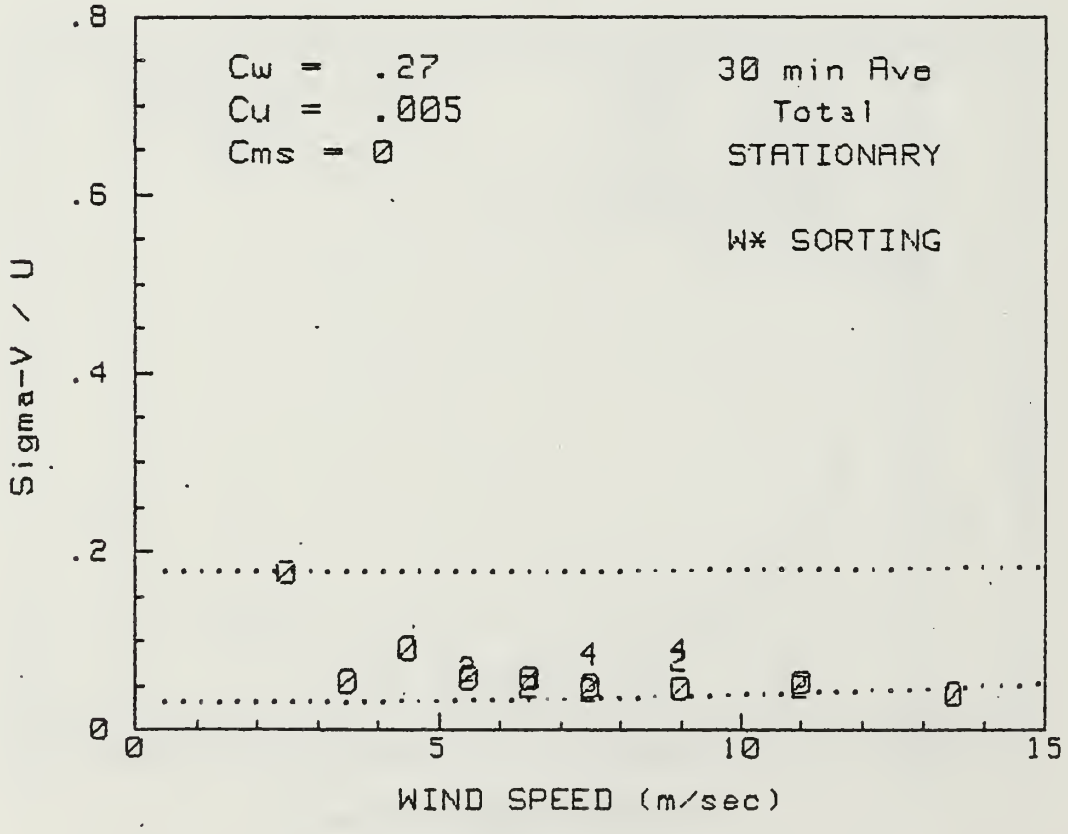
Cw = .27
Cu = .005
Cms = 0
30 min Ave
Total
STATIONARY
W* SORTING
Sigma-V / U
WIND SPEED (m/sec)
0
.2
.4
.6
.8
5
10
15

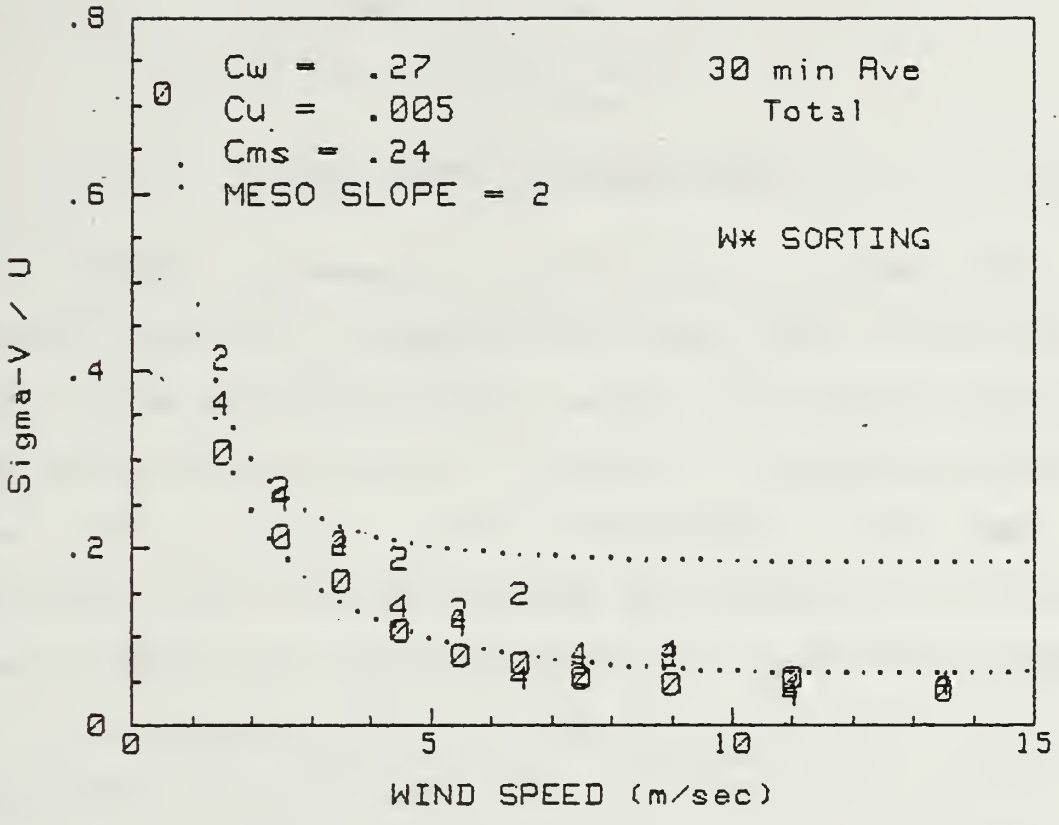
Cw = .27
Cu = .005
Cms = .24
MESO SLOPE = 2
30 min Ave
Total
W* SORTING
Sigma-V / U
WIND SPEED (m/sec)
0
.2
.4
.6
.8
5
10
15

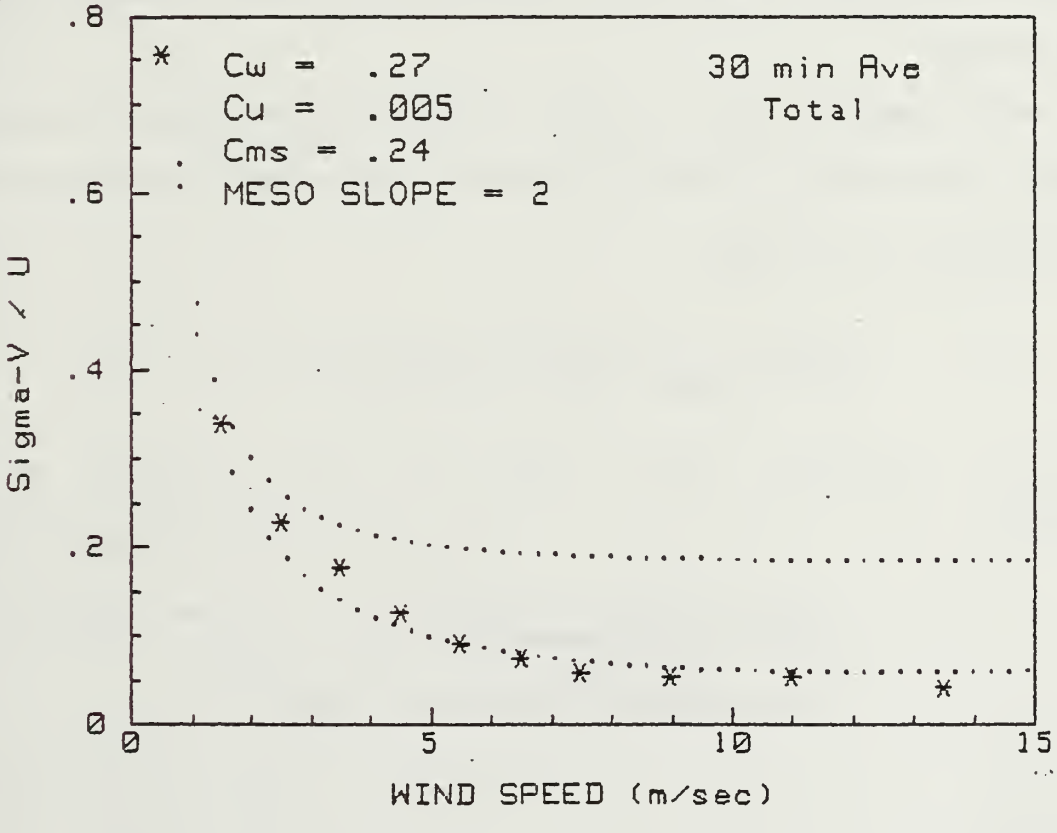
Cw = .27
Cu = .005
Cms = .24
MESO SLOPE = 2
30 min Ave
Total
Sigma-V / U
WIND SPEED (m/sec)
0
.2
.4
.6
.8
5
10
15

APPENDIX F

PUFF MODELING IMPLICATIONS

The Chemical Weapon Hazard Forecasting (CHEMFO) model developed by the Naval Environmental Predition Research Facility in Monterey, CA is a puff dispersion model used to predict the spread of chemical warfare agents, and is based on the work of Skupniewicz et al. (1984b). This model assumes a surface release with no vertical limit to the puff spread. However, that puff model only uses comparisons of relative dispersion data sets to field meteorological data for its parameterization. This thesis work can be extended to puff releases, which have operational significance to the U.S. Navy.

Skupniewicz et al. (1984a) determined estimates of short range diffusion in the horizontal plane for the transverse direction only, using

$$\sigma_y(T) = \sigma_v * T * f_y(T/t_L) \ ,$$

where:

σ_v = the standard deviation of the cross-wind velocity component,

T = the diffusion averaging time,

$f_y(T/t_L)$ = a universal function, and

t_L = the Lagrangian time scale.

The function $f_y(T/t_L)$ can be related to the puff length scale by

$$T \tilde{=} (L/U) ,$$

where

L = the dimension of the puff, and

U = the mean wind speed during the time average.

Sheih (1981) experimentally determined the "universal" function for various Pasquill-Gifford stability categories using

$$f_y(T/t_L) = [1 + (T/2t'_L)^{1/2}]^{-1} ,$$

where

t'_L = an "apparent" integral time scale.

It follows that for short range diffusion in the horizontal downwind direction

$$\sigma_x(T) = \sigma_u * T * f_x(T/t_L) ,$$

where

σ_u = the standard deviation of the downwind velocity component.

By knowing the downwind characteristic of puff growth based on $\sigma_x(T)$, the Gaussian plume dispersion model may be improved. Unfortunately, the above argument is theoretical and cannot be implemented bedause the Lagrangian time scale cannot be quantified; therefore, f_x and f_y are not known. The alternative is to utilize the relationship between σ_u and σ_v as determined in this work and project the relationship between the needed σ_x and σ_y used in puff modeling.

Skupniewicz (1984a) determined only transverse values of σ_y based on tracer experiments where actual meteorological measurements were made during selected meteorological conditions. This thesis presents a regression equation to parameterize σ_v and σ_u under many different meteorological conditions. By assuming that the relationship of turbulence to plume growth is the same for both the x and y directions, the scaling of σ_v to σ_y is expected to be the same for all σ_v. This expectation is also applied to the scaling of σ_u to σ_x for all σ_u. A relationship between σ_u and σ_v is presented earlier in this work and may provide an analogous relationship bewteen σ_y and σ_x.

This thesis has dealt with puff growth using a u, v grid based in a relative coordinate system where u is the axis along the mean wind flow. Based on this thesis, and

Panofsky and Dutton (1984), the ratio of σ_u / σ_v is approximately 1.25 $\pm$0.05. Since σ_y has been established as a function of σ_v, and $_x$ is proposed to be a function of σ_u, it follows that there should exist a relationship such that σ_x / σ_y is also approximately 1.25 $\pm$0.05.

Incorporation of this relationship into the CHEMFO model should provide an initial attempt to more accurately portray puff growth over an open ocean.

LIST OF REFERENCES

Businger, J.A., 1973: Turbulent Transfer in the Atmospheric Surface Layer. Workshop on Micrometeorology, AMS, 67.

Davidson, K.L., 1974: Observational Results on the Influence of Stability and Wind-wave Coupling on Momentum Transfer and Turbulent Fluctuations over Ocean Waves. Boundary Layer Meteorology, 6, 305- 331.

Garratt, J.R., 1977: Review of Drag Coeffiecients over Oceans and Continents. Monthly Weather Review, 105, 915.

Hojstrup, J., 1981: A Simple Model for the Adjustment of Velocity Spectra in Unstable Conditions Downstream of an Abrupt Change in Roughness and Heat Flux. Boundary Layer Meteorology, 21, 341-356.

_____, 1982: Velocity Spectra in the Unstable Planetary Boundary Layer. J. Atmos. Sci., 39, 2239.

Kaimal, J.C., J.C. Wyngaard, D.A. Haugen, O.R. Cote, Y. Izumi, S.J. Caughey and C.J. Readings, 1976: Turbulence Structure in the Convective Boundary Layer. J. Atmos. Sci., 33, 2152-2169.

Kaimal, J.C., 1978: Horizontal Velocity Spectra in an Unstable Surface Layer. Atmos. Sci., 35, 18-23.

Naval Postgraduate School, 1980: Naval Postgraduate School Shipboard and Aircraft Meteorological Equipment. Report 61-80-017 PR, Naval Postgraduate School, Monterey, CA, 22 pp.

Panofsky, H.A. and J.A. Dutton, 1984: Atmospheric Turbulence, 1st ed., John Wiley & Sons, Inc., 397 pp.

Schacher, G.E., D.E. Spiel, C.W. Fairall, K.L. Davidson, C.A. Leonard and C.H. Reheis, 1982: California Coastal Offshore Transport and Diffusion Experiments- Meteorological Conditions and Data. Report 61-82-007, Naval Postgraduate School, Monterey, CA, 380 pp.

Schacher, G.E., 1986: Parameterization of Overwater Horizontal Wind Variability. Report 61-86-014, Naval Postgraduate School, Monterey, CA, 211 pp.

Sheih, C., 1981: Pasquill-Taylor Dispersion Parameters Overwater Near Shore. Atmos. Environ., 15, 101-105.

Skupniewicz, C.E. and G.E. Schacher, 1984: Measured Plume Dispersion Parameters Over Water, Volume I. Report 61-84-012, Naval Postgraduate School, Monterey, CA, 101 pp.

_____, 1984: Assessment of the Performance of an In-Field Gaussian Plume/Puff Model for Overwater Use. Report 61-85-002, Naval Postgraduate School, Monterey, CA, 55 pp.

Vandenberg AFB, DET 30, 2WS, 1982: Terminal Forecast Reference Notebook. Vandenberg AFB, CA, 98 pp.

INITIAL DISTRIBUTION LIST

		No. Copies
1.	Defense Technical Information Center Cameron Station Alexandria, Virginia 22304-6145	2
2.	Library, Code 0142 Naval Postgraduate School Monterey, California 93943-5002	2
3.	Chairman (Code 68Mr) Department of Oceanography Naval Postgraduate School Monterey, California 93943-5004	1
4.	Chairman (Code 63Rd) Department of Meteorology Naval Postgraduate School Monterey, California 93943-5004	1
5.	Director Naval Oceanography Division Naval Observatory 34th and Massachusetts Avenue NW Washington, D.C. 20390	1
6.	Commander Naval Oceanography Command NSTL Station Bay St. Louis, Missouri 39522	1
7.	Commanding Officer Naval Oceanographic Office NSTL Station Bay St. Louis, Missouri 39522	1
8.	Commanding Officer Fleet Numerical Oceanography Center Monterey, California 93940	1
9.	Commanding Officer Naval Ocean Research and Development Activity NSTL Station Bay St. Louis, Missouri 39522	1

10. Commanding Officer — 2
Naval Environmental Prediction
Research Facility
Monterey, California 93940

11. Chairman, Oceanography Department — 1
U.S. Naval Academy
Annapolis, Maryland 21402

12. Chief of Naval Research — 1
800 N. Quincy Street
Arlington, Virginia 22217

13. Office of Naval Research (Code 420) — 1
Naval Ocean Research and Development
Activity
800 N. Quincy Street
Arlington, Virginia 22217

14. Scientific Liaison Office — 1
Office of Naval Research
Scripps Institution of Oceanography
La Jolla, California 92037

15. Library — 1
Scripps Institution of Oceanography
P.O. Box 2367
La Jolla, California 92037

16. Library — 1
Department of Oceanography
University of Washington
Seattle, Washington 98105

17. Library — 1
CICESE
P.O. Box 4803
San Ysidro, California 92073

18. Library — 1
School of Oceanography
Oregon State University
Corvallis, Oregon 97331

19. Commander — 1
Oceanographic Systems Pacific
Box 1390
Pearl Harbor, Hawaii 96860

20. Chief, Ocean Services Division — 1
National Oceanic and Atmospheric Administration
8060 Thirteenth Street
Silver Springs, Maryland 20910

21. Library — 1
Moss Landing Marine Lab
California State Colleges
Sandholdt Road
Moss Landing, California 95039

22. Library Acquisitions — 1
National Center for Atmospheric Research
P.O. Box 3000
Boulder, Colorado 80307

23. NAVSEASYSCOM — 1
Damage Control Branch
Code 55X25
Bldg NC-2
Washington, D.C. 20362-5101

24. Professor G.E. Schacher — 4
Dean of Science
Naval Postgraduate School
Monterey, California 93943-5004

25. Professor K.L. Davidson, Code 63Ds — 1
Department of Meteorology
Naval Postgraduate School
Monterey, California 93943-5004

26. Mr. Tom Yencha, Code G51 — 1
Naval Surface Weapons Center
Dahlgren, Virginia 22448

27. CDR James D. Branum — 1
2682 Olivestone Way
San Jose, California 95132

28. LT Tim Dowding — 2
6 Robin Way
Westerly, Rhode Island 02891

29. Dr. Donald L. Shearer — 1
TRC Environmental Consultants, Inc.
8775 E. Orchard Road, Suite 816
Englewood, Colorado 80111

30. Dr. Bert Galloway, Code 3917 — 1
Naval Weapons Center
China Lake, California 93555

31. Dr. Gloria Patton — 1
Theater Nuclear Warfare Project Office
Department of Navy
Washington, D.C. 20360

32. CDR S.G. Colgan, Code 420B — 1
Office of Naval Research
800 N. Quincy Street
Arlington, Virginia 22217

33. Mr. Dirk Herkhof — 1
Minerals Management Service
Pacific OCS Office
1340 West 6th Street Rm. 200
Los Angeles, California 90017

34. Mr. Robert Harrison — 1
Western Oil and Gas Assn.
727 West 7th Street
Los Angeles, California 90017

Thesis
D70153 Dowding
c.1 Parameterization of
horizontal wind velocity
variability.